1-29-2009

Study of the current-voltage relation for a single C-60 transistor

Anita Parmar

Anita Parmar
Candidate

Physics and Astronomy
Department

This dissertation is approved, and it is acceptable in quality and form for publication on microfilm:

Approved by the Dissertation Committee:

, Chairperson

Dec 5, 2008

Dec 5 2008

Dec 5, 2008

Accepted:

Dean, Graduate School

DEC 0 8 2008
Date

Study of the Current-Voltage Relation for a Single C_{60} Transistor

by

Anita Parmar

B.S., Physics, McGill University, Montreal 2000
M.S., Physics, University of New Mexico, 2003

DISSERTATION

Submitted in Partial Fulfillment of the
Requirements for the Degree of

Doctor of Philosophy
Physics

The University of New Mexico

Albuquerque, New Mexico

December, 2008

Dedication

To dear Uncle Tom.

Acknowledgments

The journey towards attaining this degree has been made much easier with the help of my teachers, friends and family.

I would like to thank my teachers first, especially my advisor Dr. David Dunlap for accepting me as his student and for sharing his unique perspective on and remarkable enthusiasm for this subject, and physics in general. I am also grateful to the members of my dissertation committee, Dr. John Grey, Dr. Nitant Kenkre, and Dr. Sudhakar Prasad, for their patience and valuable critiques of this work. I would like to thank all of my past physics professors, because each has contributed to shaping my understanding of this vast subject. Great physics teachers are few and far between, and crafting a compelling lecture is something that we all aspire to, so I would like to thank in particular the best professor that I have ever encountered, Dr. Ivan Deutsch. Female role models in this field are even more rare, and I am very grateful for Dr. Susan Atlas' presence in the department.

I would like to thank Doug Weintraub from the Office of Graduate Studies for being incredibly helpful while completing the administrative aspect of this process.

I am very lucky to have always been surrounded by the most amazing group of friends. I can't thank them enough for being so good to me, and for making the past years memorable, tolerable, and lots of fun. I would like to thank the best office mate ever, Tianjian Lu, for his great company and friendship. I am extremely grateful to Dr. Denise Wallen for her mentorship and guidance. I would like to especially thank my close friends Dave, Sonja, Tanya, Wendy, Iris, Jane, and Nina.

Finally, I am incredibly lucky to have the love and support of my family and Kiran's family. Kiran has remained supportive throughout this experience, and is the most admirable person that I know. I would like to thank my sisters, Surita, Karan, and Sharan, with whom I grow closer every year, and who have been a constant source of strength. I am especially grateful to Sharan for her guidance and friendship. My parents, Swarn and Amarjit, have given me more than I could ever thank them for, and I am the most grateful to them for all that they have done for me.

Study of the Current-Voltage Relation for a Single C_{60} Transistor

by

Anita Parmar

ABSTRACT OF DISSERTATION

Submitted in Partial Fulfillment of the

Requirements for the Degree of

Doctor of Philosophy

Physics

The University of New Mexico

Albuquerque, New Mexico

December, 2008

Study of the Current-Voltage Relation for a Single C_{60} Transistor

by

Anita Parmar

B.S., Physics, McGill University, Montreal 2000
M.S., Physics, University of New Mexico, 2003

Ph.D., Physics, University of New Mexico, 2008

Abstract

The beginning of this century saw the pioneering fabrication of a single molecular transistor using a single C_{60} molecule between gold nanowires, and inspired experimentalists and theorists alike to focus on studying phonon assisted transport through nanoscale electronic devices. We have formulated an electron tunnelling model for the current-voltage (I-V) relationship for a C_{60} molecular transistor that reproduces trends observed in the experimental I-V curves. A uniform one dimensional tight-binding lattice is used to model the transistor system, with a central defect site representing the molecule. The current is written as a function of tunnelling rates on and off of the molecule, where the rates are calculated using Fermi's Golden Rule and a Green function technique called the Renormalized Perturbation Expansion. In calculating the tunnelling rates, a deeper understanding of the trends that are seen in the experimental data is attained, and certain new features of the system

are uncovered. First, incorporating the degeneracy of the tunnelling state into the expression for the current allows the prediction of the degree of asymmetry in the saturation values for forward and reverse bias current. Also, using the relative sizes of the source-drain voltage gaps for forward and reverse bias current, and the relative sizes of the initial steps in current, we show that the C_{60} molecule is negatively charged when in a nanometre sized gap between two gold nanowires. Finally, an experimental method for measuring the effect that varying the gate voltage has on the size of the voltage gap between the tunnelling level of the molecule and the Fermi level of the electrodes is obtained.

Contents

List of Figures

List of Tables

Chapter 1

Introduction

1.1 Single Molecule Transistors

Molecular electronic applications have become the most promising prospect for minimizing electronic circuit dimensions and enhancing performance [Dat95, MAR98] however as recently as a few decades ago the idea of measuring the current through a single molecule was a daring proposition at best [AR74, Car83]. Not only has it become possible to isolate single molecules, but recent experiments continue to improve techniques for fabricating molecular switches, gates and charge transfer mechanisms [JMAR97, AMAR98, Joa02]. There have been several successful experiments reporting transport through a single molecule [MAR97, HP00, JP02, WL02, RHMS02, NZB02] demonstrating the potential for the development of molecular transistors. Most conventional transistors are based on silicon, and there is a limit to the number that fit in a given area. The advent of molecular transistors would circumvent this issue and allow for faster circuits that occupy less space, and consume less power with a reduced potential for overheating.

This thesis examines a transistor whose conducting element is a single C_{60} molecule.

The current voltage behaviour for the transistor is modeled by a set of rate equations [BS01, KM03a, MAM04]. The rates are calculated using time dependent perturbation theory for a Hamiltonian describing the movement of a single charge on a tight binding chain. The motion of the charge is coupled to the vibrational motion of the molecule. Our model provides insight other properties of the transistor; one of our main findings is a method to determine the equilibrium charge state of C_{60} from the characteristics of the current-voltage data.

1.1.1 Fabrication

Transistors control the flow of current in electronic devices and are considered the fundamental building blocks that drive everything from computers and cell phones to household appliances. Conventional transistors are semiconductor devices that regulate electron flow via a barrier, and although they can be used independently, they are more commonly combined as integrated circuits to amplify or switch electronic signals [HH89]. The physical system of H. Park et al. published in Volume 407 of Nature magazine in 2000 [HP00] is one of the first to extend the idea of electron tunnelling through quantum dots to tunnelling through molecules, resulting in the construction of a molecular transistor. While several experiments have been performed on molecule scale systems that demonstrate similar current-voltage characteristics, arising from phonon assisted tunnelling [TN02, YA03, KN02, HP99, EB02, MJ06, ANP05, JP02, CKS03, KM03a], the data that was produced in the Park experiment will be used to gauge the validity of the model that is developed in this thesis. Further information about the experimental techniques used in the fabrication of molecular transistors can be found in the above cited references.

The single molecule transistor of Park et al. is comprised of gold electrodes sandwiching an isolated C_{60} molecule, built on top of an insulating layer of SiO_2 that rests on a degenerately doped silicon wafer, as illustrated in Figure 1.1.

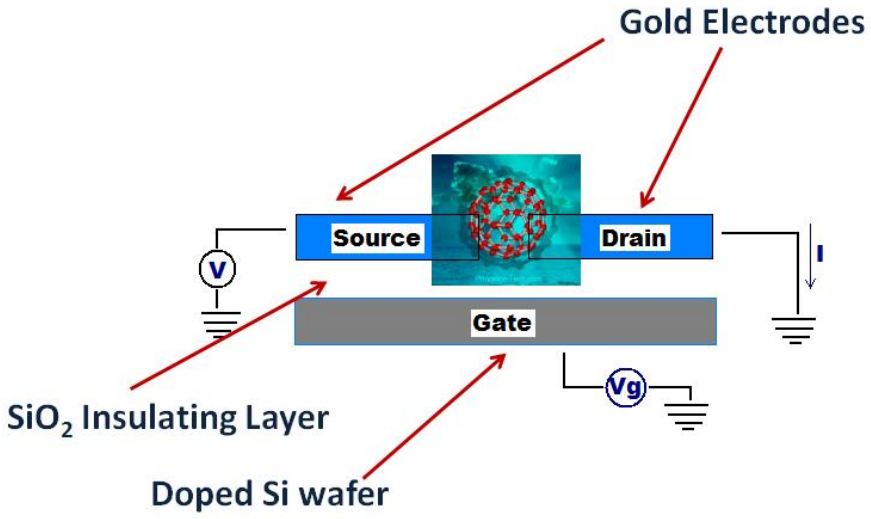

Figure 1.1: Schematic illustration of the primary components of a C_{60} single molecule transistor.

The silicon layer acts as the gate electrode, and modulates the electrostatic potential of the C_{60} molecule. In this particular example, the construction of the transistors was accomplished at low cryogenic temperatures ($T = 1.5K$). Unbroken gold wires were made using electron beam lithography and covered with a dilute solution of C_{60} molecules in toluene, and then a small gap was created in the wires using a break junction technique by the process of electromigration. A high current was passed through the wires, each of which burned out at their weakest point. It was anticipated that for some wires a C_{60} molecule could become sandwiched in the gap where the wires burned out, facilitating conduction. When the conductance of the broken wires was measured, about ten percent of the gold wires exhibited enhanced conductance, as compared to the remainder, indicating that these were wires whose gaps were occupied by C_{60} molecules. The low incidence of molecular presence within the tunnel junctions implies that the probability of more than one molecule bridging the gap is very small. Although the size of the gap is on the order of $10\mathring{A}$, and the C_{60} molecules are roughly $7\mathring{A}$ in diameter, multiple molecules could be present in

the gap since the lateral size of the electrodes is on the order of 100nm. Figure 1.2 shows typical sizes associated with the C_{60} transistor.

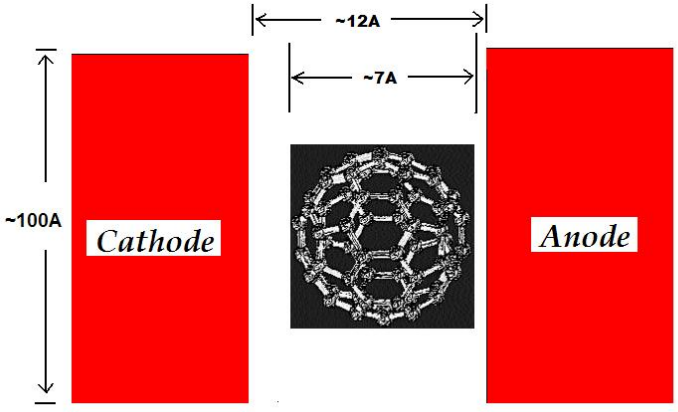

Figure 1.2: Typical size of the components of a C_{60} single molecule transistor (not to scale).

1.1.2 I-V Data

An example of data showing the current-voltage behaviour for a C_{60} transistor is shown in Figure 1.3. The independent axis of the data maps the source-drain (bias) voltage, V_{SD}, in millivolts, which is the voltage applied across the electrodes, and the dependent axis maps the current in nanoamperes. The different curves represent different gate voltages, V_G. The curves for which the bias voltage is positive will be referred to as "forward bias" and the negative bias curves as "reverse bias". Positive bias takes electrons from the left electrode to the right electrode, or from the source-cathode to the drain-anode.

The data exhibits several notable features, for instance the current is initially strongly suppressed, and then progresses in a step like pattern. The width of the region of zero conductance ("conductance gap") was found to be a reversible function

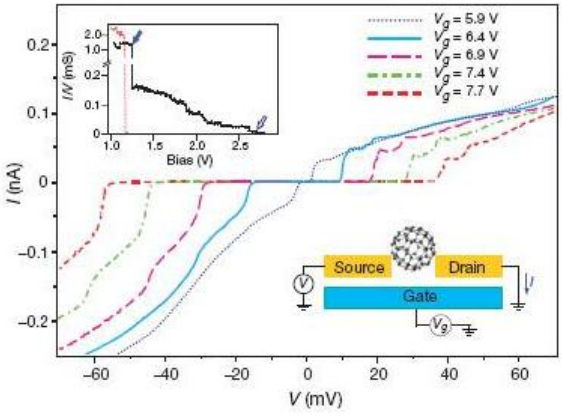

Figure 1.3: Sample data showing current-voltage curves for a single C_{60} transistor at 1.5K [Par00]. The upper inset plots the current through the connected electrodes while a large bias is applied. The five curves are for different gate voltages. The dependent axis plots the source-drain current while the independent axis plots the source drain voltage (V_{SD}). The drain is the cathode when $V_{SD} > 0$. When C_{60} is closer to the drain, it is described as on the left side of the junction.

of the gate voltage (V_g). Although the conductance gap can be reduced to zero, the gate voltage at which this occurs is device dependent.

Conductance Gap

Tuning the gate voltage adjusts the molecular level that is available for electron transport, which in turn affects the size of the conductance gap. For the case of the system at hand, this level is the lowest unoccupied molecular orbital (LUMO) for C_{60}. The position of the LUMO is fixed by V_g prior to the application of V_{sd}. Once V_{sd} is turned on, the size of the conductance gap varies depending on the voltage that must be applied to align the LUMO with the fermi level of one of the electrodes (depending on the direction of current flow and the charge of the molecule). In other words, the conductance gap is a reflection of the energy that is required to add an electron to the C_{60} molecule (or to remove one from it). The maximum conductance gap that was observed by the experimenters exceeded $270mV$, indicating that the

charging energy of C_{60} in this geometry can be greater than $270meV$. At the value of V_g where the conductance gap vanishes, the LUMO level is aligned with the Fermi level of the electrodes, and there are two different charge states of C_{60} where the energy of the system is identical. The gate voltage where this occurs is defined as V_c. The alignment of the levels is shown Figure 1.4.

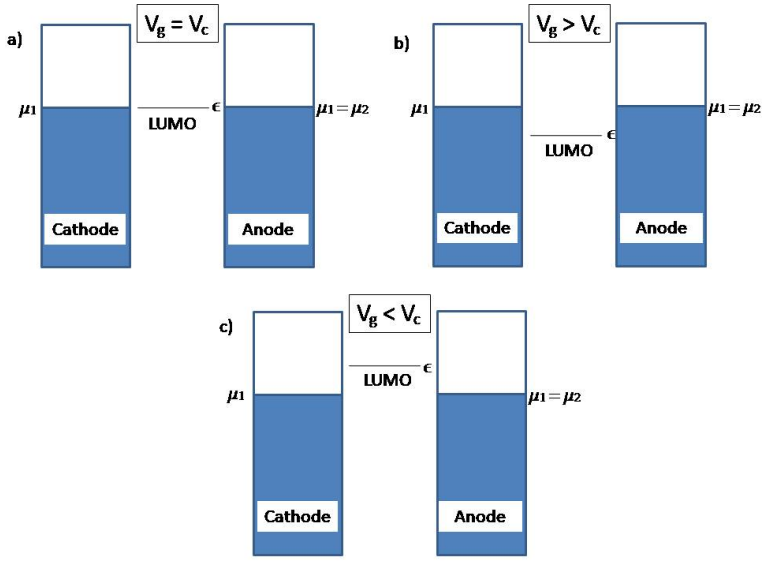

Figure 1.4: Illustration of various gate voltages. a) $V_g = V_c$: The LUMO (ϵ)is aligned with the fermi levels of the electrodes (μ_1 and μ_2), and the two charge states C_{60}^{1-} and C_{60} are equally likely. b) $V_g > V_c$: The molecule is charged prior to the application of a bias voltage, meaning that the equilibrium charge state is C_{60}^{1-}. c) $V_g < V_c$: The molecule is neutral prior to the application of a bias voltage, meaning that the equilibrium charge state is C_{60}.

If V_g is greater than V_c then the molecule is initially charged, while if V_g is less than V_c the molecule is initially neutral. Both of these cases are illustrated in Figure 1.4. This also implies that the C_{60} molecule is charged prior to the application of a bias voltage in the case of the data that is shown in Figure 1.3, because increasing the gate voltage from $5.9V$ to $7.7V$ monotonically increases the source drain gap. Inspection of the data shows that the conductance gap would vanish for some value of V_g that is less than $5.9V$. The fact that C_{60} is initially charged will be confirmed

using an alternate method in this thesis.

Equilibrium Charge State

The equilibrium charge state for C_{60} is defined as its charge state prior to the application of a bias voltage, and it is dependent on the gate voltage. For C_{60} between gold electrodes, the equilibrium charge state is believed to be neutral or singly negatively charged [Par00]. Because the current flows with the addition or subtraction of a single electron from the molecule, the two charge states that occur when the bias voltage is applied can either be C_{60}^{0} and C_{60}^{1-} or C_{60}^{1-} and C_{60}^{2-}. It can be easily estimated that the latter two charge states are separated by a much larger energy gap than the other two charge states. This, we will argue below, makes it more likely that the two participating charge states are C_{60}^{0} and C_{60}^{1-}.

To estimate the charging energies, consider the molecule to be the inner sphere of a spherical capacitor. If the the outer sphere is taken to be infinitely large and the inner sphere has a radius R, then the potential between the concentric spheres with a charge of $-Q$ on the outer sphere and $+Q$ on the inner one is

$$V = -\int_{\infty}^{R} \frac{kQ}{r^2} dr = \frac{kQ}{R}, \tag{1.1}$$

where the Coulomb force constant k is defined as $\frac{1}{4\pi\epsilon_0}$. The capacitance is therefore

$$C = \frac{Q}{V} = \frac{R}{k}. \tag{1.2}$$

Using $R \approx 7\mathring{A}$ for the radius of C_{60} [DDE96], and estimating the dielectric constant for free space, $k \approx 9\text{x}10^{9}\frac{Nm^2}{C^2}$, an approximate value for the capacitance is $C \approx 8\text{x}10^{-20}F$. To charge the capacitor to a final amount Q, the work required is

$$W = \frac{1}{2}\frac{\mathrm{Q}^2}{C} \tag{1.3}$$

Using $Q = 1.6\text{x}10^{-19}C$ for the charge of an electron, an estimate of the difference in energy between the neutral and singly ionized states, C_{60}^{0} and C_{60}^{1-}, is about $2eV$.

Since the energy is proportional to Q^2, the difference in energy between the singly and double ionized states, C_{60}^{1-} and C_{60}^{2-}, is $2eV(2^2 - 1^2) = 6eV$.

These energies are to be compared with the work function of gold, $\Phi = 5.1eV$. To align the fermi energy of gold with the energy of the C_{60}^{1-} ion, we require that

$$-\Phi \approx W - eV_{\text{gate}}. \tag{1.4}$$

This implies that

$$eV_{\text{gate}} \approx 7eV; \qquad \text{for } C_{60}^{1-} \tag{1.5}$$

$$eV_{\text{gate}} \approx 11eV; \qquad \text{for } C_{60}^{2-}. \tag{1.6}$$

The range of gate voltages in Figure 1.3 is 5.9-7.7V. This implies that the C_{60}^{2-} is beyond the range of the applied experimental gate voltages.

Vibrational Coupling

Another feature of the data in Figure 1.3 is the step progression of the current, in equal increments of voltage. Each step occurs when a new quantized excitation becomes energetically accessible to a tunnelling electron. For all devices studied by Park et al. the excitation energy was approximately 5meV, and it is observed on both sides of V_c indicating that it is an excitation of both C_{60} and C_{60}^{1-}. The excitation energy has been attributed to vibrational quanta of the centre of mass oscillation of the C_{60}^{0} molecule within the potential that confines it to the gold surface, as illustrated schematically in Figure 1.5.

Based on previous experimental and theoretical studies [DDE96, CJA93] of C_{60} on gold, the van der Waals interaction between C_{60} and the electrodes can be approximated by a Lennard-Jones potential [RH93]. If the equilibrium coupling is estimated with a harmonic potential, then the vibrational quanta of $5meV$ corresponds to a

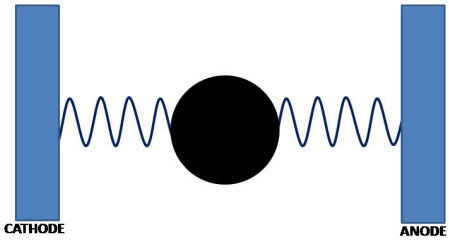

Figure 1.5: Centre of mass oscillation of C_{60} between the gold electrodes.

vibrational frequency of approximately 1.2 THz. This is in agreement with estimates from theoretical studies [DDE96, CJA93]. Theoretical estimates assume a one-sided coupling, however if the coupling between C_{60} and the two electrodes is taken to be very asymmetrical, then the calculation is not significantly affected. In its charged state C_{60} is further attracted to its image charge in the metal electrode. To first order, this should shorten the bond distance by a small amount. The modification of the vibrational frequency should be a second order effect.

The steps in the current can be explained by coupling the electron motion with the vibrational modes of the molecule [SR93]. As can be seen from Figure 1.6, the vibrational modes become available in integer increments as the bias voltage is applied.

For tunnelling in the forward bias direction, the single participating state spreads into a manifold of vibrational levels, a "comb". Tunnelling onto the molecule is facilitated when a tooth of the absorption comb overlaps the fermi sea of the cathode. Tunnelling off of the molecule is facilitated when a tooth of the emission comb no longer overlaps the fermi sea of the anode. This will be discussed in detail in Chapters 6 and 7.

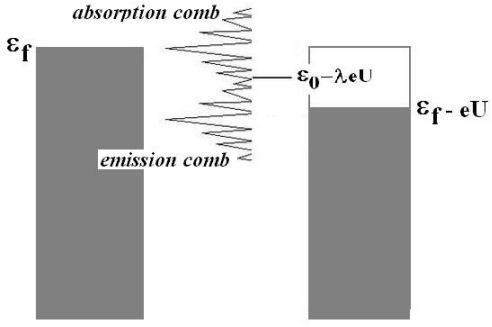

Figure 1.6: Coupling of electron tunnelling with the centre of mass oscillation of the C_{60} molecule.

1.2 Model System

In this thesis we will model the current voltage response for the C_{60} molecular transistor using a one-dimensional tight binding model [BF03, BF04, LYG97, BS01]. Tunnelling rates that incorporate the vibrational coupling will be derived in order to produce current-voltage curves that are in very good agreement with published data.

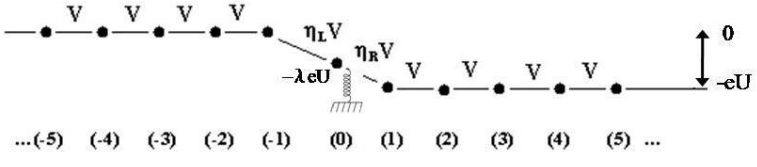

Figure 1.7: Illustration of the model system for the C_{60} molecular transistor.

An illustration of the model system is shown in Figure 1.7. The figure shows two one-sided chains of sites strongly coupled by an interaction matrix element $V \sim 1eV$ [Bev86], which represent the gold electrodes. The bandwidth of $4V$ is to be

associated with the conduction bandwidth of gold [Bev86]. The central defect site is the LUMO level of the C_{60} molecule, and is weakly coupled to the remainder of the chain via a matrix element that is reduced by a dimensionless coupling parameter $\eta \ll 1$. The coupling to the left and right of the molecular site is labelled differently in order to allow for variation in the position of the molecule within the junction. The source drain voltage is incorporated by changing the site energies of the electrodes and the molecule. The parameter λ is used to divide the source-drain voltage between the gaps to the left and right of the molecule. If the total distance across the junction is defined as l, the distance of the molecule from the cathode as d_1, the distance of the molecule from the anode as d_2, and the radius of the molecule is defined as R, then

$$l = (d_1 + \mathrm{R}) + (d_2 + \mathrm{R}), \tag{1.7}$$

and taking C_{60} as an equipotential surface, an estimate of the voltage drop at the position of the molecule is λU, where $\lambda = \frac{d_1 + \mathrm{R}}{l}$.

This work follows the typical methods of scanning tunnelling microscopy (STM) literature, with the exception of work by Kenrke, Biscarini, and Bustamante [VMK92, VMK95, FB95, BK99] that involves an analysis of STM images, where certain I-V characteristics are investigated through the calculation of propagators. Their system has a discrete number of channels for electron transport, in contrast to the sequential single electron tunnelling of the C_{60} system, and consequently their model incorporates interference effects which arise from coherent transport through multiple pathways. Because there is no evidence for these interference effects in our problem, we follow the simpler incoherent (hopping) analysis.

While this calculation is a standard approach for studying transport through single molecules [CJ00, EK02, EK03, NR03, XR03, MAM04, KvO05, BF03], and coulomb blockade systems [Naz89, MHD90, SMG90, IG91], our approach reveals

some new insight into the system which we feel is worthwhile to demonstrate. Nevertheless, our primary findings are not dependent on our method, and are as follows:

1. The saturation values for forward and reverse bias current are expected to differ by a factor of six. Measured data suggests that this value is closer to three [HP00], and the standard technique of considering only the spin asymmetry predicts a factor of two [BF03, MAM04], which suggest that the asymmetry is not completely understood.

2. The equilibrium charge of a C_{60} molecule placed in a nanometre sized gap between gold is estimated to be negative.

3. The effect that tuning the gate voltage has on the size of the voltage gap between the Fermi level of the electrodes and the tunnelling level on the molecule can be determined using only the relative sizes of the forward and reverse bias voltage gaps.

1.2.1 Outline

The properties of the C_{60} molecule that pertain to the model are discussed in Chapter 2. A rate equation for the current is derived in Chapter 3. This is used to predict the equilibrium charge state of the molecule in Chapter 4. A mathematical description of the Green function technique that will be used to find expressions for the rates is detailed in Chapter 5. This technique is applied to the physical system at hand in Chapter 6, where detailed expressions for the tunnelling rates onto and off of the molecule are derived. Chapter 7 is the concluding chapter, where the results are discussed, and compared with experimental findings.

Chapter 2

Properties of the C_{60} Molecule

2.1 Discovery and Relevance

A broad spectrum of physical science research has recently involved fullerene molecules, especially the closed cage, nearly spherical C_{60} molecule, which was designated the "1991 Molecule of the Year" on the cover of Science magazine [Jr.91]. The Nobel prize for Chemistry in 1996 was awarded to Robert F. Curl Jr., Sir Harold W. Kroto and Richard E. Smalley for their experimental verification of the existence of fullerenes in 1985. The name was chosen by Kroto and Smalley because of the resemblance of C_{60} molecules to geodesic domes that were first built in the United States by the architect R. Buckminster Fuller. Figure 2.1 shows a famous North American geodesic dome, the Montréal Biosphère, formerly the U.S. Pavillion from Expo '67, that is situated on Île Sainte-Hélène in Montréal, Canada and was designed by Fuller. This is also the origin of the common reference to C_{60} molecules as "buckminsterfullerenes" or "buckyballs". The word fullerene is now used to refer to the entire class of closed cage molecules consisting of only carbon atoms.

Fullerenes are the most recently discovered class of carbon allotropes. An al-

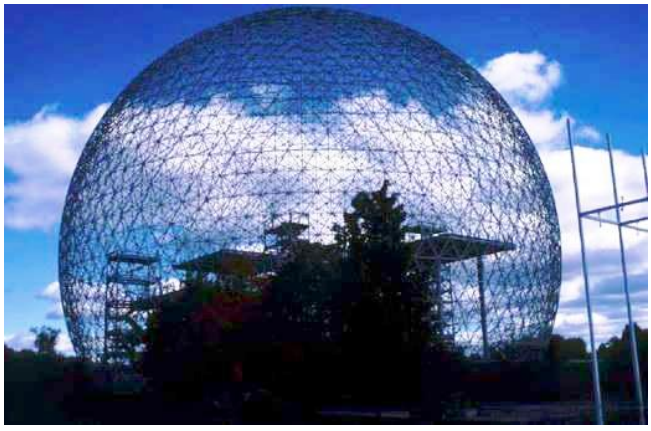

Figure 2.1: The Montréal Biosphère [Bri].

lotrope is a unique molecular configuration made of pure carbon. Examples of familiar carbon allotropes are diamond and graphite. Fullerenes are made of pentagonal and hexagonal rings of carbon. While their geometry is very similar to that of graphite, which exists in the form of a sheet of linked hexagonal carbon rings, the presence of pentagonal rings in fullerene structures results in their deviation from planar configurations. The combination of pentagonal and hexagonal rings in fullerenes allows them to exist structurally in the form of hollow spheres, ellipsoids, or tubes. The cylindrically shaped fullerenes can be thought of as a rolled up sheet of hexagonal rings capped at either end by a C_{60} hemisphere and are better known as carbon nanotubes or buckytubes.

The most extensively studied fullerene is the C_{60} molecule. Isolated C_{60} exists in the form of a slightly irregular truncated (cut off) icosahedron, which is a polyhedron with thirty-two plane faces, and is the highest possible molecular point group symmetry. The shape is more easily recognized as that used in the construction of soccer balls. Knowledge of the geometrical form of C_{60} predates the discovery of the molecule by several centuries, as evidenced by a rendition of a regular truncated icosahedron by Leonardo da Vinci in about the year 1500. This may give some insight into how the Italians accomplished their recent World Cup victory. Icosahedral

molecules were also theorized to exist several decades before their experimental discovery. Tisza (1933) [Tis33] considered the point group symmetry for icosahedral molecules, and Osawa (1970) [Osa70] suggested that an icosahedral C_{60} molecule might be chemically stable, however their work was not appreciated until the experimental stability of the C_{60} molecule in the gas phase was established by Kroto, Smalley, Curl and their collaborators in the 1980s [KHOS85].

2.2 Geometrical Form

A fullerene may be defined as a closed cage molecule that consists only of carbon molecules, and contains only hexagonal and pentagonal faces. Figures 2.2 and 2.3 illustrate the geometrical shape of the C_{60} fullerene molecule.

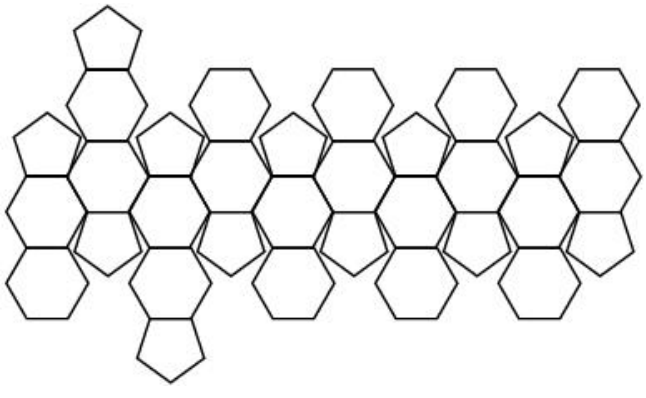

Figure 2.2: The pentagon/hexagon pattern in buckyballs is clear in an unfolded image of the structure. Figure taken from Reference [Mat].

Using Euler's theorem for polyhedra, it can be shown that all fullerenes are made up of exactly twelve pentagonal faces and an arbitrary number of hexagonal faces. Euler's theorem for polyhedra states that the number of faces added to the number of vertices in a polyhedron is equal to two greater than the number of edges,

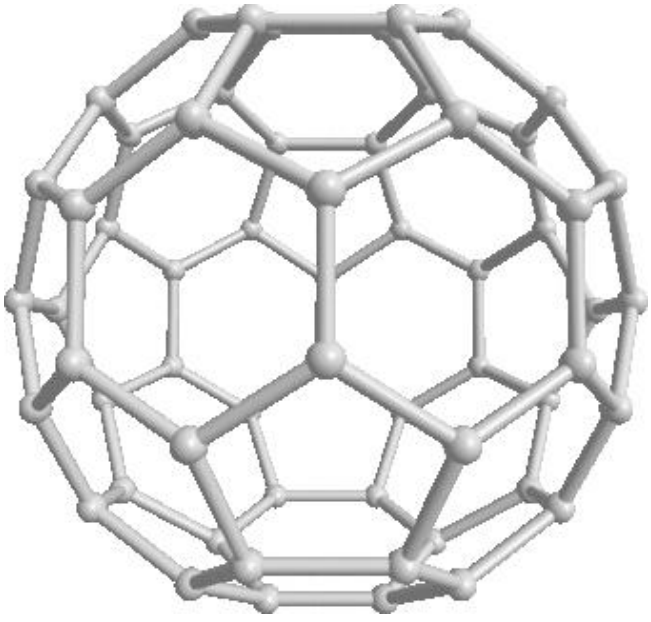

Figure 2.3: Example of a buckyball. Figure taken from Reference [DDE96].

$$f + v = e + 2. \tag{2.1}$$

The variables f, v, and e represent the numbers of faces, vertices, and edges of any polyhedron. For fullerenes, the faces are either hexagonal or pentagonal, so we can replace f with $h + p$. The number of edges is equal to $\frac{5p+6h}{2}$ since each edge touches two faces, and the number of vertices is equal to $\frac{5p+6h}{3}$ since each vertex touches three faces.

Rewriting the Euler equation with respect to these newly defined parameters gives

$$h + p + \frac{(5p + 6h)}{3} = \frac{(5p + 6h)}{2} + 2, \tag{2.2}$$

which leaves

$$p = 12. \tag{2.3}$$

Setting the number of vertices equal to sixty confirms that the number of hexagonal faces in the C_{60} molecule is twenty. By setting the number of vertices equal to twenty it can be seen that if C_{20} existed as a carbon cage molecule it would have twelve pentagonal faces and no hexagons. Inspection of the C_{60} molecular structure (Figure 2.2) shows that each pentagonal ring is surrounded by five hexagonal rings. This is energetically favourable because adjacent pentagons would lead to higher local curvature on the sphere, and therefore more strain. The tendency for pentagons to be separated by one or more hexagons is called the isolated pentagon rule [Kro87], and is the reason that C_{20} is not a naturally occurring fullerene. The smallest fullerene to satisfy the isolated pentagon rule is C_{60}. This is why fullerenes with fewer than sixty carbon atoms are less likely to be found in nature, and in fact no fullerenes with fewer than sixty carbon atoms are found in the soot that is commonly used to extract fullerenes.

The sixty carbon atoms in C_{60} are located at the vertices of the icosahedron, and as shown in Figures 2.2 and 2.3, each site is identical. Of the three C-C bonds that originate from each Carbon atom in the molecule, there are two distinct types of bonds. One forms an edge between neighbouring hexagons, while the other forms the edge between a hexagon and a pentagon. The average nearest-neighbour C-C distance, $a_{C-C} = 1.44$Å [JBY92], is found using these two bond lengths. The hexagon-pentagon bond is a single bond ($a_5 = 1.46$Å) [JBY92], while the hexagon-hexagon bond is a double bond ($a_6 = 1.40$Å) [JBY92]. The bond lengths can be measured using nuclear magnetic resonance (NMR) techniques or neutron diffraction. The two methods yield slightly different lengths; the values quoted in this section are derived from NMR. Because a regular truncated icosahedron has ninety edges of equal length, the slight difference in bond lengths is the reason that C_{60} is technically an irregular truncated icosahedron. Since its deviation from a regular polyhedron is so slight, C_{60} is often called a regular truncated icosahedron in the literature.

Using the icosahedral geometry, the average nearest-neighbour distances between

pentagonal faces can be used to calculate the size of the C_{60} molecule. Using the values given above, and treating the carbon atoms as points, the diameter can be shown to be 7.09Å [JBY92]. NMR measurements give a diameter of 7.10 ± 0.07Å [JBY92].

2.3 Physical Properties

It is largely due to their unique physical properties that the C_{60} molecule and related fullerenes have been studied extensively in recent years. The notable properties of C_{60} include its relatively high temperature superconductivity with $T_C = 33K$, and the approximate one-dimensional electrical behaviour of fullerene-related nanotubules [Heb93]. Because of these and other traits, the discovery of C_{60} has proven very useful to a variety of scientists. For chemists their existence presents an entirely new family of fullerene based compounds for study, for earth scientists it facilitates the investigation of shungite, a very old, carbon-rich mineral deposit that contains fullerenes, and for materials scientists fullerenes allow the assembly of monodisperse (polymers with one molecular mass) nanostructures of various forms including films and crystals. There are also several potential applications for engineers, such as their usefulness in optical limiting and switching devices, and in photoconductor applications for photoresist applications. They also have been used in the construction of single electron transistors, which is our interest in this thesis.

Table 2.1 lists some basic physical constants for the C_{60} molecule. The electron affinity of a molecule or atom is the energy required to detach an electron from a singly charged negative ion. It can also be defined as the energy that is released when an electron is attached to a neutral molecule or atom. The ionization potential of a molecule or atom is the energy required to remove an electron from the isolated molecule or atom. The n^{th} ionization potential is the energy required to remove the n^{th} electron after $n-1$ electrons have been removed. The ionization potential can

Table 2.1: Physical Constants for the Isolated C_{60} Molecule [DDE96, Heb93]

QUANTITY	VALUE
Average C-C distance	1.44 Å
C-C bond length on a pentagon	1.46 Å
C-C bond length on a hexagon	1.40 Å
C_{60} mean ball diameter	7.10 Å
C_{60} ball outer diameter	10.34 Å
Moment of inertia I	1.0 x 10^{-43} kg m^2
Volume per C_{60}	1.87 x $10^{-22}/cm^3$
Number of distinct C sites	1
Number of distinct C-C bonds	2
Binding energy per atom	7.40 eV
Electron affinity	2.65±0.05 eV
First ionization potential	7.58 eV
Second ionization potential	11.5 eV
HOMO-LUMO band gap for solid C_{60}	1.6±0.2 eV
HOMO-LUMO energy gap for isolated C_{60}	4.9 eV
Phonon mean free path	50 Å

be thought of as a measure of the strength by which electrons are bound; the greater the ionization potential, the harder it is to remove an electron.

For electronic applications the difference in energy between the highest occupied molecular orbital (HOMO) and the lowest unoccupied molecular orbital (LUMO) plays a key role. An experimental measure of the HOMO-LUMO gap for isolated C_{60} molecules can be calculated from the difference between the first ionization potential and the electron affinity. The values for I_P and E_A that are listed in Table 2.1 are determined from photo-electron spectroscopy of gas phase samples, and give an estimate of

$$I_P - E_A \approx 7.58eV - 2.65eV \approx 4.93eV \tag{2.4}$$

for the HOMO-LUMO gap of isolated C_{60} molecules. In solutions and in the solid state the size of the gap diminishes because of electron screening associated with

neighbouring molecules, and it has an experimentally determined value of 1.6 ± 0.2 eV for solid C_{60} [Heb93].

2.4 Electronic Structure of Isolated C_{60}

The electronic structure of C_{60} is influenced by the slight non-uniformity in its bonds, in particular by the presence of single bonds along the edges of the pentagonal rings and a double bond between the hexagonal rings. For the purpose of this study detailed calculations of electronic levels are not necessary, and so only the basic aspects of the electronic structure will be described. A simple approach is to imagine constructing the C_{60} molecule from isolated carbon atoms. Specifically, a single carbon atom has two localized (1s) core electrons and 4 valence electrons in the sp^3 hybrid orbital. If sixty isolated carbon atoms collapse to form a sphere that is bonded with sp^2 hybridized orbitals, then three of the four valence electrons from each atom will form a σ bonding network (three sp^2 hybridized orbitals) leaving sixty p orbitals from the remaining valence electrons. Therefore, there is a single p_z orbital centered on each of the atoms comprising the fullerene molecule. Using a Hückel molecular orbital (HMO) approximation, the σ bonding network is treated separately from the π bond formation that results from the sixty valence electrons. Figure 2.4 illustrates the HMO representation for the molecular orbital diagram. There are sixty molecular orbitals since we began with sixty p_z orbitals. The HOMO-LUMO gap between the thirty highest occupied orbitals and the thirty lowest unoccupied orbitals can be shown to be very large in this approximation. This approximation neglects the spherical shape of the fullerene, since the local curvature at each carbon site means that the hybridization is not purely sp^2 as it would be for a planar configuration such as graphite. The effect of the curvature is a mixing of the carbon 2s orbital with the π orbitals, and results in an enhanced electron affinity for C_{60} that is measured to be 2.65eV [VEH04].

LUMO Filling for C_{60}

The distribution of the sixty π electrons in C_{60} can be determined to first approximation using Hückel calculations, resulting in the level structure shown in Figure 2.4.

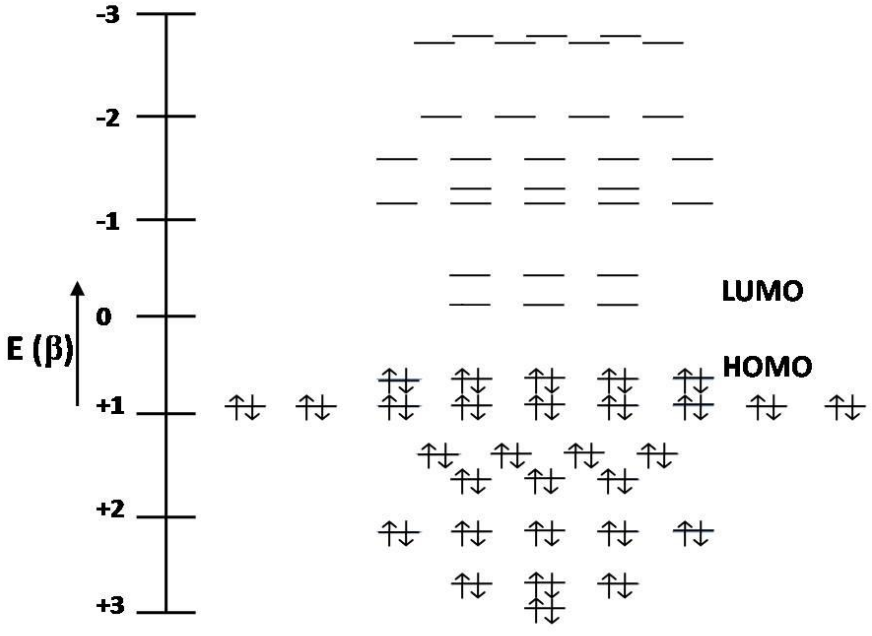

Figure 2.4: Electronic Structure Diagram for the 60 π electrons in isolated C_{60} based on a Hückel energy calculation.

The five valence (HOMO) levels of C_{60} can hold ten electrons, and the three conducting (LUMO) levels can hold six electrons. The formation of the anions of C_{60} is not entirely straightforward due to the non-linear structure of the molecule. The C_{60}^{1-}, C_{60}^{2-}, and C_{60}^{3-} anions are formed according to Hund's rules [Cha88] and the Pauli Exclusion Principle. The levels are filled so that the total angular momentum is maximized, which minimizes the electron-electron repulsion, and no two electrons of identical spin can occupy the same level. This means that the first three electrons are added so that the orbitals are singly occupied by particles of the same spin.

Based on these rules, there are six ways to form C_{60}^{1-}, six ways to form C_{60}^{2-} and two ways to form the C_{60}^{3-} anion. If the position of the first electron is taken into account, then there are only two positions for the second electron. Taking the positions of the first two electrons into account, there is only one position for the third electron. An example of one way to form the first three anions is shown in Figure 2.5.

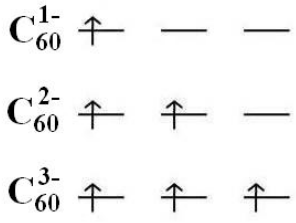

Figure 2.5: Filling of degenerate molecular orbitals according to Hund's rule and the Pauli exclusion principal.

The formation of higher order anions of C_{60} is more complicated because the electronic configuration that is the lowest in energy for C_{60}^{4-} occurs with a physical distortion of the molecule. The distortion is a result of the Jahn-Teller (JT) effect, which occurs when there is a degeneracy present. The JT effect breaks the degeneracy so that the overall energy of the distorted C_{60}^{4-} anion is lower then that of undistorted C_{60}^{4-}. The physical result of this distortion is that the molecule is stretched from a sphere to an ellipsoid, which allows a greater physical separation of the excess electrons, as shown in Figure 2.6. The result of the distortion is that the degeneracy of the three LUMO levels is broken. The LUMO level splitting for the higher anions of C_{60} is illustrated in Figure 2.7.

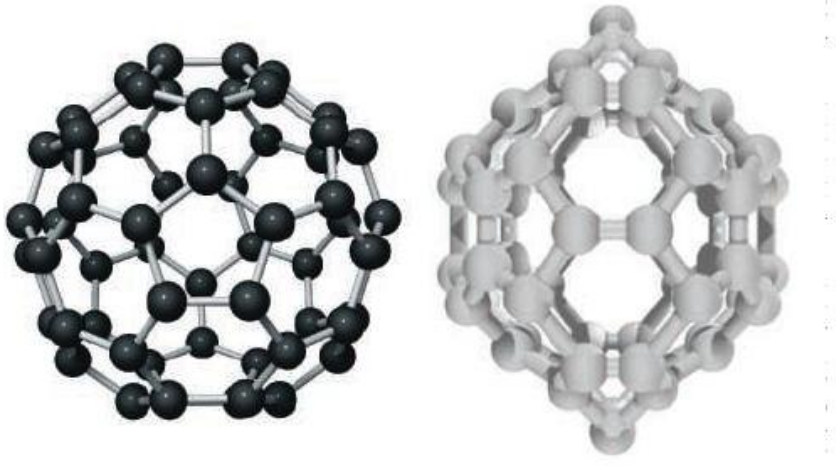

Figure 2.6: Jahn-Teller distortion of the C_{60}^{4-} anion. Figure taken from Reference [O'S05].

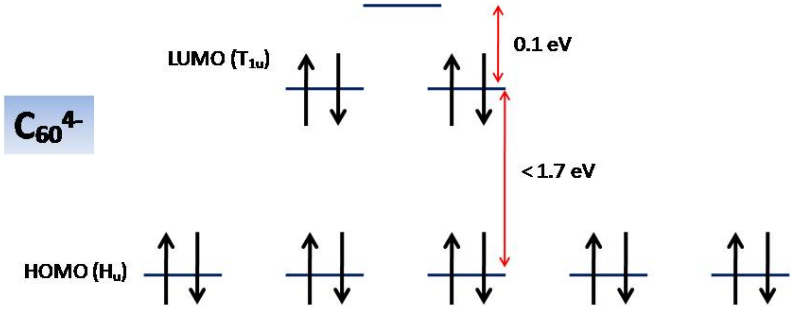

Figure 2.7: HOMO-LUMO band-gap for JT distorted C_{60}^{4-}. Figure taken from Reference [O'S05].

Enumerating the ways to create the anions of C_{60} will be relevant in the following

chapter, where a tunnelling expression for the current is derived for a single molecule C_{60} transistor.

Summary:

The five "valence" HOMO levels for the C_{60} molecule are completely filled. The three "conduction" LUMO levels can hold three electrons; more than three cause JT distortion.

Chapter 3

Master Equation and Current

3.1 Introduction

Based on electrochemical and photoelectron spectroscopic studies of C_{60} on gold, the equilibrium charge state of the C_{60} molecule when in the molecular transistor configuration is assumed to be either neutral, C_{60}^{0}, or singly ionized, C_{60}^{1-} [DDE96], where the term "equilibrium charge state" refers to the net charge on the molecule in the absence of an applied source-drain voltage, and within the range of experimental gate voltages. The position of the C_{60} molecule in the junction is also not expected to be symmetric with respect to its distance from either wire [HP00]. These details are relevant because it will be shown that the predicted current-voltage behaviour of the transistor is different for each charge state when it is assumed that the molecule has an asymmetrical position in the junction.

Here we will discuss the I-V relation on the level of a master equation [MA60]. A detailed derivation of the rates that will go into this expression will follow in the subsequent chapter, while this section focuses on finding an expression for the current. The expression will be shown to depend on the number of degenerate orbitals that

are available to a tunnelling electron. In particular, it is important to consider the number of degenerate LUMO's for C_{60}, which is shown to be three in Figure 2.4 in Chapter 1.

In experimental realizations of molecular transistors the electrodes are usually weakly coupled to the molecule [NR03], so it is common to approach electron tunnelling onto a molecular orbital that is coupled to phonon modes with a model based on rate equations [BF03, BF04, ET05]. Because the transport across the molecular junction is slow, an electron 'hopping' model is appropriate. The relevant components of the transistor are a single C_{60} molecule sandwiched between two thin gold electrodes. The system is modeled as a one dimensional, tight binding lattice with a central defect site. The defect site represents the molecule, and the sites to its left and right represent the electrodes. An expression for the current is formulated in the weak coupling limit, where the electron tunnels incoherently from cathode to molecule to anode and vice versa. In the weak coupling regime, it is assumed that the tunnelling time is the largest time scale in the system, or more specifically that the tunnelling takes longer than the time for vibrational relaxation, so that the vibrational relaxation occurs between successive tunnel events [BF03]. It is also assumed that the fermi seas in the two electrodes remain in equilibrium at all times. In the following section, an expression for the current based on the electron hopping rates in this regime will be formulated.

The single molecule transistors are comprised of gold electrodes sandwiching isolated C_{60} molecules, built on top of an insulating layer of SiO_2 that rests on a degenerately doped silicon wafer. The silicon layer acts as the gate electrode and modulates the electrostatic potential of the C_{60} molecule. It can therefore tune the alignment of the LUMO with the fermi level of the gold electrodes. By deriving the tunnelling current in two ways it will be demonstrated that treating each electron tunnelling event as a transition between two molecular states is simpler than explicitly considering transitions between charged and uncharged molecular states,

and it also naturally accounts for the rules for filling an arbitrary number of valence molecular orbitals.

3.2 Formalism

3.2.1 Degenerate Molecular Orbitals

A current that is based on tunnelling rates is dependent on the number of molecular orbitals that are energetically available to a tunnelling electron. For the C_{60} single electron transistor, the three degenerate LUMO levels participate in the tunnelling process that is comprised of two events. One event occurs from either electrode onto the molecule, and the other event is from the molecule onto either electrode. It is conceivable that tunnelling onto certain levels may contribute more strongly to the current than tunnelling onto others. For example, one might expect that an orbital that is perpendicular the cathode anode pathway should not contribute at all to the current. Thus it appears that simply augmenting the tunnelling rates by the numer of available degenerate orbitals is insufficient, and that other considerations such as spatial orientation are also important. We show that this is not true.

A tight binding "toy" system will be used to explore this process, and it will be shown that all of the levels contribute equally to the current. This is because their energy degeneracy allows the eigenstates of the tight binding system to be expressed in a basis where they all contribute equally to the tunnelling process, regardless of their orientation.

Consider a "toy" model for the molecule consisting of a tightly bound three site ring, with sites $n_i = 1, 2, 3$ that are strongly coupled by a matrix element J as shown in Figure 3.1.

If the site energies are set to zero, then the Hamiltonian for the system can be

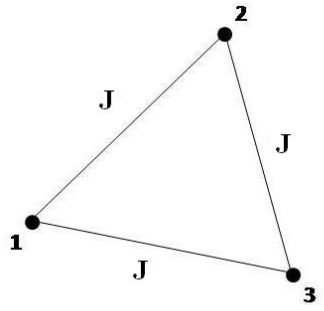

Figure 3.1: Three site chain as a toy model of the C_{60} molecule, with periodic boundary conditions.

written as

$$\begin{aligned} H &= J\left(|1><2| + |2><3| + |3><1|\right. \\ &\quad \left. + \left(|2><1| + |3><2| + |1><3|\right)\right., \end{aligned} \tag{3.1}$$

or equivalently, in matrix form as

$$H = \begin{pmatrix} 0 & J & J \\ J & 0 & J \\ J & J & 0 \end{pmatrix}. \tag{3.2}$$

The energy eigenvalues for the system are $\{2J, -J, -J\}$. The normalized eigenfunction corresponding to the nondegenerate eigenvalue $(2J)$ is:

$$|k_0> = \frac{1}{\sqrt{3}}(|1> + |2> + |3>). \tag{3.3}$$

The degenerate eigenspace can be spanned with the following eigenvectors

$$|k_+> = \frac{1}{\sqrt{3}}(e^{\frac{2\pi i}{3}}|1> + e^{\frac{-2\pi i}{3}}|2> + |3>) \tag{3.4}$$

$$|k_-> = \frac{1}{\sqrt{3}}(e^{\frac{-2\pi i}{3}}|1> + e^{\frac{2\pi i}{3}}|2> + |3>), \tag{3.5}$$

but any linear combination of these two states would work equally well. The complete set of states $\{k_0, k_+, k_-\}$ can be used to describe any state of the system.

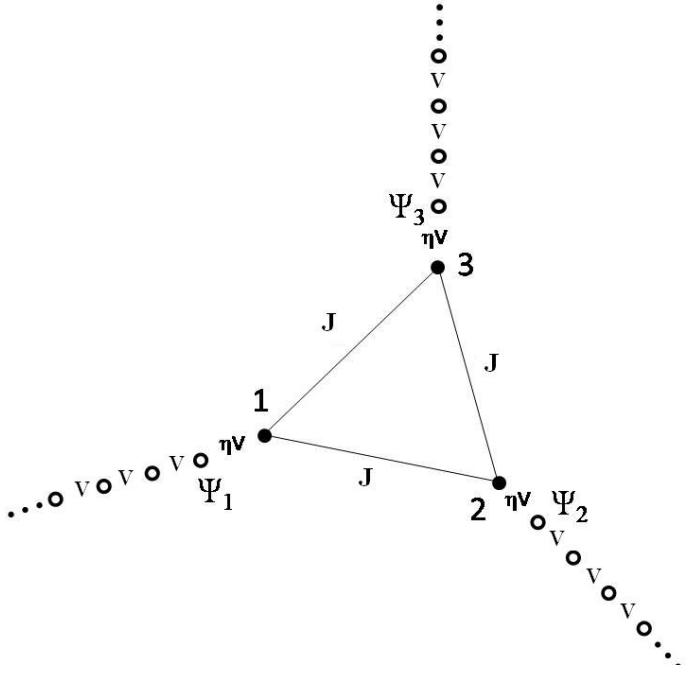

Figure 3.2: Model of the "toy" system that is used to explore the participation of the degenerate orbitals in the tunnelling rate. Each site of the three site ring is now coupled to an electrode, through which a tunnelling electron, $|q>$, can enter and exit the ring.

Figure 3.2 shows an augmented system, where each site is weakly connected to an electrode. This is a "toy" system, that will be used to illustrate the participation

of the degenerate orbitals in the tunnelling rates on and off of the ring. The labels $\{\Psi_i\}$ are introduced as labels for the sites nearest to the ring on the tight binding chains that comprise the electrodes. The sites $\{\Psi_i\}$ are weakly coupled to the ring via a reduced potential given by ηV. The strength of the coupling can be tuned with the parameter η, where $\eta \ll 1$ since the electrode-molecule coupling is assumed to be sufficiently small. The energy spectrum in the leads is assumed to overlap $|k_+>$ and $|k_->$, but $|k_0>$ is well above the fermi level and can be ignored.

The coupling of one of the leads with the system can be described by an interaction Hamiltonian,

$$H_1 = \eta V \left(|\Psi_i >< i| + |i >< \Psi_i| \right), \tag{3.6}$$

where $i = 1, 2$ or 3. For example tunnelling from the third electrode onto the ring would be described by

$$H_1 = \eta V \left(|\Psi_3 >< 3| + |3 >< \Psi_3| \right). \tag{3.7}$$

Fermi's Golden Rule

The transition rate from one state to another, Γ, can be found using Fermi's Golden Rule. This rate is often referred to as the decay rate, since it is related to the mean lifetime of the state τ by $\Gamma = 1/\tau$. Using Fermi's Golden Rule, the transition rate from an initial state i to a final state f can be written as [Sak94]:

$$R_{f \leftarrow i} = \frac{2\pi}{\hbar} | < f|H_1|i > |^2 \delta(E_i - E_f), \tag{3.8}$$

with a sum over a continuum of final states implied. The delta function enforces the condition that transitions only happen between states with equal energy $E_i = E_f$.

Tunnelling Rate

Writing the delta function, $\delta(E_i - E_f)$, as a Fourier transform, the transition rate for an electron to hop from an electrode onto the system can be written as,

$$\Gamma_{on} = \frac{1}{\hbar^2}\int_{-\infty}^{\infty} dt \sum_j < \Psi_i|e^{iH_0 t/\hbar}H_1 e^{-iH_0 t/\hbar}|k_j >< k_j|H_1|\Psi_i >, \tag{3.9}$$

where we have used the fact that

$$\left(\frac{1}{2\pi\hbar}\right)\int_{-\infty}^{\infty} dt e^{iE_a t/\hbar}e^{-iE_b t/\hbar} = \delta(E_a - E_b). \tag{3.10}$$

Let us evaluate the rate to tunnel from a Bloch state in the electrodes, $|q >$ with energy ε_q, to a state on the molecule. For example, to evaluate the rate for an electron to tunnel onto the system from the third electrode we set $i = 3$ in Equation 3.9. Using the complete set of eigenstates, $\{k_0, k_+, k_-\}$, we obtain

$$\Gamma_{on,q} = \left(\frac{2\pi}{\hbar}\right)\left(|< q|H_1|k_+ >|^2 + |< q|H_1|k_- >|^2\right)\delta(\varepsilon_q + V), \tag{3.11}$$

where the argument of the delta function arises from the energy, -V, of the states k_+, k_-. Writing

$$< q|H_1|k_+ >=< q|\Psi_3 >< \Psi_3|H_1|k_+ >=< q|\Psi_3 > \cdot \eta V \cdot \frac{1}{\sqrt{3}}, \tag{3.12}$$

the on rate can be written as,

$$\begin{aligned}\Gamma_{on,q} &= \left(\frac{2\pi}{\hbar}\right) |< q|\Psi_3 >|^2 \\ &\quad \times \left(|< \Psi_3|H_1|k_+ >|^2 + |< \Psi_3|H_1|k_- >|^2\right) \delta(\varepsilon_q + V) \\ &= \left(\frac{2\pi}{\hbar}\right) |< q|\Psi_3 >|^2 (\frac{1}{3} + \frac{1}{3})(\eta V)^2 \delta(\varepsilon_q + V) \\ &= \frac{4\pi}{3\hbar}(\eta V)^2 |< q|\Psi_3 >|^2 \delta(\varepsilon_q + V). \end{aligned} \tag{3.13}$$

The rate may be rewritten as

$$\Gamma_{on,q} = \frac{2}{3}\left[\frac{2\pi}{\hbar}(\eta V)^2 |< q|\Psi_3 >|^2 \delta(\varepsilon_q + V)\right], \tag{3.14}$$

which emphasizes the factor of $\frac{2}{3}$. The significance of this factor is that of the three molecular states, two of them are energetically available to a tunnelling particle.

Next consider the case of an electron tunnelling off of the ring, and onto electrode number three. Suppose that there is one electron on the molecule, and the temperature is low so that it is either in the $|k_+>$ or the $|k_->$ state. Since the energy of both of these states is -V, the rate to tunnel onto the electrode will be zero unless the fermi level is below -V.

The rate to tunnel off of the molecule will be

$$\Gamma_{off,q\leftarrow k_+} = \Gamma_{off,q\leftarrow k_-} = \frac{1}{3}\left[\frac{2\pi}{\hbar}(\eta V)^2 |< q|\Psi_3 >|^2 \delta(\varepsilon_q + V)\right]. \tag{3.15}$$

The prefactor in the case of tunnelling off of the molecule is $\frac{1}{3}$ because $|< k_+|3 >|^2 = \frac{1}{3}$. Assuming that thermal relaxation takes place between hops, the overall rate for one electron to tunnel off of the ring is the thermal average of the two rates,

$$\begin{aligned}\Gamma_{off,q} &= \frac{1}{2}\Gamma_{off,q\leftarrow k_+} + \frac{1}{2}\Gamma_{off,q\leftarrow k_-} \\ &= \frac{1}{3}\left[\frac{2\pi}{\hbar}(\eta V)^2|<q|\Psi_3>|^2\delta(\varepsilon_q + V)\right]. \end{aligned} \tag{3.16}$$

Notice that this is $\frac{1}{2}$ of the rate to tunnel on the ring. This is not surprising because the rate is proportional to the density of final states, and there are two final states for the on rate and only one for the off rate. Spin has been neglected for this discussion.

The choice of the eigenstates $|k_->$ and $|k_+>$ was arbitrary, and any linear combination of the two would also span the degenerate eigenspace of the ring system. An equivalent pair of eigenstates that can be used in place of the $|k_->$ and $|k_+>$ eigenstates are the following:

$$|+> = \frac{1}{\sqrt{2}}(k_+ + k_-) = \frac{1}{\sqrt{6}}(-|1> -|2> +2|3>) \tag{3.17}$$

$$|-> = \frac{1}{\sqrt{2}}(k_+ - k_-) = -i\sqrt{\frac{1}{2}}(|1> +|2>). \tag{3.18}$$

In contrast to the $|k_->$ and $|k_+>$ states, which both have identical spatial overlaps with the third electrode, now only the $|+>$ state overlaps the third electrode in this case. Thus the tunnelling rates onto the ring will show whether spatial orientation affects the tunnelling rates. Using the new eigenstates, the on rate is

$$\begin{aligned}
\Gamma_{on,q} &= \left(\frac{2\pi}{\hbar}\right) |<q|\Psi_3>|^2 \\
&\quad \times \left(|<\Psi_3|H_1|+>|^2 + |<\Psi_3|H_1|->|^2\right) \delta(\varepsilon_q + V) \\
&= \left(\frac{2\pi}{\hbar}\right) |<q|\Psi_3>|^2 (\frac{2}{\sqrt{6}})^2 (\eta V)^2 \delta(\varepsilon_q + V) \\
&= \frac{4\pi}{3\hbar}(\eta V)^2 |<q|\Psi_3>|^2 \delta(\varepsilon_q + V) \\
&= \frac{2}{3}\left[\frac{2\pi}{\hbar}(\eta V)^2 |<q|\Psi_3>|^2 \delta(\varepsilon_q + V)\right]. \qquad (3.19)
\end{aligned}$$

This is the same result that was obtained using the $|k_+>$ and $|k_->$ states. The rates for tunnelling off of the ring when the $|+>$ and $|->$ eigenstates are used are

$$\Gamma_{off,q\leftarrow+} = \frac{2}{3}\left[\frac{2\pi}{\hbar}(\eta V)^2 |<q|\Psi_3>|^2 \delta(\varepsilon_q + V)\right]; \qquad (3.20)$$

$$\Gamma_{off,q\leftarrow-} = 0. \qquad (3.21)$$

The thermal average of these rates gives an identical result to that which was obtained for the $|k_+>$ and $|k_->$ eigenstates,

$$\begin{aligned}
\Gamma_{off,q} &= \frac{1}{2}\Gamma_{off,q\leftarrow+} + \frac{1}{2}\Gamma_{off,q\leftarrow+} \\
&= \frac{1}{3}\left[\frac{2\pi}{\hbar}(\eta V)^2 |<q|\Psi_3>|^2 \delta(\varepsilon_q + V)\right]. \qquad (3.22)
\end{aligned}$$

This example is an illustration of a more general result that the tunnelling rate onto the ring system is independent of the number of orbitals that spatially overlap the tunnelling path, and it just scales with the number of energetically available

orbitals. This means that all three of the degenerate LUMO levels for C_{60} should be considered in the formation of a hopping rate expression for the current across the molecular transistor.

3.3 Tunnelling Rate Expressions

A rate expression for the current will be derived following the approach of Datta [Dat95], using a method that considers each of the six degenerate LUMO levels of C_{60} distinctly, and will be referred to as the molecular transition picture. This method is simpler than the usual approach taken in the literature [MAM04, BF03] when dealing with a system with multiply degenerate HOMO and/or LUMO levels, which is the case for the C_{60} transistor system. Before approaching the full three level LUMO system from the molecular transition point of view, its validity is proven by comparison with the conventional electron tunnelling picture. For simplicity, this will be done for the case of only one LUMO level.

3.3.1 Conventional Electron Tunnelling Picture

The primary concern when finding an expression for the current across the C_{60} transistor is the probability that the molecular site is occupied. This probability is a function of the tunnelling rates onto the molecule, Γ_{mc} and Γ_{ma}, and the tunnelling rates off of the molecule, Γ_{cm} and Γ_{am}. Here we have introduced a compact notation, Γ_{ab}, which means the rate for tunnelling from "b to a". The subscripts that will be used are molecule (m), cathode (c), and anode (a). Thus Γ_{mc} is the rate to tunnel from cathode to molecule, for example. The rates are illustrated in Figure 3.3.

The application of a forward biased voltage lowers the fermi level of the anode with respect to the cathode, which means that forward biased current is the result of

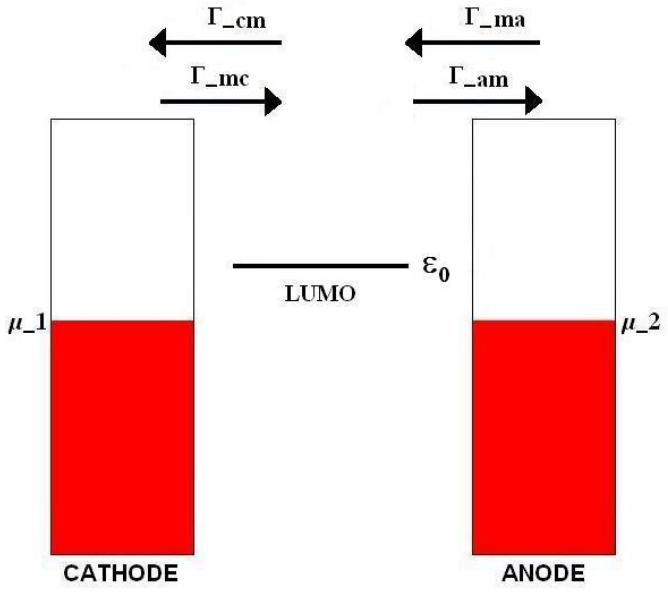

Figure 3.3: Illustration of the electron tunnelling picture. Γ_{ij} are the tunnelling rates, μ_1 and μ_2 are the fermi levels of the electrodes, and ε_0 is the energy of the LUMO level.

an electron tunnelling from the cathode to the anode. Reverse biased current is the result of an applied voltage that lowers the fermi level of the cathode with respect to the anode, and electrons tunnel from anode to cathode.

For the case of one LUMO level and an initially neutral molecule, there are two participating charge states for the C_{60} molecule, neutral and singly ionized. By limiting the molecule to single ionization, the Coulomb repulsion potential on the molecule is effectively set to infinity. Because the spin of the tunnelling electrons must be considered, there are three possible occupation states: unoccupied, and occupied by an electron of either spin up or spin down. The probability that the molecular site is occupied is defined as $P_m^{\uparrow}$ or $P_m^{\downarrow}$, where the subscript arrows indicate the spin of the tunnelling electron, and the probability that it is unoccupied as P_m^0. The equations describing the time evolution of these probabilities are

$$\frac{dP_m^{\uparrow}}{dt} = P_m^0\Gamma_{mc} + P_m^0\Gamma_{ma} - P_m^{\uparrow}\Gamma_{cm} - P_m^{\uparrow}\Gamma_{am} \tag{3.23}$$

$$\frac{dP_m^{\downarrow}}{dt} = P_m^0\Gamma_{mc} + P_m^0\Gamma_{ma} - P_m^{\downarrow}\Gamma_{cm} - P_m^{\downarrow}\Gamma_{am} \tag{3.24}$$

$$\frac{dP_m^0}{dt} = \left(P_m^{\uparrow} + P_m^{\downarrow}\right)\Gamma_{cm} + \left(P_m^{\uparrow} + P_m^{\downarrow}\right)\Gamma_{am} - 2P_m^0\Gamma_{mc} - 2P_m^0\Gamma_{ma}. \tag{3.25}$$

Using the additional constraint that the probabilities to sum to one,

$$P_m^{\uparrow} + P_m^{\downarrow} + P_m^0 = 1,$$

the steady state probabilities for the occupation of the molecular site can be determined:

$$P_m^{\uparrow} = P_m^{\downarrow} = \frac{\Gamma_{mc} + \Gamma_{ma}}{\Gamma_{cm} + \Gamma_{am} + 2(\Gamma_{mc} + \Gamma_{ma})} \tag{3.26}$$

$$P_m^0 = \frac{\Gamma_{cm} + \Gamma_{am}}{\Gamma_{cm} + \Gamma_{am} + 2(\Gamma_{mc} + \Gamma_{ma})}. \tag{3.27}$$

Current

The current can be found by considering the probability flux across either the cathode-molecule bond (left) or molecule-anode bond (right). Using the C-M bond, the current can be written in terms of the steady state solutions to the master equation and the tunnelling rates as follows,

$$
\begin{aligned}
I &= -e\{\begin{pmatrix} Probability \\ system\ is\ in \\ P_m^0\ state \end{pmatrix}\begin{pmatrix} Rate\ to \\ transition\ to \\ P_m^{\uparrow}\ from\ left \end{pmatrix} + \begin{pmatrix} Probability \\ system\ is\ in \\ P_m^0\ state \end{pmatrix}\begin{pmatrix} Rate\ to \\ transition\ to \\ P_m^{\downarrow}\ from\ left \end{pmatrix} \\
&\quad - \begin{pmatrix} Probability \\ system\ is\ in \\ P_m^{\uparrow}\ state \end{pmatrix}\begin{pmatrix} Rate\ to \\ transition\ to \\ P_m^0\ from\ left \end{pmatrix} - \begin{pmatrix} Probability \\ system\ is\ in \\ P_m^{\downarrow}\ state \end{pmatrix}\begin{pmatrix} Rate\ to \\ transition\ to \\ P_m^0\ from\ left \end{pmatrix}\} \\
&= -e\left(2P_m^0\Gamma_{mc} - P_m^{\uparrow}\Gamma_{cm} - P_m^{\downarrow}\Gamma_{cm}\right) \\
&= (-2e)\frac{\Gamma_{mc}\Gamma_{am} - \Gamma_{ma}\Gamma_{cm}}{\Gamma_{cm} + \Gamma_{am} + 2(\Gamma_{mc} + \Gamma_{ma})}. \qquad (3.28)
\end{aligned}
$$

As mentioned earlier, higher order corrections to the current such as spin flip transitions (i.e. $P_m^{\uparrow} \rightarrow P_m^{\downarrow}$) are neglected.

The expression for the current is the sum of a forward biased current and the reverse biased current,

$$I = I_{fb} + I_{rb}. \qquad (3.29)$$

The first term in the sum is the forward biased current, and contains the tunnelling events that are strongly favoured when an applied bias voltage lowers the fermi level of the anode with respect to the cathode,

$$I_{fb} = -2e\frac{\Gamma_{mc}\Gamma_{am}}{\Gamma_{cm} + \Gamma_{am} + 2(\Gamma_{mc} + \Gamma_{ma})}. \qquad (3.30)$$

The second term is the reverse bias current, and is strongly favoured when an applied voltage lowers the fermi energy of the cathode with respect to the anode,

$$I_{rb} = 2e\frac{\Gamma_{ma}\Gamma_{cm}}{\Gamma_{cm} + \Gamma_{am} + 2(\Gamma_{mc} + \Gamma_{ma})}. \tag{3.31}$$

Since tunnelling rates in the direction opposing the applied bias voltage are small, the expressions for the forward and reverse biased current can be approximated for non-zero voltage. For forward biased current Γ_{cm} and Γ_{ma} are small, and for the reverse biased current Γ_{mc} and Γ_{am} are small, which gives the following simplified expressions:

$$I_{fb} \approx -2e\frac{\Gamma_{mc}\Gamma_{am}}{\Gamma_{am} + 2\Gamma_{mc}}, \tag{3.32}$$

$$I_{rb} \approx 2e\frac{\Gamma_{ma}\Gamma_{cm}}{\Gamma_{cm} + 2\Gamma_{ma}}. \tag{3.33}$$

Limiting Values of the Current

Since there is no inherent symmetry in the formation of a break junction, the molecule is likely to be positioned to one side of the junction more than the other [Par00], so it is useful to make a further approximation, taking the limit in which the molecule is coupled much more strongly to one electrode than the other. First consider the case where the molecule is closer to the cathode.

The dominant tunnelling rates are between the molecule and the cathode since we expect the rates to depend exponentially with distance, with a decay length of $\sim 1\mathring{A}$. Assuming that the time for a particle to tunnel from the cathode to the molecule is much shorter than the time to tunnel from the anode to the molecule, the hop between the anode and molecule will be the rate limiting hop.

For forward biased current the rate limiting step is Γ_{am}, and so $\Gamma_{am} \ll \Gamma_{mc}$, allowing Equation 3.32 to be written approximately as

$$\begin{aligned} I_{fb} &\approx -2e\frac{\Gamma_{mc}\Gamma_{am}}{2\Gamma_{mc}} \\ &= -e\Gamma_{am}. \end{aligned} \tag{3.34}$$

For reverse biased current the rate limiting step is Γ_{ma}, which means that $\Gamma_{ma} \ll \Gamma_{cm}$ and Equation 3.33 may be written approximately as

$$\begin{aligned} I_{rb} &\approx 2e\frac{\Gamma_{ma}\Gamma_{cm}}{\Gamma_{cm}} \\ &= 2e\Gamma_{ma}. \end{aligned} \tag{3.35}$$

Alternately, if the molecule were positioned closer to the anode then the tunnelling rates between the anode and molecule would dominate the expressions, and the rate limiting hop would be between the cathode and the molecule. In such a case, the expressions for the current would reduce to:

$$I_{fb} \approx -2e\Gamma_{mc}; \tag{3.36}$$

$$I_{rb} \approx e\Gamma_{cm}. \tag{3.37}$$

Regardless of which side of the junction the molecule is on, the limiting value for the current is proportional to the slower tunnelling rate. For this reason it is said that the current for the C_{60} transistor is dominated by the "rate limiting hop". This is expected since the two hops are sequential in taking the electron from one electrode to another. Of greater interest is the factor of two by which the expressions for the forward and reverse biased current differ for both configurations. When the molecule

is closer to the cathode, the reverse biased current is larger than the forward biased current by a factor of two. When the molecule is closer to the anode, the forward biased current is larger by a factor of two. The data that has been published for the C_{60} molecular transistor shows a clear asymmetry with respect to magnitude of the forward and reverse biased curves, so this factor will be important in predicting the location of the molecule in the junction.

The analysis we have just presented is straightforward for the case of an initially neutral molecule and a non-degenerate LUMO level. However, enumerating the different charge states becomes more complicated when additional LUMO levels are introduced. Many difficulties can be avoided with the introduction of an alternate method for deriving the current, which we present in the next section.

3.3.2 Molecular Transition Picture

Following the approach of Datta [Dat95], we have developed an alternate formulation of the current that is more amenable to a degenerate system such as C_{60}. In the "molecular transition picture", the spin of the tunnelling electrons is explicitly incorporated into the calculation for the current by considering each tunnelling possibility as a distinct level. Instead of considering spin up and spin down electrons tunnelling onto the molecule, a more formulaic method is to think of the tunnelling state on the molecule as a multi-state system, where each state represents a possible tunnelling event, as illustrated in Figure 3.4.

The multi-state molecular level is shown in Figure 3.4 for the case of a non-degenerate LUMO level, like the one considered in the last section. The lowest lying state (00) represents the molecule in the neutral charge state, and the two intermediate states (01 and 10) represent the singly ionized spin up and spin down states. The highest energy state (11) represents the doubly ionized state of the molecule, which has already been discussed as inaccessible in experimental realizations of the

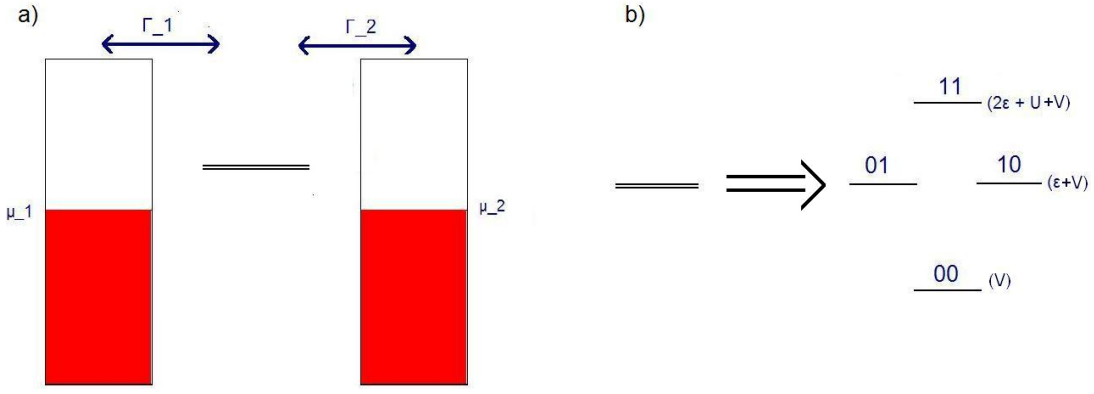

Figure 3.4: Transformation from single two site energy level to multi-level system. (a) The tunnelling rates across the metal-molecule bonds are given by Γ_i, and the fermi energies are given by μ_i. (b) The molecular level is now replaced by a system of levels that represents the possible charge states for the molecule. The increase in potential due to the presence of one excess electron on the molecule is given by ε, and the increase in potential due to the presence of two excess electrons on the molecule is given by U.

C_{60} transistor. The diagram for the molecular levels that participate in the current is shown in Figure 3.5.

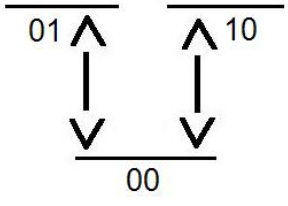

Figure 3.5: Allowed transitions when the current corresponds to neutral and singly ionized C_{60}.

The parameters in Figure 3.4 are defined as follows: ε is the increase in potential due to the presence of one excess electron onto the molecule, U is the increase in potential due to double ionization (the Coulomb repulsion potential) when transitioning from either the 01 or 10 state to the 11 state, Γ_1 is the tunnelling rate (in either direction) across the cathode-molecule bond, and Γ_2 is the tunnelling rate

across the anode-molecule bond. The fermi energies in the cathode and anode are given by μ_1 and μ_2.

The tunnelling rates can always be written as a product, $\Gamma_i = \gamma_i f_i$ or $\Gamma_i = \gamma_i(1 - f_i)$, where f_i is the fermi function of the metal electrode 1 or 2, corresponding to cathode and anode respectively. Tunnelling onto the molecule is given by $\Gamma_i = \gamma_i f_i$, where the argument of the fermi function is equal to the energy of the final state. The tunnelling rate off of the molecule is $\Gamma_i = \gamma_i(1 - f_i) \equiv \gamma_i \overline{f_i}$, and in this case the argument of the fermi function is equal to the energy of the initial state, since these tunnelling events require the presence of a hole with the energy of the tunnelling electron.

As shown in Figure 3.4, there are two ways to tunnel onto the molecule if the 11 state is excluded. These can be expressed using the above defined variables as,

$$00 \longmapsto 01 = \frac{1}{2}\gamma_1 f_1(\varepsilon) + \frac{1}{2}\gamma_2 f_2(\varepsilon) \tag{3.38}$$

$$00 \longmapsto 10 = \frac{1}{2}\gamma_1 f_1(\varepsilon) + \frac{1}{2}\gamma_2 f_2(\varepsilon) \tag{3.39}$$

$$. \tag{3.40}$$

Each term is the sum of two rates, the rate to tunnel from the cathode and and that from the anode. The factors of one half indicate the probability that the tunnelling particle is spin up or spin down. Similarly, the two ways to tunnel off of the molecule are,

$$01 \longmapsto 00 = \frac{1}{2}\gamma_1 \overline{f_1}(\varepsilon) + \frac{1}{2}\gamma_2 \overline{f_2}(\varepsilon) \tag{3.41}$$

$$10 \longmapsto 00 = \frac{1}{2}\gamma_1 \overline{f_1}(\varepsilon) + \frac{1}{2}\gamma_2 \overline{f_2}(\varepsilon), \tag{3.42}$$

where $\overline{f_i} = 1 - f_i$.

The subscript on γ determines whether the tunnelling event occurs between the molecule and the cathode (1) or the molecule and the anode (2). The upward transition rates (an electron tunnelling onto the molecule) are multiplied by the Fermi function, and the downward transition rates (a hole tunnelling onto the molecule or an electron tunnelling off) are multiplied by one minus the Fermi function. For the C_{60} system, because only one excess electron is allowed on the molecule at a time, the argument of the Fermi function is the same for all of the rates that correspond to a given initial charge state.

These expressions can be combined to find the time evolution of the occupation probabilities. Defining P_j as the probability that the j^{th} state is occupied, where j can equal 00, 01 or 10, the equations describing the rate of change of the occupation probabilities is

$$\frac{d}{dt}\begin{pmatrix} P_{00} \\ P_{01} \\ P_{10} \end{pmatrix} = \begin{pmatrix} -(00 \longmapsto 01 + 00 \longmapsto 10) & 01 \longmapsto 00 & 10 \longmapsto 00 \\ 00 \longmapsto 01 & -01 \longmapsto 0 & 0 \\ 00 \longmapsto 10 & 0 & -10 \longmapsto 00 \end{pmatrix} \begin{pmatrix} P_{00} \\ P_{01} \\ P_{10} \end{pmatrix}. \quad (3.43)$$

In addition, the probabilities are constrained by conservation of probability,

$$P_{00} + P_{01} + P_{10} = 1. \quad (3.44)$$

Equilibrium Charge State = Neutral

There are two potential charge states to consider for the C_{60} transistor, neutral and singly ionized. For comparison with the prior derivation of the hopping current, the first case that will be analyzed is an initially neutral molecule. If the molecule is neutral prior to the application of a bias voltage, then the electron tunnelling events are transitions between a single initial state, 00, and two final states, 01 and 10. In steady state the probabilities do not change in time, so the rate equations are reduced to

$$\begin{aligned}
\dot{P_{00}} &= 0 = -\left[\gamma_1 f_1(\varepsilon) + \gamma_2 f_2(\varepsilon)\right] P_{00} + \frac{1}{2}\left[\gamma_1 \overline{f_1}(\varepsilon) + \gamma_2 \overline{f_2}(\varepsilon)\right] (P_{01} + P_{10}) \\
\dot{P_{01}} &= 0 = \frac{1}{2}\left[\gamma_1 f_1(\varepsilon) + \gamma_2 f_2(\varepsilon)\right] P_{00} - \frac{1}{2}\left[\gamma_1 \overline{f_1}(\varepsilon) + \gamma_2 \overline{f_2}(\varepsilon)\right] P_{01} \\
\dot{P_{10}} &= 0 = \frac{1}{2}\left[\gamma_1 f_1(\varepsilon) + \gamma_2 f_2(\varepsilon)\right] P_{00} - \frac{1}{2}\left[\gamma_1 \overline{f_1}(\varepsilon) + \gamma_2 \overline{f_2}(\varepsilon)\right] P_{10}, \qquad (3.45)
\end{aligned}$$

and the equation for conservation of probability is

$$P_{00} + P_{01} + P_{10} = 1. \qquad (3.46)$$

The argument of the Fermi functions, ε, is equal to $\varepsilon_0 - \lambda eU$ for our model system, where eU was defined in the introductory chapter to represent the source-drain voltage. The solutions of these equations are the steady state probabilities,

$$P_{00} = \frac{\gamma_1 \overline{f_1} + \gamma_2 \overline{f_2}}{\left[\gamma_1 \overline{f_1} + \gamma_2 \overline{f_2}\right] + 2\left[\gamma_1 f_1 + \gamma_2 f_2\right]} \qquad (3.47)$$

$$P_{01} = P_{10} = \frac{\gamma_1 f_1 + \gamma_2 f_2}{\left[\gamma_1 \overline{f_1} + \gamma_2 \overline{f_2}\right] + 2\left[\gamma_1 f_1 + \gamma_2 f_2\right]}. \qquad (3.48)$$

With the above expressions, the current can be found in the same way as the previous section. Using the flux across the cathode-molecule bond, the current may be expressed in terms of the hopping rates as:

$$\begin{aligned} I &= -e\{\begin{pmatrix} Probability \\ system\ is\ in \\ 00\ state \end{pmatrix}\begin{pmatrix} Rate\ to \\ transition\ to \\ 01\ from\ left \end{pmatrix} + \begin{pmatrix} Probability \\ system\ is\ in \\ 00\ state \end{pmatrix}\begin{pmatrix} Rate\ to \\ transition\ to \\ 10\ from\ left \end{pmatrix} \\ &\quad - \begin{pmatrix} Probability \\ system\ is\ in \\ 01\ state \end{pmatrix}\begin{pmatrix} Rate\ to \\ transition\ to \\ 00\ from\ left \end{pmatrix} - \begin{pmatrix} Probability \\ system\ is\ in \\ 10\ state \end{pmatrix}\begin{pmatrix} Rate\ to \\ transition\ to \\ 00\ from\ left \end{pmatrix}\} \\ &= -e\left[P_{00}\gamma_1 f_1 + P_{00}\gamma_1 f_1 - P_{01}\gamma_1\overline{f_1} - P_{10}\gamma_1\overline{f_1}\right] \\ &= (-2e)\frac{\gamma_1 f_1\gamma_2\overline{f_2} - \gamma_2 f_2\gamma_1\overline{f_1}}{\left(\gamma_1\overline{f_1} + \gamma_2\overline{f_2}\right) + 2\left(\gamma_1 f_1 + \gamma_2 f_2\right)} \end{aligned}$$

As expected, this result is identical to the one that was obtained without the transformation to the multi-level system, where the current was found to be

$$I = (-2e)\frac{\Gamma_{mc}\Gamma_{am} - \Gamma_{ma}\Gamma_{cm}}{\Gamma_{cm} + \Gamma_{am} + 2\left(\Gamma_{mc} + \Gamma_{ma}\right)}. \tag{3.49}$$

The two expressions for the current can be compared by equating the following parameters:

$$\begin{aligned}
\Gamma_{mc} &= \gamma_1 f_1 \\
\Gamma_{ma} &= \gamma_2 f_2 \\
\Gamma_{cm} &= \gamma_1 \overline{f_1} \\
\Gamma_{am} &= \gamma_2 \overline{f_2}.
\end{aligned}$$

Making the above substitutions confirms that both methods yield identical expressions.

An alternate way of comparing the two expressions is to check that the multi-level expression yields the same limiting result for the case of an asymmetrically positioned molecule. Tunnelling occurs in the forward bias direction when the potential of the anode is lowered with respect to the cathode, and all reverse bias terms can be neglected. Tunnelling occurs in the reverse bias direction when the potential of the cathode is lowered with respect to the anode, and the forward bias terms can be neglected. This gives the following expressions:

$$I_{fb} = (-2e)\frac{\gamma_1 f_1 \gamma_2 \overline{f_2}}{\gamma_2 \overline{f_2} + 2\gamma_1 f_1} \tag{3.50}$$

$$I_{rb} = (2e)\frac{\gamma_2 f_2 \gamma_1 \overline{f_1}}{\gamma_1 \overline{f_1} + 2\gamma_2 f_2}. \tag{3.51}$$

For a molecule that sits closer to the cathode, the expressions reduce to:

$$I_{fb} \approx -e\gamma_2 \overline{f_2} \tag{3.52}$$

$$I_{rb} \approx 2e\gamma_2 f_2, \tag{3.53}$$

and for a molecule that sits closer to the anode, the expressions reduce to:

$$I_{fb} \approx -2e\gamma_2\overline{f_2} \tag{3.54}$$

$$I_{rb} \approx e\gamma_2 f_2. \tag{3.55}$$

These results are identical to those that were obtained by following the standard electron tunnelling method.

It is interesting to note that if the spin of the tunnelling particles is neglected, then the following (incorrect) result is obtained:

$$I = (-e)\frac{\Gamma_{mc}\Gamma_{am} - \Gamma_{ma}\Gamma_{cm}}{\Gamma_{cm} + \Gamma_{am} + \Gamma_{mc} + \Gamma_{ma}}. \tag{3.56}$$

In this case, the limiting values for the current when the molecule is positioned closer to the cathode than to the anode are:

$$I_{fb} = -e\frac{\Gamma_{mc}\Gamma_{am}}{\Gamma_{mc} + \Gamma_{am}} \approx -e\Gamma_{am} \tag{3.57}$$

$$I_{rb} = e\frac{\Gamma_{ma}\Gamma_{cm}}{\Gamma_{ma} + \Gamma_{cm}} \approx e\Gamma_{ma}, \tag{3.58}$$

and the limiting values for the current when the molecule is positioned closer to the anode are:

$$I_{fb} \approx -e\Gamma_{mc} \tag{3.59}$$

$$I_{rb} \approx e\Gamma_{cm}. \tag{3.60}$$

The asymmetry that distinguishes the forward bias from the reverse bias current is absent when the spin of the tunnelling particle is neglected.

Equilibrium Charge State = Singly Ionized

If the C_{60} molecule is singly ionized prior to the application of a bias voltage, then the tunnelling events correspond to transitions between two states, 01 and 10, and one state 00.

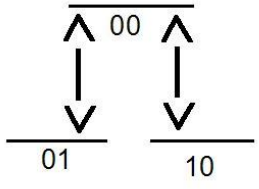

Figure 3.6: Allowed transitions when the current corresponds to an equilibrium charge state of C_{60}^{1-}.

The occupation probabilities that determine the current are still P_{01}, P_{10} and P_{00}, and although the essential factors for determining the current, the initial and final molecular states, have reversed their roles, the evolution equations describing the probability that the molecular site is occupied remain the same. Since the current is dependent on the flux of electrons across either metal-molecule bond, it is clear that is independent of the initial charge state of the molecule,

$$I_{C_{60}^{0}\rightarrow C_{60}^{1-}} = I_{C_{60}^{1-}\rightarrow C_{60}^{0}} = -2e\frac{\gamma_1 f_1 \gamma_2 \overline{f_2} - \gamma_2 f_2 \gamma_1 \overline{f_1}}{\left(\gamma_1 \overline{f_1} + \gamma_2 \overline{f_2}\right) + 2\left(\gamma_1 f_1 + \gamma_2 f_2\right)}. \tag{3.61}$$

If the transition was from singly ionized to doubly ionized C_{60}, then the probabilities of interest would be P_{01} and P_{10} (probabilities for single ionization), and P_{11} (probability for double ionization), and their steady state solutions would yield a slightly different expression for the current,

$$I_{C_{60}^{1-}\rightarrow C_{60}^{2-}} = (-2e)\frac{\gamma_1 f_1 \gamma_2 \overline{f_2} - \gamma_2 f_2 \gamma_1 \overline{f_1}}{\gamma_1 f_1 + \gamma_2 f_2 + 2\left(\gamma_1 \overline{f_1} + \gamma_2 \overline{f_2}\right)}. \tag{3.62}$$

The expressions in Equations 3.61 and 3.62 only differ by a shift in the factor of 2 in their denominators. This shift results in different limiting values for the current when the molecule is positioned asymmetrically in the gap between the gold wires. Current representing transitions between singly and doubly ionized C_{60} would exhibit behaviour opposite to that of current representing transitions between neutral and singly ionized C_{60}.

By envisioning the transport through a molecular transistor as arising from a transition between two charge states of a given molecule, the current can always be calculated with relative ease, provided that the molecular structure of the molecule is known. This is because the method only relies on a knowledge of the degeneracy of the two transition states.

3.4 D-Fold Degeneracy

The derivation of the current can be generalized for transitions between an arbitrary number of equilibrium and excited states. This is not the same thing as saying that it can be written in general for a transition between two particular charge states. This is because the number of initial and final states that correspond to an initial and final charge state depends on the molecule in question. Although this was possible for single degeneracy, as shown in the previous section, for degeneracies higher than one the transition diagrams are dependent on the rules for filling the valence levels of the molecule in question. In other words, this can't be done without a knowledge of the geometry and electronic structure of the molecule being studied.

Relating the charge states to the number of ways to tunnel on and off the molecule

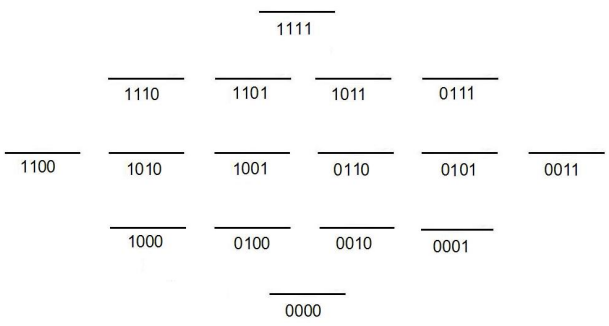

Figure 3.7: Degeneracy of states for a system with a two-fold degenerate LUMO where only the Pauli Exclusion Principle is considered. The labelling is as follows: $\{a, b, c, d\}$ represents {Level 1, Spin up; Level 1, Spin down; Level 2, Spin up; Level 2, Spin down}.

is straightforward when only the Pauli Exclusion Principle is considered. In that case, the diagram for two-fold degeneracy would be as shown in Figure 3.7 with sixteen levels in total. For a level that is labelled $\{a, b, c, d\}$ in Figure 3.7, the variables represent the following states: {Level 1, Spin up; Level 1, Spin down; Level 2, Spin up; Level 2, Spin down}. Using simple combinatorial analysis, it can be shown that the number of levels in a diagram for higher order degeneracies is equal to 2^{2d}, where d is the number of degenerate states. The full diagram for three-fold degeneracy would have sixty-four levels in total, the diagram for four-fold degeneracy would have one hundred twenty-eight levels, and so on. The general relation can be found by considering a d-fold degenerate LUMO. The lowest rung of the molecular transition diagram, representing the neutral state, will have one level, or equivalently $2d$ choose zero. The next rung, representing a LUMO containing one electron, will have $2d$ levels, or equivalently $2d$ choose one. The next rung will have $2d$ choose two levels, and so on until the highest rung which will have $2d$ choose $2d$, or one, level. The number of levels can easily be summed using the binomial theorem,

$$\sum_{C=0}^{2d} \binom{2d}{C} = 2^{2d}. \tag{3.63}$$

When all possible configurations for filling the molecular orbitals are included, the current is easily written as a function of the initial and final charge of the molecule by relating the number of states, N, with a particular charge state, C, as

$$N = \binom{2d}{C}. \tag{3.64}$$

Since filling the LUMO depends on the structure of the molecule in question, and must obey the fermion rules for filling degenerate orbitals, this basic model is incorrect. A more reasonable molecular transition diagram for a two-fold degenerate LUMO is shown in Figure 3.8, however even this diagram is not universally correct for any system with two degenerate LUMO levels because certain systems could exhibit symmetry breaking effects, such as the Jahn-Teller effect, that would break the degeneracy of the two levels.

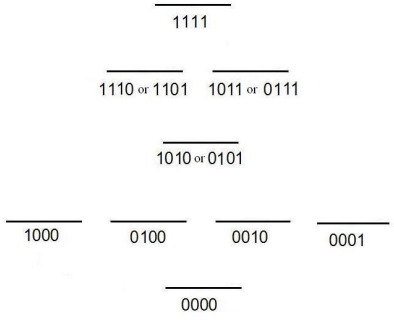

Figure 3.8: Degeneracy of transitions for a system with a two-fold degenerate LUMO.

A general expression for the current based on the number of ways to tunnel on and off the molecule can be constructed by extending the derivation as follows: if there are x ways to tunnel onto the molecule, and y ways to tunnel off, then the current current is

$$I = xy(-e)\frac{\gamma_1 f_1 \gamma_2 \overline{f_2} - \gamma_2 f_2 \gamma_1 \overline{f_1}}{x\left(\gamma_1 f_1 + \gamma_2 f_2\right) + y\left(\gamma_1 \overline{f_1} + \gamma_2 \overline{f_2}\right)}. \tag{3.65}$$

For C_{60}, the relevant molecular transition diagram is shown in Figure 3.9. There are six ways to tunnel onto the molecule, and one way to tunnel off so a tunnelling expression for the current is

$$I = -6e\frac{\gamma_1 f_1 \gamma_2 \overline{f_2} - \gamma_2 f_2 \gamma_1 \overline{f_1}}{6\left(\gamma_1 f_1 + \gamma_2 f_2\right) + \left(\gamma_1 \overline{f_1} + \gamma_2 \overline{f_2}\right)}. \tag{3.66}$$

Expressed as a function of Γ_{ab}, the current is

$$I = (-6e)\frac{\Gamma_{mc}\Gamma_{am} - \Gamma_{ma}\Gamma_{cm}}{\Gamma_{cm} + \Gamma_{am} + 6\left(\Gamma_{mc} + \Gamma_{ma}\right)}. \tag{3.67}$$

This can be compared to Equation 3.28, where only the spin degeneracy was considered. The inclusion of the LUMO degeneracy results in the replacement of the factor of 2 with a factor of 6.

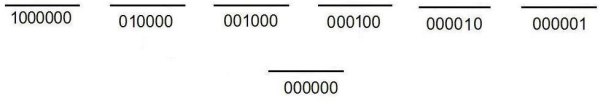

Figure 3.9: Degeneracy of the neutral to singly ionized transition for a system with three-fold degenerate excited states.

Comparison of Forward and Reverse Bias Current for C_{60}

For an initially neutral molecule, the expressions for the forward and reverse bias current are:

$$I_{fb} = -6e\frac{\gamma_1 f_1 \gamma_2 \overline{f_2}}{\gamma_2 \overline{f_2} + 6\gamma_1 f_1} \tag{3.68}$$

$$I_{rb} = 6e\frac{\gamma_2 f_2 \gamma_1 \overline{f_1}}{\gamma_1 \overline{f_1} + 6\gamma_2 f_2}. \tag{3.69}$$

For a molecule that is closer to the cathode than the anode, these expressions reduce to

$$\lim_{\Gamma_1 \gg \Gamma_2} I_{fb} = -e\gamma_2 \overline{f_2} \tag{3.70}$$

$$\lim_{\Gamma_1 \gg \Gamma_2} I_{rb} = 6e\gamma_2 f_2 \tag{3.71}$$

and for a molecule that is closer to the anode than to the cathode, the expressions reduce to

$$\lim_{\Gamma_1 \ll \Gamma_2} I_{fb} = -6e\gamma_1 f_1 \tag{3.72}$$

$$\lim_{\Gamma_1 \ll \Gamma_2} I_{rb} = e\gamma_1 \overline{f_1}. \tag{3.73}$$

Like the generalized expression for the current, this relationship is independent of the initial charge on the molecule, and only depends on the number of initial and final states. Within the parameters of this model, where only one tunnelling electron is allowed on the molecule at a time, it is only necessary to know the relative position of the molecule in the molecular junction and the number of initial and final degenerate levels that are available to a tunnelling electron in order to write an expression for the current and to predict the relative sizes of the forward and reverse biased currents.

Summary:

The tunnelling rate onto the molecule is proportional to the number of energetically available eigenstates on the molecule.

The "Molecular Transition Picture" is introduced as an easier way to enumerate the states in the data.

The experimental data shows an asymmetry in the saturation values for the forward and reverse bias current. When the degeneracy of the LUMO is considered along with the spin of the tunnelling particle, the forward and reverse bias current curves are expected to saturate at different values. Based only on the degeneracy considerations, depending on which side of the junction the molecule resides on, one bias is predicted to saturate at $\frac{1}{6}$ of the value of the other bias.

This can be compared to the result from considering a non-degenerate tunnelling orbital, where an asymmetry of 2 is found for the relative saturation values.

Chapter 4

Equilibrium Charge States of C_{60}

4.1 Introduction

In Chapter 1, the equilibrium charge state of C_{60} was predicted to be C_{60}^{1-} by inspection of the experimental data produced by Park et al. [HP00]. This was done by comparing the relative size of the voltage gap with the progression of the gate voltage. This prediction can be confirmed by considering the effect that the asymmetrical position of the molecule has on the gap voltage in contrast with the effect it has on the dimensionless coupling parameters, η_R and η_L. The dimensionless coupling parameters describe the strength of bonds between the C_{60} molecule and the gold electrodes, and are therefore expected to vary with respect to the position of the molecule in the junction. The relative sizes of the forward and reverse bias voltage gaps is also dependent on the degree of asymmetry in the molecule's position, allowing a relationship between the coupling parameters and the voltage gap to be induced. The relationship will be examined using a one dimensional, tight binding chain of sites with a central defect site, representing the molecule between the gold electrodes.

4.2 Equilibrium Charge States

In order to explore the effect of the two possible initial charge states, C_{60}^{0} and C_{60}^{1-}, on the current voltage curves it is not necessary to consider the degeneracy of the LUMO so the molecule is drawn as a one site system. Also, because we are examining the equilibrium charge state, i.e. the charge of the molecule in the absence of an applied source-drain voltage, it is not necessary to consider a voltage drop across the molecular junction. The model system for this section is thus comprised of two uniform, one-dimensional, semi-infinite tight binding chains that are separated by a central defect site. The tight binding chains represent the metal leads, and are coupled to the central site, which represents the molecule, via a reduced potential, $\eta_L V$ and $\eta_R V$, as shown in Figure 4.1.

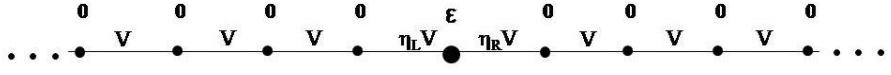

Figure 4.1: Tight binding representation of the C_{60} transistor, where the molecule is represented as a single site on the chain, and has the potential to hold two electrons, one with spin up, and one with spin down.

Using this system, the different possibilities for tunnelling on the molecule can be explored. Because Coulomb repulsion prevents double ionization, the ion C_{60}^{2-} does not participate for the range of applied voltages considered. If the molecule is initially neutral, an electron will hop onto the molecule and then hop off of it before another can come on. If it is initially ionized, an electron will first hop off of the molecule and then another will hop onto it.

4.2.1 Case 1: $\varepsilon_0 > \mu$

The first case assumes that the energy of the LUMO is greater then the fermi level of the electrodes before the source drain voltage is applied, as shown in Part (a) of Figure 4.2.

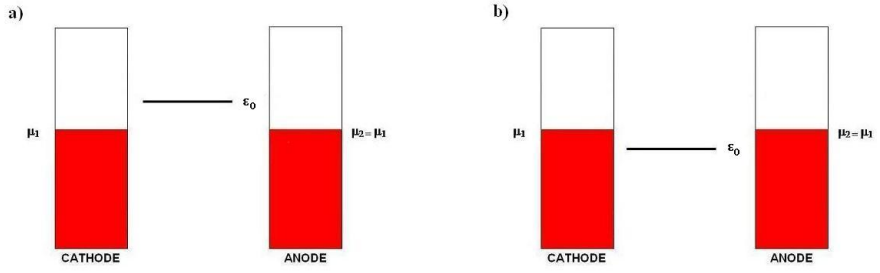

Figure 4.2: (a) Case 1: The molecule is initially neutral. (b) Case 2: The molecule is initially charged.

In this case the molecule will be unoccupied prior to the application of the bias voltage, meaning that the equilibrium charge state is neutral. As the bias voltage is applied, the LUMO will move into the tunnelling regime, as shown in Part (a) of Figure 4.3.

Once the energy level has been lowered to the fermi level of the cathode, an electron will be able to hop on the molecule from the cathode. Coulomb repulsion prevents more then one tunnelling particle from occupying the molecule at a time, so the electron must then then hop off before another can hop on.

4.2.2 Case 2: $\varepsilon_0 < \mu$

If the energy of the LUMO is less then the fermi level of the electrodes before the source drain voltage is applied, then the molecule will have one excess electron on it in equilibrium. Its equilibrium charge state will be singly ionized, as shown in Part

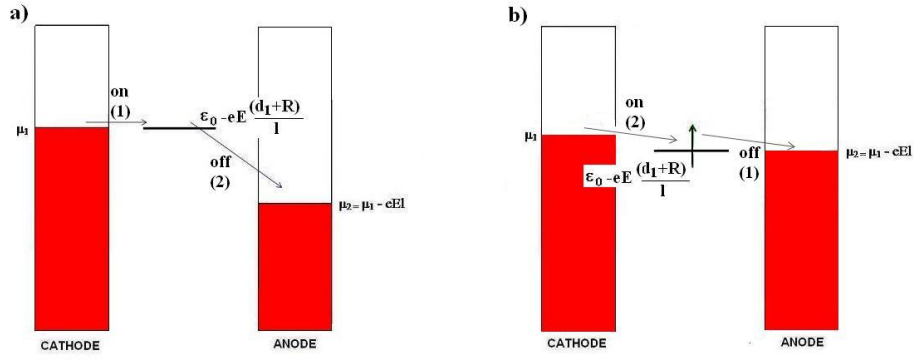

Figure 4.3: (a) Case 1: The current is turned on by an electron hop onto the molecule when the applied voltage brings the molecular level into the energy range of the tunnelling electron. This electron tunnels off before another may tunnel onto the molecule. (b) Case 2: Current is turned on by an electron hop off of the molecule, followed by a hop on the molecule, and so on.

(b) of Figure 4.2.

The application of a bias voltage lowers the fermi level of the anode until it is aligned with the LUMO of the molecule, as shown in Part (b) of Figure 4.3.

At this point, the electron will hop off of the molecule into an unoccupied state of the anode, and another will hop onto the molecule from the cathode.

4.3 Analysis of Forward and Reverse Bias Asymmetry

The current voltage data for the C_{60} single molecule transistor exhibits two distinct asymmetries. The relative size of the forward and the reverse bias currents is consistently unequal over a range of gate voltages. In the case of the data published by Park et al., shown in Figure 4.4, the magnitude of the forward bias curves is smaller then that of the reverse bias curves. Also, the relative size of the voltage gaps, the

voltage that is applied before the current turns on, is consistently different for forward and reverse bias. In the case of the data shown in Figure 4.4, the voltage gaps are smaller for forward bias curves relative to reverse bias curves that are measured at the same gate voltage.

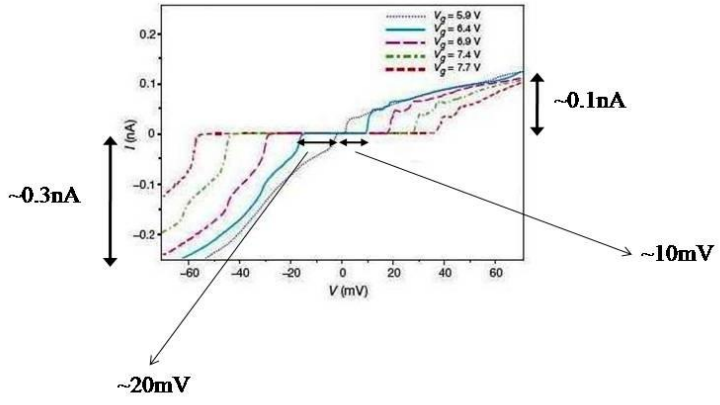

Figure 4.4: Experimental current-voltage curves for a single C_{60} transistor from Reference [Par00]. Approximate values are given for the two notable asymmetries in the data. An example of the asymmetry in the saturation value for the current is given for the curve measured at $V_g = 5.9V$ and an example for the asymmetry in the gap voltage is given for the curve measured at $V_g = 6.4V$.

4.3.1 Relative Magnitude of I-V Curves

We have already discussed the fact that when the molecule is asymmetrically coupled to the leads, there is a rate limiting hop that dominates the current. If $\eta_R \ll \eta_L$, or equivalently if the rate to tunnel onto the molecule from the right Γ_2 is less than the rate to tunnel from the left Γ_1, then the rate limiting hop will be between the molecule and the electrode to the right (the anode). The only time that this will not be true is if hopping between the left electrode and the molecule is blocked due to the alignment of the fermi level with the molecular level. If tunnelling is

completely blocked then the current is zero, and this has no effect. When the energy level is approaching the fermi level, then the tunnelling is only partially blocked, and there is a small voltage window where tunnelling between the molecule and the left electrode is dominant in the expression for the current, but this is not important for our analysis.

If $\eta_L \ll \eta_R$, or equivalently if the rate to tunnel onto the molecule from the right Γ_2 is greater than the rate to tunnel from the left Γ_1, then the rate limiting hop will be between the molecule and the electrode to the left (the cathode).

Recall that the dominant terms in the current for forward and reverse bias applied voltages were found to be

$$\begin{aligned} I_{fb}^{\eta_L>\eta_R} &= -e\gamma_2\overline{f_2} \\ I_{rb}^{\eta_L>\eta_R} &= 6e\gamma_2 f_2 \\ I_{fb}^{\eta_L<\eta_R} &= -6e\gamma_1 f_1 \\ I_{rb}^{\eta_L<\eta_R} &= e\gamma_1\overline{f_1}. \end{aligned} \tag{4.1}$$

For the case of a one site model, the asymmetry in magnitude between the forward and reverse bias current manifests itself as a factor of 2 in the equations. This is because for a charged molecule, the rate for tunnelling off the molecule is smaller than the rate for tunnelling on by a factor of 2 due to spin. For a singly charged ion, the spin of the extra electron will be either up or down, and in tunnelling off it will "see" only half of the unoccupied density of states in the metal. On the other hand, to put an electron on an uncharged molecule it doesn't matter whether the spin is up or down so the entire density of states of the metal comes into the rate calculation.

When the degeneracy of the LUMO for C_{60} is considered, the factor of 2 becomes a factor of 6. Although an electron tunnelling off of the molecule still sees one half of

the unoccupied density of states, and the entire density of states is considered for an electron tunnelling on, the electron tunnelling on has three orbitals to choose from now instead of only one. The factors multiply to give an overall asymmetry factor of 6 for the off rate versus the on rate.

4.3.2 Relative Magnitude of Voltage Gaps

The size of the gap between the electrodes is on the order of 1nm [Par00]. If this distance is defined as l, and the electric field between the electrodes is assumed to be uniform, then the potential energy of a charge -e in the gap between the electrodes is $-eEl$. This energy can be split into two parts, $-eE(d_1 + R)$ and $-eE(d_2 + R)$, where

$$l = d_1 + d_2 + 2R. \tag{4.2}$$

The division of the gap is illustrated in Figure 4.5.

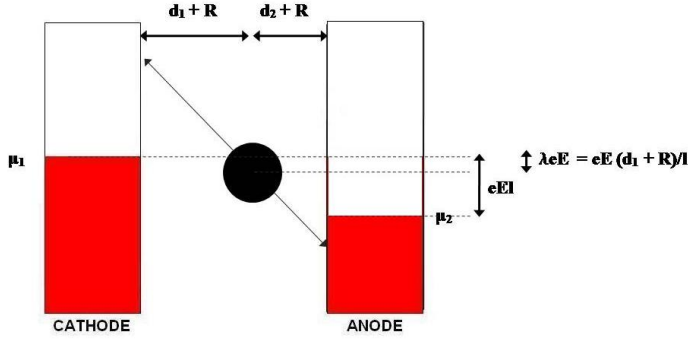

Figure 4.5: An electron has potential energy $-eE(d_1 + R)$ between the cathode and the molecule, and $-eE(d_2 + R)$ between the molecule and the anode.

The energies $eE(d_1 + R)$ and $eE(d_2 + R)$ can be used to derive an expression for

the voltage gap, which is the source-drain voltage that is applied before the current turns on.

Voltage Gap for Case 1

As shown in Figure 4.3, for Case 1 the current turns on when the one-electron state is aligned with the fermi level of the cathode. This occurs when

$$\varepsilon_0 - \mu_1 = eE(d_1 + R). \tag{4.3}$$

This can be rewritten as

$$eEl = eV_{gap}^{forward} = \frac{l}{d_1 + R}\left(\varepsilon_0 - \mu_1\right). \tag{4.4}$$

For reverse bias, the voltage gap is similarly given by

$$eV_{gap}^{reverse} = \frac{l}{d_2 + R}\left(\varepsilon_0 - \mu_1\right). \tag{4.5}$$

It is useful to notice that adding the reciprocals of the voltage gaps eliminates the dependence on d_1, d_2, R, and l,

$$\begin{aligned} \frac{1}{eV_{gap}^{forward}} + \frac{1}{eV_{gap}^{reverse}} &= \frac{1}{\varepsilon_0 - \mu_1}\left(\frac{d_1 + R}{l} + \frac{d_2 + R}{l}\right) \\ &= \frac{1}{\varepsilon_0 - \mu_1}. \end{aligned} \tag{4.6}$$

We see that the difference in energy between the fermi level of the electrodes and the tunnelling state can be measured directly using only the voltage gaps.

Voltage Gap for Case 2

For Case 2, the current turns on when the one-electron state is aligned with the fermi level of the anode, since the first event is a hop off of the molecule. This occurs when

$$\mu_1 - \varepsilon_0 = eE(d_2 + R). \tag{4.7}$$

This can be rearranged as the equation for Case 1 was to give the following expression for the voltage gap:

$$eV_{gap}^{forward} = \frac{l}{d_2 + R}\left(\mu_1 - \varepsilon_0\right). \tag{4.8}$$

And similarly, the gap for reverse bias is:

$$eV_{gap}^{reverse} = \frac{l}{d_1 + R}\left(\mu_1 - \varepsilon_0\right). \tag{4.9}$$

In this case, the energy difference between the tunnelling state and the fermi level of the electrodes can also be calculated using only the forward and reverse bias voltage gaps:

$$\frac{1}{eV_{gap}^{forward}} + \frac{1}{eV_{gap}^{reverse}} = \frac{1}{\mu_1 - \varepsilon_0}. \tag{4.10}$$

This can be used to determine how ε_0 changes with gate voltage.

4.4 Relating the Two Asymmetries

The distances between the molecule and the electrodes, d_1 and d_2, and the coupling parameters, η_L and η_R, are expected to be related since a weak coupling to a particular electrode should correspond to a longer tunnelling distance. By introducing the variable α, defined as the wavefactor overlap decay parameter, the variables can be related in the following way:

$$\eta_L = \eta_0 e^{-\alpha d_1} \tag{4.11}$$

$$\eta_R = \eta_0 e^{-\alpha d_2}. \tag{4.12}$$

If d_1 is large then η_L will be small and the path between the left electrode and the molecule will be the limiting step in the current. For large d_2, the coupling to the right, η_R, will be small and the path between the right electrode and the molecule will be the limiting step.

For Case 1, when the charge of the molecule is neutral prior to the application of the source-drain voltage, the ratio of the forward to the reverse voltage gap

$$\frac{V_{gap}^{forward}}{V_{gap}^{reverse}} = \frac{d_2 + R}{d_1 + R}, \tag{4.13}$$

is found by dividing Equation 4.4 by Equation 4.5. If $d_2 > d_1$, then $V_g^f > V_g^r$, and if $d_2 < d_1$, then $V_g^f < V_g^r$.

Let us now relate the information about the voltage gaps to the current asymmetry caused by the spin degeneracy that was discussed in Section 4.3.1. In that section we saw that if the coupling to the cathode, η_L, was greater than the coupling

to the anode, η_R, then the rate limiting step for forward bias is the hop off of the molecule onto the anode, and the rate limiting step for reverse bias is the hop on the molecule from the anode. The magnitude of the forward bias current will be $\frac{1}{6}$ the magnitude of the reverse bias current in this case. This implies that $d_1 < d_2$, which implies that $V_g^f > V_g^r$. In other words, when the forward voltage gap is larger than the reverse voltage gap, the magnitude of the forward current will be smaller than the reverse current. This correlation can be expressed as the following product

$$P = \left(|I_{fb}| - |I_{rb}|\right)\left(V_g^f - V_g^r\right). \tag{4.14}$$

P (which has units of power) will be negative in this case.

For Case 2, where the equilibrium charge state is singly ionized, the ratio is

$$\frac{V_{gap}^{forward}}{V_{gap}^{reverse}} = \frac{d_2 + R}{d_1 + R}, \tag{4.15}$$

which is the reciprocal of the result shown in Equation 4.13, for an initially neutral molecule. In this case, if $d_1 > d_2$, then $V_g^f > V_g^r$, and if $d_1 < d_2$, then $V_g^f < V_g^r$. This implies that if the forward voltage gap is larger than the reverse gap, the magnitude of the forward bias current will be larger than the reverse current, or if the forward voltage gap is smaller than the reverse gap, the magnitude of the forward bias current will also be smaller than the reverse current. In this case, P will be positive.

In summary, the correlation parameter determines the charge state as follows:

$$P = \begin{cases} \text{positive, then equilibrium charge state is charged;} \\ \text{negative, then equilibrium charge state is neutral.} \end{cases} \tag{4.16}$$

Looking at the data of Park et al. [HP00] shown in Figure 4.4, we see that $|I_{fb}| < |I_{rb}|$ and $|V_{gap}^{fb}| < |V_{gap}^{rb}|$. This means that $P > 0$ for the data, and that C_{60} is initially charged in equilibrium.

This analysis has been carried out under the assumption that the participating state is the LUMO. It can also be shown that the same result applies when the participating state is the HOMO.

Summary:

By comparing the asymmetries in the current and the voltage gap that are observed in the experimental data for a C_{60} transistor, the equilibrium charge state of the molecule can be determined. A convenient way to combine the asymmetries is through the correlation function P, where P is defined as follows:

$$P = (I_{fb} - I_{rb})(V_{fb} - V_{rb}).$$

If P is positive, then the molecule is occupied in equilibrium. If P is negative, then the molecule is not occupied in equilibrium. Using this function, the published data for the C_{60} single molecule transistor indicates that C_{60} is initially negatively charged when in the molecular transistor configuration.

Also, adding the inverse of the voltage gaps gives an experimental measure of the difference in energy between the fermi level of the electrodes and the energy of the tunnelling orbital. This can be used to determine how ε_0 changes with the gate voltage.

Chapter 5

The Renormalized Perturbation Expansion

5.1 Introduction

The formalism of the Renormalized Perturbation Expansion (RPE) is well suited for constructing the Green functions for the single molecule transistor system. This section will provide an introduction to the RPE method, emphasizing the aspects that apply to the problem at hand. A more complete treatment of the approach can be found in Appendix B of Reference [Eco06], upon which most of this discussion is based. Renormalization refers to a collection of techniques for obtaining physical relationships between observable quantities when they are found to be infinite through standard methods. In the RPE an infinite sum representation of the Green function is equated to an equivalent finite representation, allowing expressions for physical observables to be easily constructed. It is a useful method for calculating Green functions for tight binding lattices with a small number of defects. Although the transistor system will be treated as a one-dimensional system, the method can be extended to higher dimensions.

5.2 Notation

5.2.1 Definition of Functions

Green functions are useful for solving inhomogeneous differential equations

$$\mathbf{L}(\mathbf{r})\Psi = f(\mathbf{r})\Psi, \tag{5.1}$$

and may be defined as the solutions of generalized equations of the following form

$$[z - \mathbf{L}(\mathbf{r})]\, \mathbf{G}(\mathbf{r}, \mathbf{r}'; z) = \delta(\mathbf{r} - \mathbf{r}'). \tag{5.2}$$

The variable z is equal to the fourier transform variable. It is a complex variable with real and imaginary parts, $z = X + iY$, and $\mathbf{L}(\mathbf{r})$ is a linear, time-independent, Hermitian, differential operator with a complete set of eigenfunctions,

$$\mathbf{L}(\mathbf{r})\phi_n(\mathbf{r}) = \lambda_n \phi_n(\mathbf{r}). \tag{5.3}$$

It is convenient to use an orthonormal representation of the complete set $\{\phi_n(\mathbf{r})\}$ that satisfies the same boundary conditions as $\mathbf{G}(\mathbf{r}, \mathbf{r}'; z)$. The index n may take on both discrete and continuous values depending on the spectrum of eigenvalues for $\mathbf{L}$. Also, the completeness of the eigenfunctions means that any well-behaved function defined on Ω and satisfying the appropriate boundary conditions can be written as a linear combination of the eigenfunctions,

$$\psi(\mathbf{r}) = \sum_n c_n \phi_n(\mathbf{r}), \tag{5.4}$$

which means that

$$\sum_n \phi_n(\mathbf{r})\phi_n^*(\mathbf{r}') = \delta(\mathbf{r}-\mathbf{r}'). \tag{5.5}$$

This can easily be shown by multiplying Equation 5.4 by ϕ_m^* and integrating over $\mathbf{r}$. Because of the orthonormality of the set $\{\phi_n(\mathbf{r})\}$, the following relation is true:

$$\int_\Omega \phi_m^* \psi\left(\mathbf{r}\prime\right) d\mathbf{r}' = \sum_n c_n \int_\Omega \phi_m^* \phi_n d\mathbf{r}' = c_m. \tag{5.6}$$

Substituting Equation 5.6 into Equation 5.4 gives:

$$\psi(\mathbf{r}) = \int_\Omega \left\{ \sum_m \phi_m^*(\mathbf{r}')\phi_m(\mathbf{r}) \right\} \psi(\mathbf{r}')d\mathbf{r}'. \tag{5.7}$$

For Equation 5.7 to be true for any ψ, its kernel, $\sum_m \phi_m^*(\mathbf{r}')\phi_m(\mathbf{r})$, must be equal to $\delta(\mathbf{r}-\mathbf{r}')$.

5.2.2 Dirac Notation

For the derivation of the renormalized perurbation expansion it is useful to introduce Dirac notation, where the relevant functions are written with respect to $|\mathbf{r}\rangle$, the eigenvector of the position operator. The following set of equations defines the transformation from functional form to Dirac notation:

$$\phi_n(\mathbf{r}) = \langle \mathbf{r}|\phi_n\rangle\,, \quad \phi_n^*(\mathbf{r}) = \langle \phi_n|\mathbf{r}\rangle \tag{5.8}$$

$$\delta(\mathbf{r}-\mathbf{r}')\mathbf{L}(\mathbf{r}) \equiv \langle\mathbf{r}|\mathbf{L}|\mathbf{r}'\rangle \tag{5.9}$$

$$\mathbf{G}(\mathbf{r},\mathbf{r}';z) \equiv \langle\mathbf{r}|\mathbf{G}(z)|\mathbf{r}'\rangle \tag{5.10}$$

$$\delta(\mathbf{r}-\mathbf{r}') = \langle\mathbf{r}|\mathbf{r}'\rangle \tag{5.11}$$

$$\int d\mathbf{r}|\mathbf{r}\rangle\langle\mathbf{r}| = 1. \tag{5.12}$$

With this new notation the orthonormality of the eigenfunctions and Equations 5.2, 5.3 and 5.5 can be written as:

$$\langle\phi_n|\phi_m\rangle = \delta_{nm} \tag{5.13}$$

$$(z-\mathbf{L})\mathbf{G}(z) = 1 \tag{5.14}$$

$$\mathbf{L}|\phi_n\rangle = \lambda_n|\phi_n\rangle \tag{5.15}$$

$$\sum_n |\phi_n\rangle\langle\phi_n| = 1. \tag{5.16}$$

The original notation can be recovered by taking the inner product with $\langle\mathbf{r}|$ and $|\mathbf{r}'\rangle$. Aside from simplifying the algebra, the Dirac notation allows one to express all equations in **k**-space, which is equivalent to taking the Fourier transform of the original equations with respect to **r** and **r**′.

In applying the RPE method to the C_{60} molecular transistor, the system will be modeled as a 1-dimensional infinite lattice and G(**m**,**m**) will be equal to the amplitude in reciprocal space to find an electron on site **m** given that it began there.

If all eigenvalues of $z-\mathbf{L}$ are non-zero, meaning that $z \neq \{\lambda_n\}$, then Equation 5.14 can be formally solved,

$$\mathbf{G}(z) = \frac{1}{z-\mathbf{L}}. \tag{5.17}$$

The Green function can be written in with respect to a basis set by inserting a complete set of states (Equation 5.16) into Equation 5.17,

$$\begin{aligned}\mathbf{G}(z) &= \frac{1}{z-\mathbf{L}}\sum_n |\phi_n\rangle\langle\phi_n| \\ &= \sum_n \frac{1}{z-\mathbf{L}}|\phi_n\rangle\langle\phi_n| \\ &= \sum_n \frac{|\phi_n\rangle\langle\phi_n|}{z-\lambda_n}. \end{aligned} \tag{5.18}$$

The final form of Equation 5.18 was obtained using the relation $f(L)|\phi_n\rangle = f(\lambda_n)|\phi_n\rangle$, which is valid for any well-behaved function $f(L)$. Equation 5.18 can be rewritten as follows in order to incorporate a general eigenspectrum:

$$G(z) = \sum_n{}' \frac{|\phi_n\rangle\langle\phi_n|}{z-\lambda_n} + \int' dn \frac{|\phi_n\rangle\langle\phi_n|}{z-\lambda_n}. \tag{5.19}$$

All of the eigenvalues of L are real since it is an Hermitian operator. Therefore, if $\mathrm{Im}\{z\} \neq 0$, then $z \neq \{\lambda_n\}$ and G(z) is analytic in the complex z-plane, except for the parts of the real z-axis that correspond to the eigenvalues of L. This means that G(z) has simple poles at the discrete eigenvalues of L, or conversely that the poles of G(z) give the discrete eigenvalues of L.

5.3 Renormalized Perturbation Expansion for a Tight Binding Problem

Consider a tight binding Hamiltonian, $H = H_0 + H_1$. H_0 is a Hamiltonian with known energy levels, $\{\varepsilon_\mathbf{l}\}$, and eigenstates, $\{|\mathbf{l}\rangle\}$, and represents the site energies

for infinite 1-dimensional tight binding lattice. H_1 is a perturbation to H_0, and represents the coupling, V, between nearest neighbouring sites on the lattice. The Hamiltonians are written in Dirac notation as:

$$H_0 = \sum_{\mathbf{l}} \varepsilon_{\mathbf{l}} |\mathbf{l}\rangle\langle\mathbf{l}| \tag{5.20}$$

$$H_1 = \sum_{\mathbf{l},\mathbf{m}}^{*} V |\mathbf{l}\rangle\langle\mathbf{m}|. \tag{5.21}$$

The asterisk above the second summation is a reminder that the outer product in H_1 applies only to neighbouring sites due to the assumption of a tight binding system. Also, for ease of calculation the set representing the eigenstates of H_0, $\{|\mathbf{l}\rangle\}$, is taken to be orthonormal so the inner product between elements is the following:

$$\langle\mathbf{l}|\mathbf{m}\rangle = \delta_{\mathbf{l},\mathbf{m}}. \tag{5.22}$$

The eigenspectra for the full Hamiltonian, H, and the unperturbed Hamiltonian, H_0 are defined as follows:

$$\begin{aligned} H\Psi_n &= \Lambda_n \Psi_n \\ H_0\psi_n &= \lambda_n \psi_n, \end{aligned}$$

where $\{\Lambda_n\}$ is defined as the set of eigenvalues for the full Hamiltonian and $\{\lambda_n\}$ is defined as the set of eigenvalues for the unperturbed Hamiltonian. If it is assumed that z does not equal any of the eigenvalues of H nor H_0 ($z \neq \{\Lambda_n\}$, $z \neq \{\lambda_n\}$) then Equation 5.17 can be used to expand G(z) as follows:

$$G(z) = (z - H)^{-1} = (z - H_0 - H_1)^{-1} \ , \ G_0 = (z - H_0)^{-1} \tag{5.23}$$

$$\begin{aligned} G(z) &= (G_0^{-1} - H_1)^{-1} &&= G_0 G_0^{-1} (G_0^{-1} - H_1)^{-1} \\ &&&= G_0 (1 - H_1 G_0)^{-1} \\ &&&= G_0 (1 + H_1 G_0 + H_1 G_0 H_1 G_0 + \ldots) \\ &&&= G_0 + G_0 H_1 G_0 + G_0 H_1 G_0 H_1 G_0 + \ldots \end{aligned} \tag{5.24}$$

The relation $A^{-1}B^{-1} = (BA)^{-1}$ was used to simplify the expression. The matrix elements in the above expression can be found by taking the inner product with $\langle \mathbf{l}|$ and $|\mathbf{m}\rangle$, which gives the probability to find a particle at site $\mathbf{m}$ given that it begins at site $\mathbf{l}$ in a lattice of arbitrary dimension. This gives an infinite sum representation for the Green function,

$$\begin{aligned} G(\mathbf{l}, \mathbf{m}) &= \langle \mathbf{l}|G|\mathbf{m}\rangle \\ &= G_0(\mathbf{l}, \mathbf{m}) + \sum_{\mathbf{n}_1, \mathbf{n}_2} G_0(\mathbf{l}, \mathbf{n}_1) \langle \mathbf{n}_1|H_1|\mathbf{n}_2\rangle G_0(\mathbf{n}_2, \mathbf{m}) \\ &\quad + \sum_{\mathbf{n}_1, \mathbf{n}_2, \mathbf{n}_3, \mathbf{n}_4} G_0(\mathbf{l}, \mathbf{n}_1) \langle \mathbf{n}_1|H_1|\mathbf{n}_2\rangle G_0(\mathbf{n}_2, \mathbf{n}_3) \langle \mathbf{n}_3|H_1|\mathbf{n}_4\rangle G_0(\mathbf{n}_4, \mathbf{m}) + \ldots \end{aligned} \tag{5.25}$$

This expression may be simplified by recalling that the Hamiltonian only couples neighbouring sites,

$$\langle \mathbf{l}|H_1|\mathbf{m}\rangle = V \delta_{\mathbf{l}, \mathbf{m}+1}, \tag{5.26}$$

and also by rewriting the expression for the Green function,

$$G_0(\mathbf{l},\mathbf{m}) = \delta_{\mathbf{l},\mathbf{m}} G_0(\mathbf{l}). \tag{5.27}$$

With these changes, the Green function expression reduces to:

$$\begin{aligned} G(\mathbf{l},\mathbf{m}) &= \delta_{\mathbf{l},\mathbf{m}}\, G_0(\mathbf{l}) + G_0(\mathbf{l})\, V\, G_0(\mathbf{m})\, \delta_{\mathbf{l},\mathbf{m}+1} \\ &+ \sum_{\alpha} G_0(\mathbf{l})\, V\, G_0(\alpha)\, V\, G_0(\mathbf{m}) + \ldots \end{aligned} \tag{5.28}$$

The diagonal matrix elements of the Green function ($G(\mathbf{l},\mathbf{l})$) are often referred to as 'locators', and the off diagonal elements ($G(\mathbf{l},\mathbf{m})$) as 'propagators' because each term in the above sum represents a different path from site $\mathbf{l}$ to site $\mathbf{m}$ on the lattice, where the path is comprised of steps that connect a given lattice site to a nearest neighbour. The first term in Equation 5.28 is a path from site $\mathbf{l}$ to site $\mathbf{l}$ (or equivalently, from $\mathbf{m}$ to $\mathbf{m}$). The second term represents all paths from any nearest neighbouring site of $\mathbf{l}$ to $\mathbf{l}$ (note that the sites are labeled in bold in order to account for higher dimensinal lattices). The third term represents all paths from the nearest neighbour of the nearest neighbour of $\mathbf{l}$ to $\mathbf{l}$, and so on. In fact, there is a one to one correspondence between the set of all possible paths connecting site $\mathbf{l}$ to site $\mathbf{m}$ on the lattice and the terms in the above summation,

$$G(\mathbf{l},\mathbf{m}) = \sum(\text{all paths connecting site l to site m}). \tag{5.29}$$

To enumerate the paths, a basis set of paths that connect site $\mathbf{l}$ to site $\mathbf{l}$ is constructed. These paths, called skeleton paths, are self-avoiding paths that connect site $\mathbf{l}$ to site $\mathbf{m}$ directly, without revisiting any site, and without any extraneous excursions over the remainder of the lattice. The red and blue paths connecting site

l to site **m** in Figure 5.1 are examples of skeleton paths. Each skeleton paths is the foundation for a family of paths, whose members connect the two sites via all possible decorated skeleton paths, where a decorated skeleton path is the original path, decorated with any number of allowed excursions over the lattice. The green arrows in Figure 5.1 are examples of decorations of the red and blue skeleton paths. The Green function can be written more precisely now,

$$G(\mathbf{l},\mathbf{m}) = \sum_{\text{Decorations}} \{\text{Skeleton Paths}\}\,. \tag{5.30}$$

To evaluate the summation the following notation will be used: Each lattice site that is contained in a given path is counted as a factor of $G_0(\mathbf{n})$. Each step connecting lattice sites contained in the path is counted as a factor of V.

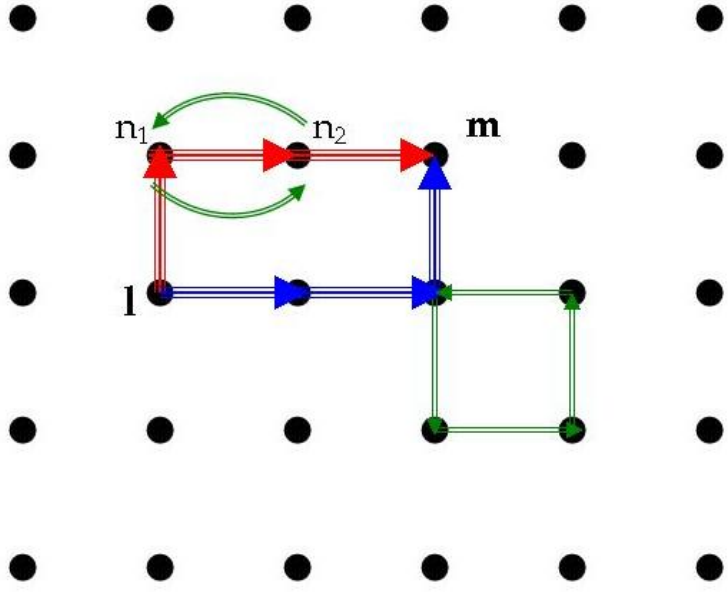

Figure 5.1: Sample pathways from site **l** to site **m** in a 2-d lattice.

Using this notation, the red skeleton path including the green decoration depicted in Figure 5.1 is expressed as:

$$G_0(\mathbf{l})VG_0(\mathbf{n}_1)VG_0(\mathbf{n}_2)VG_0(\mathbf{n}_1)VG_0(\mathbf{n}_2)VG_0(\mathbf{m}). \tag{5.31}$$

Equation 5.31 is equal to one element of the sixth term in Equation 5.28. The summation of elements that comprises the sixth term is equivalent to all of the distinct three step paths that connect site $\mathbf{l}$ to site $\mathbf{m}$. The blue path is an alternate three step skeleton path from site $\mathbf{l}$ to site $\mathbf{m}$, with the green portion depicting a possible decoration. It can be seen by inspection that the sum of all decorated skeleton paths connecting site $\mathbf{l}$ to site $\mathbf{m}$ is equivalent to the infinite sum representation of the Green function given in Equation 5.28.

To count all of the excursions on a particular skeleton path, recognize that any diagonal matrix element, for instance $G(\mathbf{l},\mathbf{l})$, is defined as the sum of all paths beginning and ending at the site $\mathbf{l}$. The expression in Equation 5.31 can be expanded so that it represents all decorated paths that follow the red skeleton path by replacing $G_0(\mathbf{l})$ by $G(\mathbf{l},\mathbf{l})$. Now that all possible excursions beginning and ending at site $\mathbf{l}$ have been counted, the same procedure can be applied to the next site visited in the path, being careful to make sure that site $\mathbf{l}$ is not revisited, since all excursions originating from that site have already been counted. To express this, it is convenient to adopt the notation $G(\mathbf{n}_1,\mathbf{n}_1\,[\mathbf{l}])$, which denotes the sum of all paths beginning and ending at $\mathbf{n}_1$ when it is forbidden to pass through site $\mathbf{l}$. In other words, this is the $\mathbf{n}_1,\mathbf{n}_1$ matrix element of H in the limit that $\varepsilon_{\mathbf{l}}$ approaches infinity (since $\varepsilon_{\mathbf{l}} \to \infty$ means that $G_0(\mathbf{l}) = 0$). Continuing in this way, the sum of all possible decorations of the red skeleton path in Figure 1 is:

$$G(\mathbf{l},\mathbf{l})\,V\,G(\mathbf{n}_1,\mathbf{n}_1\,[\mathbf{l}])\,V\,G(\mathbf{n}_2,\mathbf{n}_2\,[\mathbf{l},\mathbf{n}_1])\,V\,G(\mathbf{n}_3,\mathbf{n}_3\,[\mathbf{l},\mathbf{n}_1,\mathbf{n}_2]) \times V\,G(\mathbf{m},\mathbf{m}\,[\mathbf{l},\mathbf{n}_1,\mathbf{n}_2,\mathbf{n}_3]). \tag{5.32}$$

As long as all of the skeleton paths can be determined, the Green function $G(\mathbf{l}, \mathbf{m})$ can be expressed as the sum of all possible paths connecting site $\mathbf{l}$ to site $\mathbf{m}$. Equation 5.28 can be rewritten in the new formalism as:

$$G(\mathbf{l}, \mathbf{m}) = \sum_{\text{skeleton paths}} G(\mathbf{l}, \mathbf{l})\, V\, G(\mathbf{n}_1, \mathbf{n}_1, [\mathbf{l}])\, V\, G(\mathbf{n}_2, \mathbf{n}_2, [\mathbf{l}, \mathbf{n}_1])\, V \\ .... V\, G(\mathbf{m}, \mathbf{m}[\mathbf{l}, \mathbf{n}_1, \mathbf{n}_2, ...]). \tag{5.33}$$

Using this notation, the diagonal matrix elements take the following form:

$$G(\mathbf{l}, \mathbf{l}) = G_0(\mathbf{l}) + \sum_{\text{skeleton paths}} G(\mathbf{l}, \mathbf{l})\, V\, G(\mathbf{n}_1, \mathbf{n}_1, [\mathbf{l}])\, V .... V\, G_0(\mathbf{l}). \tag{5.34}$$

The final term of all skeleton paths for diagonal matrix elements, $G(\mathbf{l}, \mathbf{l})$, will always be $G_0(\mathbf{l})$ since all decorations originating from site $\mathbf{l}$ were counted in the first term of the path. A 'self-energy' expression can also be identified, $\Delta(\mathbf{l})$, in Equation 5.34 that represents the electron's interaction with the remainder of the chain:

$$\Delta(\mathbf{n}) \equiv \sum_{\text{skeleton paths}} V\, G(\mathbf{n}_1, \mathbf{n}_1, [\mathbf{l}])\, V G(\mathbf{n}_2, \mathbf{n}_2, [\mathbf{n_1}, \mathbf{l}])\, V .... V. \tag{5.35}$$

The Green function representing site locators, Equation 5.34, can be rewritten in terms of the self-energy,

$$G(\mathbf{l}, \mathbf{l}) = G_0(\mathbf{l}) + G(\mathbf{l}, \mathbf{l})\, \Delta(\mathbf{l})\, G_0(\mathbf{l}). \tag{5.36}$$

Finally, we can solve Equation 5.36 to obtain an expression for the site locator,

$$G(\mathbf{l},\mathbf{l};z) = \frac{G_0(\mathbf{l})}{1 - G_0(\mathbf{l})\,\Delta(\mathbf{l};z)} = \frac{1}{z - \varepsilon_{\mathbf{l}} - \Delta(\mathbf{l};z)}. \tag{5.37}$$

The expressions for $G(\mathbf{l},\mathbf{m})$, $G(\mathbf{l},\mathbf{l})$ and $\Delta(\mathbf{l})$ are known as the renormalized perturbation expansion (RPE) equations. The price that is paid for the achievement of simple summations over self-avoiding paths is the complicated Green functions that are entangled within them. The RPE can be reapplied to evaluate functions such as $G(\mathbf{n}_1,\mathbf{n}_1[\mathbf{n}_2,\mathbf{n}_3,...])$, iterating the procedure until the expressions are fully simplified. This procedure is demonstrated in the following section.

5.4 Example: One Dimensional Infinite Chain

Although convergence of the RPE equations is not always assured, the method works well for several paradigm systems such as Bethe lattices, which are related to Cayley trees. A Cayley tree with a connectivity of q is formed by drawing q bonds from an isolated vertex. The q vertices at the ends of the bonds form the first shell of the lattice. This procedure is continued iteratively, where $(q-1)$ bonds are drawn from each new extremity. The second shell is comprised of the second set of $q(q-1)$ vertices, the third shell from the next set of $q(q-1)^2$ vertices, and so on. The $n_t h$ shell contains $q(q-1)^{n-1}$ vertices. A Bethe lattice can be thought of as the limit of an infinite Cayley tree, [AP95]. A Bethe lattice has no surface, and its connectivity k is defined to be $q-1$. A Bethe lattice with $k=2$ is shown in Figure 5.2.

The model for the C_{60} transistor system is an infinite one dimensional chain (a Bethe lattice with connectivity equal to one) with a central defect site. Because of this, it is useful to demonstrate the iteration procedure on an infinite, uniform, one dimensional chain, shown in Figure 5.3.

For an infinite one-dimensional chain there are two self-avoiding paths originating

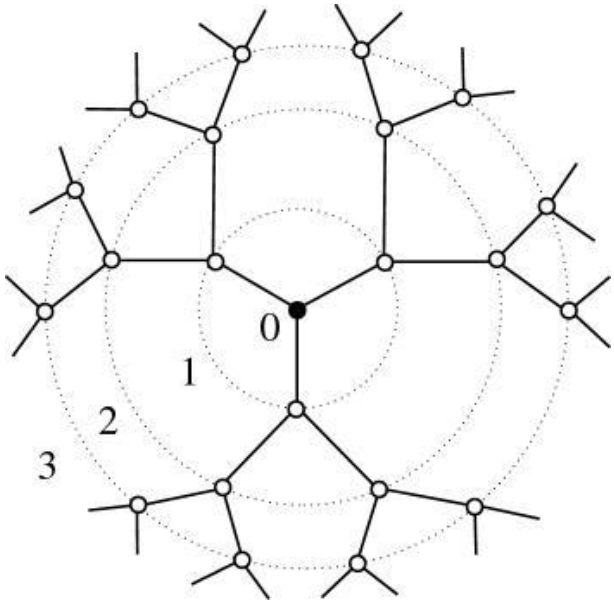

Figure 5.2: A Bethe lattice with connectivity equal to two.

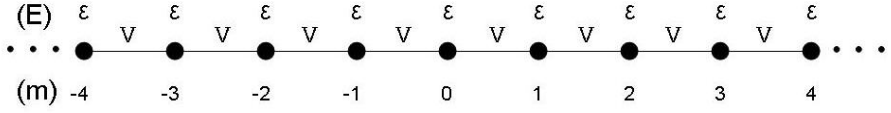

Figure 5.3: Uniform 2-dimensional chain.

from a given site, to the left and to the right of the site in question. The self energy,

$$\begin{aligned} \Delta(\mathbf{l}) &= V\,G(\mathbf{l}+1,\mathbf{l}+1[\mathbf{l}])\,V + V\,G(\mathbf{l}-1,\mathbf{l}-1[\mathbf{l}])\,V \\ &= \Delta_L + \Delta_R, \end{aligned} \tag{5.38}$$

is the sum of a continuation to the left, Δ_L, and a continuation to the right, Δ_R.

If the chain is assumed to be uniform, then $\Delta_L = \Delta_R$ and the self energy can be simplified to

$$\Delta(\mathbf{l}) = 2V^2 G(\mathbf{l}+1, \mathbf{l}+1[\mathbf{l}]). \tag{5.39}$$

In general, for a uniform Bethe lattice with connectivity k, the self energy is modified by replacing the overall multiplicative factor of 2 with (k+1),

$$\Delta(\mathbf{l}) = (k+1)V^2 G(\mathbf{l}+1, \mathbf{l}+1[\mathbf{l}]). \tag{5.40}$$

Next the RPE equation for $G(\mathbf{l}, \mathbf{l})$ is used (Equation 5.37) to rewrite $G(\mathbf{l}+1, \mathbf{l}+1)$ as a function of $\Delta(\mathbf{l})$,

$$G(\mathbf{l}+1, \mathbf{l}+1[\mathbf{l}]) = \frac{1}{z - \varepsilon - \Delta(\mathbf{l}+1[\mathbf{l}])}. \tag{5.41}$$

The self energy that is contained in the $\mathbf{l}+1$ locator is equal to

$$\Delta(\mathbf{l}+1[\mathbf{l}]) = V^2 G(\mathbf{l}+2, \mathbf{l}+2[\mathbf{l}+1]). \tag{5.42}$$

Notice that the multiplicative factor of two that is present in $\Delta(\mathbf{l})$ is not included in $\Delta(\mathbf{l}+1[\mathbf{l}])$ because it is a reduced self energy that only represents explorations over half of the chain. The expression for $G(\mathbf{l}+2, \mathbf{l}+2[\mathbf{l}+1])$ can be replaced with $G(\mathbf{l}+1, \mathbf{l}+1[\mathbf{l}])$ in the reduced self energy because they are equivalent for a uniform chain, and then Equation 5.42 can be replaced with Equation 5.41 to obtain a form that is independent of $\Delta(\mathbf{l})$,

$$G(\mathbf{l}+1, \mathbf{l}+1[\mathbf{l}]) = \frac{1}{z - \varepsilon - V^2 G(\mathbf{l}+1, \mathbf{l}+1[\mathbf{l}])}. \tag{5.43}$$

The solution is an equation that is quadratic in $G(\mathbf{l}+1,\mathbf{l}+1[\mathbf{l}])$,

$$(z-\varepsilon)G(\mathbf{l}+1,\mathbf{l}+1[\mathbf{l}]) - V^2G^2(\mathbf{l}+1,\mathbf{l}+1[\mathbf{l}]) = 1, \tag{5.44}$$

which gives the following double valued result for $G(\mathbf{l}+1,\mathbf{l}+1[\mathbf{l}])$:

$$G(\mathbf{l}+1,\mathbf{l}+1[\mathbf{l}]) = \frac{(z-\varepsilon) \pm \sqrt{(z-\varepsilon)^2 - 4V^2}}{2V^2} \tag{5.45}$$

$$\tag{5.46}$$

The correct solution (negative) can be chosen by taking the limit as $V \to 0$ and requiring that $G(\mathbf{l}+1,\mathbf{l}+1[\mathbf{l}]) \to \frac{1}{z-\varepsilon}$. The Green function can then be written as:

$$G(\mathbf{l}+1,\mathbf{l}+1[\mathbf{l}]) = \frac{(z-\varepsilon) - \sqrt{(z-\varepsilon)^2 - 4V^2}}{2V^2} \tag{5.47}$$

$$= \frac{2}{(z-\varepsilon) + \sqrt{(z-\varepsilon)^2 - 4V^2}}. \tag{5.48}$$

This my be substituted into Equation 5.40 to give an expression for the self energy:

$$\Delta(\mathbf{l}) = \frac{4V^2}{(z-\varepsilon) + \sqrt{(z-\varepsilon)^2 - 4V^2}}. \tag{5.49}$$

And finally, this self-energy can be substituted into the RPE equation for the Green function, Equation 5.37, to give the well-known expression for the site $\mathbf{l}$ locator for a uniform one-dimensional tight-binding lattice,

$$\begin{aligned} G(\mathbf{l},\mathbf{l};z) &= \frac{1}{z-\varepsilon-\frac{4V^2}{(z-\varepsilon)+\sqrt{(z-\varepsilon)^2-4V^2}}} \\ &= \frac{1}{\sqrt{(z-\varepsilon)^2-4V^2}}. \end{aligned} \tag{5.50}$$

This shows how the RPE equations can be manipulated to yield simple expressions for the Green functions of a one dimensional infinite chain. This process can be repeated for Bethe lattices of arbitrary dimension, making the RPE an ideal starting point for modeling the current-voltage characteristics of a single molecular transistors, because it allows the model to be extended to higher dimensions.

Summary:

The Renormalized Perturbation Expansion is an exact method for calculating Green functions. In order to calculate the tunnelling rates for the one dimensional lattice that is used in this thesis, the probability amplitude for a particle that begins on the mth site to remain on the mth site will be needed. In the Green function formalism this is defined as the site locator for the mth site, and is equal to:

$$G(m,m;z) = \frac{1}{z - \varepsilon_m - \Delta(m;z)}$$

The variable z is equal to the Fourier transform variable.

For a one-dimensional lattice that is infinite, tight-binding and uniform, with a site-site interaction that is defined by $< m|H|n >= V\delta_{m,n\pm1}$, the self energy is equal to:

$$\begin{aligned} \Delta(m;z) &= \Delta_L(m;z) + \Delta_R(m;z) \\ &= 2V^2 G(m \pm 1, m \pm 1[m]) \end{aligned}$$

Chapter 6

Electron Hopping Rates

6.1 Preliminary Calculation

The rates for a single electron to tunnel through the metal-molecule bonds for the C_{60} transistor system are calculated using a tight-binding model for the system. It is assumed that the electron tunnelling takes longer than vibrational relaxation, which means that the molecule relaxes to its vibrational ground state between successive tunnelling events, and that the fermi seas in the electrodes are always in equilibrium. The method for deriving the hopping rates is developed in stages, using successively more complicated model systems, eventually leading to tunnelling rates that are representative of the C_{60} molecular transistor system. The first, and simplest system that is examined is a one dimensional infinite chain with a central defect site. The central defect site represents the C_{60} molecule, more specifically the LUMO level that is active in the tunnelling process, which is weakly coupled to the uniform chains of sites to its left and right, which represent the gold wires. These sites are strongly coupled by a potential V, implying that the bandwidth of the metal is $4V$. The dimensionless coupling parameters, η_L and η_R, reduce the coupling of the defect site to the chain, and are labelled differently in order to account for the possibility

that the molecule does not reside in the centre of the junction. It is assumed that $\eta_R, \eta_L \ll 1$. This model is illustrated in Figure 6.1.

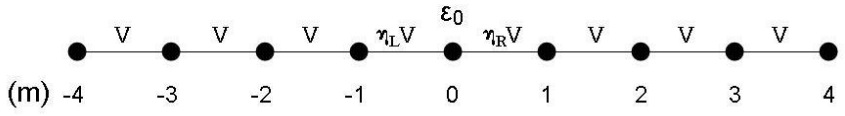

Figure 6.1: Infinite chain with a central defect site.

Without any loss of generality, the initial amplitude for a particle to begin on the zeroth (defect) site of the chain can be taken to be $-i$. Using the RPE method, an expression for the Fourier transform of the site zero propagator can be written, which is simply the amplitude for a particle that begins on site zero to remain on site zero,

$$G(0,0) = \frac{1}{z - \varepsilon_0 - \Delta_L - \Delta_R}. \tag{6.1}$$

The variable z is the Fourier variable, and ε_0 is the site energy for the defect site, which represents the energy of the LUMO. The self energies comes from excursions over the leads to the left and to the right, and can be expanded as

$$\Delta_L(0) = \eta_L^2 V^2 G(-1,-1\,[0]) \tag{6.2}$$

$$\Delta_R(0) = \eta_R^2 V^2 G(1,1\,[0]), \tag{6.3}$$

where

$$G(-1,-1[0]) = G(1,1[0]) = \frac{1}{z - \Delta}. \tag{6.4}$$

The Δ used above represents the (equivalent) self energies for all sites on an infinite, one sided, uniform chain. It therefore represents the (one-sided) self energy for all sites on the chain depicted in Figure 6.1, excluding the zeroth site. In particular, for an arbitrary Green function $G(-n, -n[-n+1])$, Δ is equal to $\Delta(-n[-n+1])$ and for $G(n, n[n-1])$, Δ is equal to $\Delta(n[n-1])$. Since the chain is infinite and all sites except the zeroth one are coupled by the same potential and have equivalent site energies, then provided that $n \neq 0$ and that the zeroth site is excluded, these expressions are equivalent for all n.

A solution for Δ can be found by closing the RPE self-consistently,

$$\begin{aligned} \Delta &= \Delta(-1[0]) = V^2 G(-2, -2[-1]) = V^2 G(-1, -1[0]) && (6.5) \\ &= \frac{V^2}{z - \Delta}. && (6.6) \end{aligned}$$

Solving the quadratic equation gives

$$\Delta = \frac{z}{2} \pm \frac{1}{2}\sqrt{z^2 - 4V^2}, \tag{6.7}$$

with the negative sign giving the correct result, as discussed for Equation 5.45.

This expression for Δ can be used to rewrite Equations 6.1, 6.2, and 6.3 for $G(1, 1[0])$, $\Delta_L(0)$ and $\Delta_R(0)$ as follows

$$\begin{aligned} G(1, 1[0]) &= G(-1, -1[0]) = \frac{2}{z + \sqrt{z^2 - 4V^2}} && (6.8) \\ \Delta_{L/R}(0) &= \frac{2(\eta_{L/R} V)^2}{z + \sqrt{z^2 - 4V^2}}. && (6.9) \end{aligned}$$

Substituting Equation 6.9 into Equation 6.1, the amplitude for a particle beginning on the zeroth site to remain on the zeroth site is

$$G(0,0) = \frac{1}{z - \varepsilon_0 - \frac{2(\eta_L V)^2}{z+\sqrt{z^2-4V^2}} - \frac{2(\eta_R V)^2}{z+\sqrt{z^2-4V^2}}}. \tag{6.10}$$

This may be simplified to the following expression

$$G(0,0) = \frac{1}{z - \varepsilon_0 - \frac{1}{2}(\eta_L^2 + \eta_R^2)(z - \sqrt{z^2-4V^2})}. \tag{6.11}$$

6.1.1 Symmetrically Coupled Defect Site

The first case that will be analyzed has the central site equally coupled to the left and right sites on the chain, which corresponds to the molecule residing in the centre of the junction. Setting η_L equal to η_R, the probability amplitude G(0,0) reduces to

$$\begin{aligned} G(0,0) &= \frac{1}{z - \varepsilon_0 - \eta^2(z - \sqrt{z^2-4V^2})} \\ &= \frac{(z - \varepsilon_0 - \eta^2 z) - \eta^2\sqrt{z^2-4V^2}}{(z - \varepsilon_0 - \eta^2 z)^2 - \eta^4(z^2-4V^2)} \\ &= \frac{z(1-\eta^2) - \varepsilon_0 - \eta^2\sqrt{z^2-4V^2}}{(1-2\eta^2)(z-z_+)(z-z_-)}. \end{aligned} \tag{6.12}$$

The Green function G(0,0) exhibits two simple poles at z_+ and z_- and two branch points at the edges of the energy band at $\pm 2V$. The two simple poles, z_+ and z_-, are equal to

$$z_\pm = \frac{\varepsilon_0(1-\eta^2)}{1-2\eta^2} \pm \frac{\eta^2}{1-2\eta^2}\sqrt{\varepsilon_0^2 - 4V^2(1-2\eta^2)}. \tag{6.13}$$

We note that the poles are complex when the bare molecular energy ε_0 lies within the bandwidth of the leads,

$$-2V\sqrt{1-2\eta^2} < \varepsilon_0 < 2V\sqrt{1-2\eta^2}, \tag{6.14}$$

where the full bandwidth $4V$ has been slightly reduced by the coupling to $4V\sqrt{1-2\eta^2}$.

The time dependence of the function can be recovered by taking the inverse Fourier transform,

$$G(0,0;t) = \frac{1}{2\pi}\int_{-\infty+i\gamma}^{\infty+i\gamma} dz\; e^{-izt}G(0,0;z). \tag{6.15}$$

To evaluate the integral, a contour that extends into the lower half of the complex plane is chosen in order to yield a vanishingly small integrand for $z = -iy$ as $y \to \infty$, and that is lifted infinitesimally above the real axis in order to avoid the singularities of G(0,0;z), as shown in Figure 6.2.

For $\eta \ll 1$, it can be shown that the dominant contribution to the integral is from the pole at z_-,

$$G(0,0;t) \simeq -i\frac{1-\eta^2}{1-2\eta^2}e^{-i\varepsilon_0\frac{1-\eta^2}{1-2\eta^2}t}e^{\frac{-\eta^2\sqrt{4V^2(1-2\eta^2)-\varepsilon_0^2}}{1-2\eta^2}t}. \tag{6.16}$$

The square of this expression gives the probability of finding the particle on site zero,

$$P(t) = |G(0,0;t)|^2 \simeq e^{-2\eta^2\frac{\sqrt{4V^2(1-2\eta^2)-\varepsilon_0^2}}{1-2\eta^2}\,t}. \tag{6.17}$$

This implies an exponential decay rate,

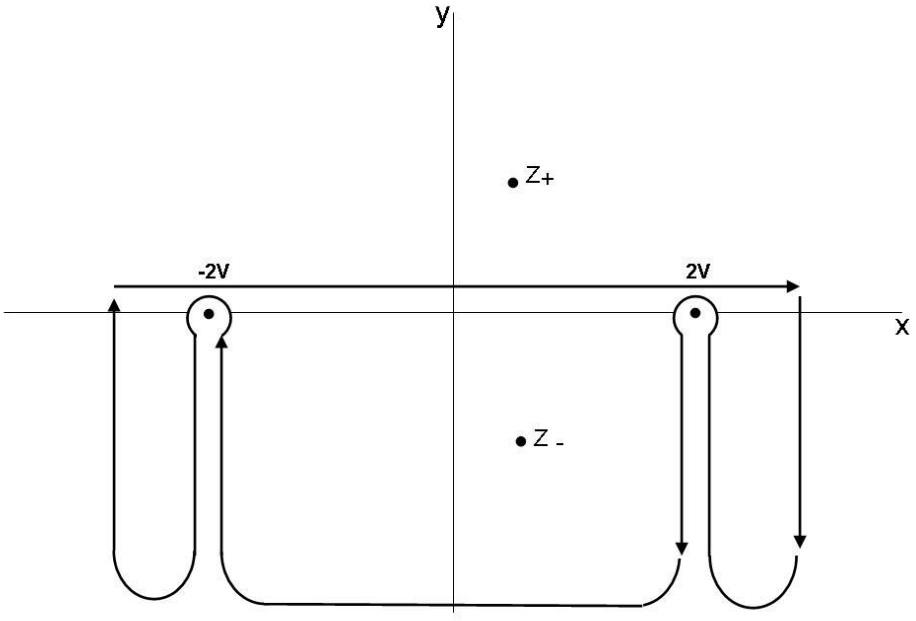

Figure 6.2: Contour for evaluation of the Fourier integral for G(0,0;z). The branch points at ±2V are avoided.

$$\begin{aligned} R &= \frac{2\eta^2}{\hbar}\frac{\sqrt{4V^2(1-2\eta^2)-\varepsilon_0^2}}{(1-2\eta^2)} \\ &= \frac{-2}{\hbar}\mathrm{Im}\{z_-\}. \end{aligned} \tag{6.18}$$

The result can be generalized by returning to the original expression for the site zero propagator,

$$G(0,0) = \frac{1}{z-\varepsilon_0-\Delta_L-\Delta_R} = \frac{1}{z-(\varepsilon_0+\Delta_L+\Delta_R)}, \tag{6.19}$$

from which it is clear that an implicit expression for the pole is

$$z_{-} = \varepsilon_0 + \Delta_L + \Delta_R. \tag{6.20}$$

Insertion of Equation 6.20 into the right hand side of Equation 6.18 shows that the rate for the particle to leave the central site can be formally expressed as the sum of the imaginary parts of the self-energies. The site energy ε_0 is excluded because it is real and does not affect the final result,

$$R = \frac{-2}{\hbar}\mathrm{Im}\{\Delta_L + \Delta_R\}. \tag{6.21}$$

It can be inferred that the two terms represent the tunnelling rates to the left and to the right. Extracting the two terms gives

$$R_L = \frac{-2}{\hbar}\mathrm{Im}\Delta_L; \tag{6.22}$$

$$R_R = \frac{-2}{\hbar}\mathrm{Im}\Delta_R. \tag{6.23}$$

We now have a general formulation for determining the decay rates from a central defect site on an otherwise uniform one dimensional chain. The decay rates are proportional to the imaginary part of the self energies. In the limit of small η, these are equivalent to the Fermi golden rule rates.

6.2 Fermi Sea Considerations

The expressions for the tunnelling rates also need to take the electron occupation of the electrodes into account. This can be accomplished in a formal way by distin-

guishing the terms in our Hamiltonian between those that refer to motion in the leads and those that represent the molecule and its coupling. From the full Hamiltonian,

$$\begin{aligned} H &= \sum_{m\neq 0,1} V(|m\rangle\langle m+1| + |m+1\rangle\langle m|) + \eta_L V(|-1\rangle\langle 0| + |0\rangle\langle -1|) \\ &\quad + \eta_R V(|1\rangle\langle 0| + |0\rangle\langle 1|) + \varepsilon_0 |0\rangle\langle 0| \end{aligned} \tag{6.24}$$

we recognize the part corresponding to the metal leads as,

$$\begin{aligned} H_{metal} &= \sum_{m=1}^{\infty} V(|m\rangle\langle m+1| + |m+1\rangle\langle m|) + \sum_{m=-1}^{-\infty} V(|m\rangle\langle m+1| + |m+1\rangle\langle m|) \\ &= H^R_{metal} + H^L_{metal}, \end{aligned} \tag{6.25}$$

on the right and left respectively, and the part corresponding to the molecule as,

$$H_{molecule} = \varepsilon_0 |0\rangle\langle 0|, \tag{6.26}$$

and finally the part that couples the molecule to the electrodes,

$$H_{int} = \eta_L V\left(|-1\rangle\langle 0| + |0\rangle\langle -1|\right) + \eta_R V\left(|1\rangle\langle 0| + |0\rangle\langle 1|\right). \tag{6.27}$$

The self energy associated with site zero can be re-expressed explicitly in terms of this Hamiltonian,

$$\Delta_L = |\langle 0|H|-1\rangle|^2 \langle -1|\frac{1}{z - H^L_{metal}}|-1\rangle; \tag{6.28}$$

$$\Delta_R = |\langle 0|H|1\rangle|^2 \langle 1|\frac{1}{z - H^R_{metal}}|1\rangle. \tag{6.29}$$

Apart from the variation in coupling to the left and right leads, the Hamiltonian is symmetric about the central site. This means that the two terms in the expression for $H^{L/R}_{metal}$ are equivalent up to the factor of η, and as in the previous section describe a one-sided infinite chain. The expressions for the self energy are also equivalent up to the factor of η.

The expression for $\langle 1|\frac{1}{z-H_{metal(R)}}|1\rangle$ can be expanded using k-space eigenstates of the metal,

$$\langle 1|\frac{1}{z - H_{metal(R)}}|1\rangle = \sum_{k,k'} \langle 1|k\rangle \langle k|\frac{1}{z - H_{metal(R)}}|k'\rangle \langle k'|1\rangle . \tag{6.30}$$

Since $\langle k|\frac{1}{z-H_{metal(R)}}|k'\rangle = \delta_{k,k'}\frac{1}{z-\varepsilon_k}$, the expression can be simplified to

$$\langle 1|\frac{1}{z - H_{metal(R)}}|1\rangle = \sum_{k} |\langle 1|k\rangle|^2 \frac{1}{z - \varepsilon_k}. \tag{6.31}$$

Therefore, the self energy can be written as an integral over the energy density ρ of k-states,

$$\Delta_R = \eta_R^2 V^2 \int d\varepsilon \rho(\varepsilon) \frac{|\langle 1|k(\varepsilon)\rangle|^2}{z - \varepsilon}. \tag{6.32}$$

The above expression can be equated to Equation 6.9 that describes the self energy for a one-sided chain, showing formally that

$$\begin{aligned}\sum_k |\langle 1|k\rangle|^2 \frac{1}{z-\varepsilon_k} &= \frac{2}{z+\sqrt{z^2-4V^2}} \\ &= \frac{z-\sqrt{z^2-4V^2}}{2V}.\end{aligned} \tag{6.33}$$

Notice that there are no poles in the right hand side expression, implying that there are no localized states that overlap the site m=1. Notice also that the Green function becomes complex when $z^2 < 4V^2$:

$$\begin{aligned}G(1,1[0]) &= \frac{1}{\eta_R^2 V^2}\Delta_R = \frac{2}{z+i\sqrt{4V^2-z^2}} \\ &= \frac{z-i\sqrt{4V^2-z^2}}{2V^2}.\end{aligned} \tag{6.34}$$

Substituting this equation into the previous equation, we find that the imaginary part of the self-energy can be written as

$$\mathrm{Im}\{\Delta_R\} = -\frac{\eta_R^2}{2}\sqrt{4V^2-z^2}. \tag{6.35}$$

We can use this to re-express equation 6.32 as

$$\begin{aligned}-\frac{\eta_R^2}{2}\sqrt{4V^2-z^2} &= \eta_R^2 V^2 \,\mathrm{Im}\lim_{\gamma\to 0}\int d\varepsilon \frac{\rho(\varepsilon)|\langle 1|k(\varepsilon)\rangle|^2}{z+i\gamma-\varepsilon} \\ -\frac{\sqrt{4V^2-z^2}}{2V^2} &= -\pi \lim_{\gamma\to 0}\int d\varepsilon \rho(\varepsilon)|\langle 1|k(\varepsilon)\rangle|^2 \frac{\gamma/\pi}{(z-\varepsilon)^2+\gamma^2} \\ &= -\pi\rho(z)|\langle 1|k(z)\rangle|^2.\end{aligned} \tag{6.36}$$

It follows that

$$\rho(\varepsilon)|\langle 1|k(\varepsilon)\rangle|^2 = \frac{\sqrt{4V^2-\varepsilon^2}}{2\pi V^2} \quad if\ \varepsilon^2 < 4V^2 \tag{6.37}$$

$$= 0 \quad if\ \varepsilon^2 > 4V^2. \tag{6.38}$$

With this, we can rewrite the self energy corresponding to the right electrode as an integral over the single particle energies explicitly in terms of an integral over energy,

$$\Delta_R = \frac{\eta_R^2}{2\pi}\int_{-2V}^{2V} d\varepsilon \frac{\sqrt{4V^2-\varepsilon^2}}{z-\varepsilon}. \tag{6.39}$$

The self energy corresponding to the left electrode is of the same form,

$$\Delta_L = \frac{\eta_L^2}{2\pi}\int_{-2V}^{2V} d\varepsilon \frac{\sqrt{4V^2-\varepsilon^2}}{z-\varepsilon}. \tag{6.40}$$

6.3 Electron Occupancy of the Electrodes

The Fermi function,

$$f(\varepsilon) = \frac{1}{e^{\beta(\varepsilon-\mu)}+1}, \tag{6.41}$$

gives the equilibrium probability that a state with energy ε will be occupied at a given temperature. The probability decays for ε above the fermi energy μ. Alternatively we can look at the probability that a given state is unoccupied, which is given by

$$\overline{f}(\varepsilon) = 1 - f(\varepsilon) = \frac{1}{1 + e^{\beta(\mu-\varepsilon)}}. \tag{6.42}$$

The probability that the electron energy states in the leads are unoccupied is taken into account in the calculation of the hopping rates by including a factor of $1-f(\varepsilon)$ in the self energy expressions, Equations 6.39 and 6.40. This accounts for the fact that many of the paths contributing to the self energy must be excluded due to occupation by other electrons in the metal. If a bias voltage is applied across the gap, the fermi function changes slightly since the applied voltage causes the fermi level of the cathode (reverse bias) or anode (forward bias) to shift according to the applied bias. Figure 6.3 illustrates the application of forward and reverse biases across the gap.

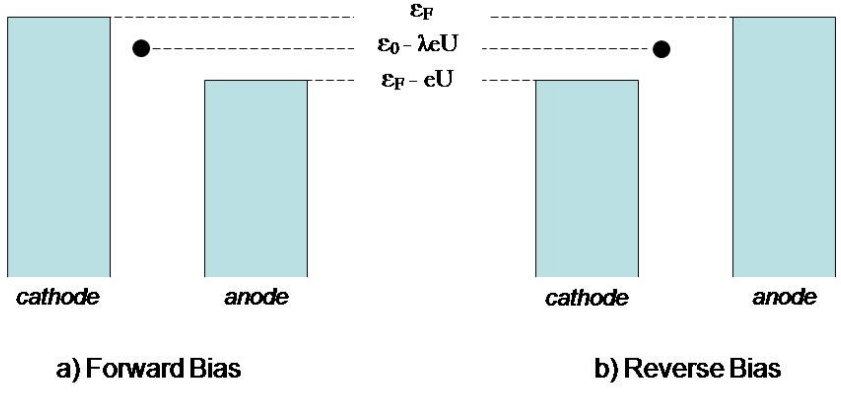

Figure 6.3: Illustration of forward and reverse bias across the electrode gap.

For a forward bias drop of eU, the right hand self energy is modified as,

$$\begin{aligned}\Delta_R &= \frac{\eta_R^2}{2\pi}\int_{-2V-eU}^{2V-eU} d\varepsilon \frac{\sqrt{4V^2-(\varepsilon+eU)^2}}{(z-\varepsilon)\left[1+e^{\beta(\mu-eU-\varepsilon)}\right]} \\ &= \frac{\eta_R^2}{2\pi}\int_{-2V}^{2V} d\widetilde{\varepsilon} \frac{\sqrt{4V^2-\widetilde{\varepsilon}^2}}{(z+eU-\widetilde{\varepsilon})\left[1+e^{\beta(\mu-\widetilde{\varepsilon})}\right]}.\end{aligned} \tag{6.43}$$

In the last line we have changed integration variable to $\widetilde{\varepsilon} = \varepsilon + eU$. The left hand self energy remains unchanged,

$$\Delta_L = \frac{\eta_L^2}{2\pi}\int_{-2V}^{2V} d\varepsilon \frac{\sqrt{4V^2-\varepsilon^2}}{(z-\varepsilon)\left[1+e^{\beta(\mu-\varepsilon)}\right]}. \tag{6.44}$$

The expressions are simplified in the limit that the temperature approaches zero, which is physically significant for the C_{60} transistor system since measurements are made at temperatures of a few Kelvin. In this limit the Fermi function acts as a step function, cutting off all energies smaller than the Fermi energy,

$$\Delta_R = \frac{\eta_R^2}{2\pi}\int_{\mu}^{2V} d\varepsilon \frac{\sqrt{4V^2-\varepsilon^2}}{z+eU-\varepsilon} \tag{6.45}$$

$$\Delta_L = \frac{\eta_L^2}{2\pi}\int_{\mu}^{2V} d\varepsilon \frac{\sqrt{4V^2-\varepsilon^2}}{z-\varepsilon}. \tag{6.46}$$

Notice that because the density of states is finite at $\varepsilon = \mu$, the expressions diverge logarithmically as $z \to (\mu - eU)$ for Δ_R or as $z \to \mu$ for Δ_L. In the neighbourhood of these divergences, the hopping rates switch on and off depending on whether the energy is above or below μ, and thus this is important for describing the I-V behaviour of the junction. The behaviour may be approximated analytically by representing the density of states as a constant in the neighbourhood of interest. Note that the integrated density of states gives,

$$\frac{1}{2\pi}\int_{-2V}^{2V} d\varepsilon\sqrt{4V^2-\varepsilon^2} = V^2 = \frac{\mathrm{w}^2}{16},$$

where w is the bandwidth, 4V. Replacing the term $\sqrt{4V^2-\varepsilon^2}/2\pi$ in Δ_R and Δ_L with the constant w/16 (which will integrate to $\mathrm{w}^2/16$) gives

$$\Delta_R \simeq \frac{\eta_R^2\mathrm{w}}{16}\int_{\mu}^{\mathrm{W}/2}\frac{d\varepsilon}{z+eU-\varepsilon} = \frac{\eta_R^2\mathrm{w}}{16}\ln\left(\frac{z+eU-\mu}{z+eU-\mathrm{w}/2}\right) \tag{6.47}$$

$$\Delta_L \simeq \frac{\eta_L^2\mathrm{w}}{16}\int_{\mu}^{\mathrm{W}/2}\frac{d\varepsilon}{z-\varepsilon} = \frac{\eta_L^2\mathrm{w}}{16}\ln\left(\frac{z-\mu}{z-\mathrm{w}/2}\right) \tag{6.48}$$

Since we must be careful to remain above the real z axis, it is convenient to rewrite $z-\mu$ as $|z-\mu|$ when it is a positive quantity and as $|z-\mu|e^{i\pi}$ when it is a negative quantity. Assuming that we can take $\mathrm{w}/2 >> z$ for any time-dependence of interest, we have $z-\mathrm{w}/2 \approx \mathrm{w}/2\, e^{i\pi}$. With this adjustment, the self-energies become

$$\Delta_R = \frac{\eta_R^2\mathrm{w}}{16}\left[-i\pi+\ln\left(\frac{z+eU-\mu}{\mathrm{w}/2}\right)\right]; \tag{6.49}$$

$$\Delta_L = \frac{\eta_L^2\mathrm{w}}{16}\left[-i\pi+\ln\left(\frac{z-\mu}{\mathrm{w}/2}\right)\right]. \tag{6.50}$$

This is known as the wide band approximation. Putting all of this together, the amplitude for an electron to remain on site zero in the Fourier domain is

$$G(0,0) = \frac{1}{z-\varepsilon_0+\lambda eU-\frac{\eta_R^2\,\mathrm{W}}{16}\ln\left(\frac{z+eU-\mu}{\mathrm{W}/2}\right)-\frac{\eta_L^2\mathrm{W}}{16}\ln\left(\frac{z-\mu}{\mathrm{W}/2}\right)+i\frac{\pi\mathrm{W}}{16}\left(\eta_R^2+\eta_L^2\right)} \tag{6.51}$$

As in Section 6.1, we can find the decay rates by evaluating the imaginary parts of the self energies at the pole z_- in the lower half-plane,

$$R_R = -\frac{\eta_R^2 \mathrm{w}}{8\hbar}\mathrm{Im}\left[-i\pi + \ln\left(\frac{z_+ eU - \mu}{\mathrm{w}/2}\right)\right]; \tag{6.52}$$

$$R_L = -\frac{\eta_L^2 \mathrm{w}}{8\hbar}\mathrm{Im}\left[-i\pi + \ln\left(\frac{z_- \mu}{\mathrm{w}/2}\right)\right]. \tag{6.53}$$

We can see that depending on the value of the pole, the inclusion of the Fermi cut-off energy results in more than one solution for the rates. If the pole lies within the band, meaning that $z > \mu$, then the argument of the logarithm is positive for both the self energy to the left and the self energy to the right, and the logarithm has no imaginary component. This means that the rates are given by

$$R_R = \frac{\eta_R^2 \mathrm{w}\pi}{8\hbar}; \tag{6.54}$$

$$R_L = \frac{\eta_L^2 \mathrm{w}}{8\hbar}. \tag{6.55}$$

If the pole lies between μ and $\mu - eU$, so that $\mu - eU < z_- < \mu$ then the argument of the logarithm in the expression for Δ_L becomes negative and thus has an imaginary component that is equal to π, causing the rate to the left to vanish. In this case the rates are given by

$$R_R = \frac{\eta_R^2 \mathrm{w}\pi}{8\hbar}; \tag{6.56}$$

$$R_L = 0. \tag{6.57}$$

If the pole is less than $\mu - eU$, then both rates vanish.

6.4 Temperature Effects

To incorporate the effect of temperature into the model, we will first return to the case of symmetric coupling ($\eta_L = \eta_R$) and examine the self energy for the case of zero bias. For those parameters, the self energy is:

$$\begin{aligned}\Delta &= \langle 0|H_{int}|-1\rangle\langle -1|\frac{1}{z-H_{metal}}|-1\rangle\langle -1|H_{int}|0\rangle + \langle 0|H_{int}|1\rangle\langle 1|\frac{1}{z-H_{metal}}|1\rangle\langle 1|H_{int}|0\rangle \\ &= \eta^2 V^2\left(\langle -1|\frac{1}{z-H_{metal}}|-1\rangle + \langle 1|\frac{1}{z-H_{metal}}|1\rangle\right) \qquad (6.58)\end{aligned}$$

The inner products $\langle -1|\frac{1}{z-H_{metal}}|-1\rangle$ and $\langle -1|\frac{1}{z-H_{metal}}|-1\rangle$ are equivalent.

Using equations 6.43 and 6.44, the self energy can be written as

$$\Delta = \frac{\eta^2}{\pi}\int_{-2V}^{2V} d\varepsilon \frac{\sqrt{4V^2-\varepsilon^2}}{(z-\varepsilon)\left[1+e^{\beta(\mu-\varepsilon)}\right]}. \qquad (6.59)$$

Setting $\mathrm{w} = 4V$ and replacing $\frac{\sqrt{4V^2-\varepsilon^2}}{2\pi}$ with the constant $\frac{\mathrm{W}}{16}$ in the wide-band approximation gives,

$$\Delta = \frac{\eta^2 \mathrm{w}}{8}\int_{-\infty}^{\mathrm{W}/2} \frac{d\varepsilon}{(z-\varepsilon)\left[1+e^{\beta(\mu-\varepsilon)}\right]}. \qquad (6.60)$$

Integrating by parts gives

$$\Delta = \frac{\eta^2 \mathrm{w}}{8}\left(-\frac{\ln(z-\varepsilon)}{1+e^{\beta(\mu-\varepsilon)}}\Big|_{-\frac{\mathrm{W}}{2}}^{\frac{\mathrm{W}}{2}} + \int_{-\frac{\mathrm{W}}{2}}^{\frac{\mathrm{W}}{2}} d\varepsilon \ln(z-\varepsilon)\frac{\beta}{4}\mathrm{sech}^2\left(\frac{\beta(\mu-\varepsilon)}{2}\right)\right) \qquad (6.61)$$

For low T, we can neglect the evaluation at the lower limit for the first term, since $e^{\beta(\mu+\mathrm{W}/2)} \gg 1$. In the second term, $\mathrm{sech}^2\left(\frac{\beta(\mu-\varepsilon)}{2}\right)$ falls off quickly on both sides of $\varepsilon = \mu$, and so it is possible to replace the limits of integration $\pm\frac{\mathrm{W}}{2}$ by $\pm\infty$. This gives

$$\Delta \approx \frac{\eta^2 \mathrm{w}}{8}\left(-\frac{\ln(z-\mathrm{w}/2)}{1+e^{\beta(\mu-\mathrm{W}/2)}} + \int_{-\infty}^{+\infty} d\varepsilon \ln(z-\varepsilon)\frac{\beta}{4}\mathrm{sech}^2\left(\frac{\beta(\mu-\varepsilon)}{2}\right)\right) \tag{6.62}$$

The factor $e^{\mu-\mathrm{W}/2}$ in the denominator of the first term can also be neglected. This approximation is excellent at low temperature due to the exponential fall-off of the Fermi function. Therefore, at this point it is sufficient to focus on the remaining integral in the above equation,

$$\int_{-\infty}^{+\infty} d\varepsilon \ln(z-\varepsilon)\frac{\beta}{4}\mathrm{sech}^2\left(\frac{\beta(\mu-\varepsilon)}{2}\right) \tag{6.63}$$

As $\mathrm{T} \to 0$, the factor $\frac{\beta}{4}\mathrm{sech}^2\left(\frac{\beta(\mu-\varepsilon)}{2}\right) \to \delta(\varepsilon-\mu)$ goes to a normalized delta function in ε, centered at μ. If we replace this term and carry out the integration, we get $\mathrm{I} = \ln(\mu-\varepsilon)$ which when substituted into Equation 6.62 gives the same result for the self energy that was found in the $T = 0$ case. Therefore we see that in order to capture the effects of finite temperature, we must be careful to retain details pertaining to the nonvanishing width. This is obviously most important when $z \simeq \mu$ so that the logarithm $\ln(z-\varepsilon)$ is quickly changing in the neighbourhood of ε, where $\mathrm{sech}^2\left(\beta(\varepsilon-\mu)\right)$ is strongly peaked.

It is with these details in mind that we suggest the following: In Equation 6.63, we will replace the strongly peaked function $\frac{\beta}{4}\mathrm{sech}^2\left(\frac{\beta(\varepsilon-\mu)}{2}\right)$ by a Lorentzian function,

$$\frac{\beta}{4}\mathrm{sech}^2\left(\frac{\beta(\mu-\varepsilon)}{2}\right) \Rightarrow \frac{\gamma/\pi}{\gamma^2+(\varepsilon-\mu)^2}, \tag{6.64}$$

centred about the same point, and with a width defined as γ that is proportional to kT. With this substitution, as $\mathrm{T} \to 0$ the Lorentzian becomes a δ-function, and the correct result is recovered. On the other hand, for finite temperatures the integral has a simple analytic form. Using the method of residues, it is straightforward to show that

$$\begin{aligned} \lim_{\mathrm{w}\to\infty} I &= \int_{-\frac{\mathrm{W}}{2}}^{\frac{\mathrm{W}}{2}} d\varepsilon \ln(z-\varepsilon)\frac{\gamma/\pi}{\gamma^2+(\varepsilon-\mu)^2} \\ &= \ln(z-\mu+i\gamma). \end{aligned} \tag{6.65}$$

Thus the self energy becomes

$$\Delta = \frac{\eta^2 \mathrm{w}}{8} \ln \frac{(z-\mu+i\gamma)}{(z-\mathrm{w}/2)}. \tag{6.66}$$

It is modified from the zero temperature form by the introduction of a complex fermi energy, where μ is now replaced with $\mu - i\gamma$.

A good choice for γ is $\gamma = \frac{4}{\pi}\mathrm{kT}$. This particular choice for the width of the Lorentzian is motivated by the fact that when the rate of change of R with z is evaluated in the neighbourhood of $z = \mu$, it agrees with the exact result:

$$\frac{dR}{dz}\Big|_{z=\mu} = \frac{\pi\eta^2\mathrm{w}}{8\mathrm{kT}}. \tag{6.67}$$

Using this value for γ, and replacing $\ln(z - \mathrm{w}/2)$ with $i\pi + ln(\mathrm{w}/2)$ for $z \ll \mathrm{w}$, we have

$$\Delta = \frac{\eta^2 \mathrm{w}}{8}\left[\ln\left(\frac{z+i\frac{4}{\pi}\mathrm{kT}-\mu}{\mathrm{w}/2}\right) - i\pi\right]. \tag{6.68}$$

For $|\mathrm{Re}(z)| \gg \mu$ we can neglect $i\frac{4}{\pi}\mathrm{kT}$ in comparison to $z-\mu$ and it follows that the rate is

$$R = -2\mathrm{Im}(\Delta) = \begin{cases} \frac{\pi\eta^2\mathrm{W}}{2} & ; z > \mu \\ 0 & ; z < \mu \end{cases}, \tag{6.69}$$

and turns on and off as expected. The transition occurs in the neighbourhood of $z = \mu$, and in this region the factor of $i\frac{4}{\pi}\mathrm{kT}$ allows the transition to occur smoothly, over a neighbourhood in energy $\mu - \frac{4}{\pi}\mathrm{kT} \leq z \leq \mu + \frac{4}{\pi}\mathrm{kT}$.

6.5 Current

The tunnelling rates that have been calculated represent the rates of decay for the occupation of the central defect site of the lattice, therefore they correspond to the rates for an electron to tunnel off of the molecule. The tunnelling rates that will be used in the master equation formulation for the current are:

$$\Gamma_{cm} = -\frac{\eta_L^2 w}{8}\mathrm{Im}\left[-i\pi + ln\left(\frac{z_-^e + i\frac{4}{\pi}kT - \mu}{w/2}\right)\right] \tag{6.70}$$

$$\Gamma_{am} = -\frac{\eta_R^2 w}{8}\mathrm{Im}\left[-i\pi + ln\left(\frac{z_-^e + i\frac{4}{\pi}kT + eU - \mu}{w/2}\right)\right] \tag{6.71}$$

Recall that the subscript $\{mc\}$ refers to tunnelling from the molecule to the cathode and the subscript $\{ma\}$ refers to a tunnelling event from the molecule to the anode. The superscript e has been added to the resonance pole as a reminder that the tunnelling particle is an electron.

To find the corresponding rates for an electron to tunnel on the molecule, we can think of a hole tunnelling off. In that case, the rates are identical to those for an electron tunnelling off except that the signs of all of the energies must be reversed.

The Green function for emission of a hole is,

$$G_h(0,0) = \frac{1}{zm - \varepsilon_0 + \lambda eU - \frac{\eta_R^2 w}{16}\ln\left(\frac{z+i\frac{4}{\pi}kT-eU+\mu}{w/2}\right) - \frac{\eta_L^2 w}{16}\ln\left(\frac{z+i\frac{4}{\pi}kT+\mu}{w/2}\right) + i\frac{\pi w}{16}(\eta_R^2+\eta_L^2)}, \tag{6.72}$$

and the hole emission rates are:

$$\Gamma_{mc} = -\frac{\eta_L^2 w}{8}\mathrm{Im}\left[-i\pi + ln\left(\frac{z_-^h + i\frac{4}{\pi}kT + \mu}{w/2}\right)\right]; \tag{6.73}$$

$$\Gamma_{ma} = -\frac{\eta_R^2 w}{8}\mathrm{Im}\left[-i\pi + ln\left(\frac{z_-^h + i\frac{4}{\pi}kT - eU + \mu}{w/2}\right)\right]. \tag{6.74}$$

6.6 Electron Phonon Coupling

The stair steps in the I-V curves seen by Park et al. [Par00] have been attributed to coupling of the electron motion with the centre of mass vibrational motion of C_{60} molecules between the gold electrodes. This aspect in incorporated in the model by including a linear site-diagonal coupling to a single harmonic oscillator of frequency ω_0:

$$\begin{aligned} H &= \sum_{m\neq 0,-1} V(|m\rangle\langle m+1| + |m+1\rangle\langle m|) + \eta_L V(|-1\rangle\langle 0| + |0\rangle\langle -1|) \\ &\quad + \eta_R V(|1\rangle\langle 0| + |0\rangle\langle 1|) + (\varepsilon_0 - \lambda e\mathrm{U})|0\rangle\langle 0| - e\mathrm{U}\sum_{m=1}^{\infty} |m\rangle\langle m| \\ &\quad + \frac{p^2}{2m} + \frac{1}{2}m\omega_0^2 x^2 + g\sqrt{2\hbar m\omega_0^3}x|0\rangle\langle 0|, \end{aligned} \tag{6.75}$$

where g is the dimensionless electron-phonon coupling constant.

In the limit of $\eta_L, \eta_R \to 0$, the molecule is isolated from the electrodes and the vibrational eigenstates are those of the displaced oscillator, which can be seen by completing the square in the vibrational potential energy term:

$$H_{vib} = \frac{p^2}{2m} + \frac{1}{2}m\omega_0^2 x^2 + g\sqrt{2\hbar m\omega_0^3}x|0><0| \tag{6.76}$$

$$= \frac{p^2}{2m} + \frac{1}{2}m\omega_0^2\left(x + g\sqrt{\frac{2\hbar}{m\omega_0}}|0><0|\right)^2 - g^2\hbar\omega_0|0><0|. \tag{6.77}$$

The oscillator will tend to relax to a displaced equilibrium position,

$$x_{eq} = -g\sqrt{\frac{2\hbar}{m\omega_0}}, \tag{6.78}$$

if the molecule is occupied by the electron. It will return to $x_{eq} = 0$ once the electron leaves.

The coordinates that decouple the vibrational motion from the electron location are obtained from the unitary transformation [GS71, Ken75],

$$\mathbb{X} = e^{\frac{i}{\hbar}x_{eq}p|0><0|}xe^{-\frac{i}{\hbar}x_{eq}p|0><0|} \tag{6.79}$$

$$= x + x_{eq}|0><0|; \tag{6.80}$$

$$\mathbb{P} = e^{\frac{i}{\hbar}x_{eq}p|0><0|}pe^{-\frac{i}{\hbar}x_{eq}p|0><0|} \tag{6.81}$$

$$= p. \tag{6.82}$$

Under the same transformation, the operators in H that govern the electron transitions are given by

$$||m \gg\ll m'|| = e^{\frac{i}{\hbar}x_{eq}p|0><0|}|m><m'|e^{-\frac{i}{\hbar}x_{eq}p|0><0|} \tag{6.83}$$

$$= |m><m'|e^{\frac{i}{\hbar}x_{eq}p\delta_{m,0}}e^{-\frac{i}{\hbar}x_{eq}p\delta_{m,0}}. \tag{6.84}$$

In this manner, the new Hamiltonion is

$$\mathbb{H} = e^{\frac{i}{\hbar}x_{eq}p|0><0|}He^{-\frac{i}{\hbar}x_{eq}p|0><0|} \tag{6.85}$$

$$\begin{aligned} = & \sum_{m\neq 0,-1} V\left(||m \gg\ll m+1|| + \text{c.c.}\right) \\ & +\eta_L V\left(||-1 \gg\ll 0||e^{-\frac{i}{\hbar}x_{eq}\mathbb{P}} + \text{c.c.}\right) + \eta_R V\left(||1 \gg\ll 0||e^{-\frac{i}{\hbar}x_{eq}\mathbb{P}} + \text{c.c.}\right) \\ & +(\varepsilon_0 - \lambda eU)||0 \gg\ll 0|| - eU\sum_{m=1}^{\infty}||m \gg\ll m|| \\ & +\frac{\mathbb{P}^2}{2m} + \frac{1}{2}m\omega_0^2\mathbb{X}^2 - g^2\hbar\omega_0||0 \gg\ll 0||. \end{aligned} \tag{6.86}$$

The advantage of this transformation is that in the limit of $\eta_L, \eta_R \to 0$ the molecular eigenstates are products of the electronic and vibrational states.

The evolution of the system state is given by

$$|\Psi >= \sum_{m,n} C_{m,n}(t)||m \gg_{site} ||n \gg_{oscillator}, \tag{6.87}$$

where $||m \gg_{site}$ gives the location of the electron and $||n \gg_{oscillator}$ gives the state of the oscillator, and where $n = 0, 1, \ldots$ is the vibrational quantum number. The Hamiltonian can be viewed as describing transitions in a semi-infinite two-dimensional site space, as shown in Figure 6.4. The diagonal coupling terms in the figure reflect the coupling of the electron motion with the oscillator state, and only occur when $|m| \leq 1$. This coupling appears in the Hamiltonian in terms of the form $\eta_L V||-1 \gg\ll 0||e^{-\frac{i}{\hbar}x_{eq}\mathbb{P}}$, etc.

In the experiments of interest, the temperature is low enough that the oscillator will relax to its ground state in equilibrium. Placing the electron on the molecule corresponds to the initial condition, $C_{m,n}(t) = \delta_{m,0}\delta_{n,0}$, assuming that there is sufficient time for the oscillator to undergo vibrational relaxation before the electron moves away. For electrical current, we are interested in the site-probabilities regardless of the state of the oscillator. For example, the probability to be at site $m = 0$ is given by,

$$P_0(t) = \sum_{n=0}^{\infty} \left|C_{n,0}(t)\right|^2 \approx \left|C_{0,0}(t)\right|^2. \tag{6.88}$$

The Green function $G(0, n; 0, 0)$ is proportional to η^2 for $\eta \neq 0$, and therefore for small η_L, η_R all terms in the sum except $n = 0$ can be neglected. In physical terms, this means that the probability that the oscillator will make a transition to

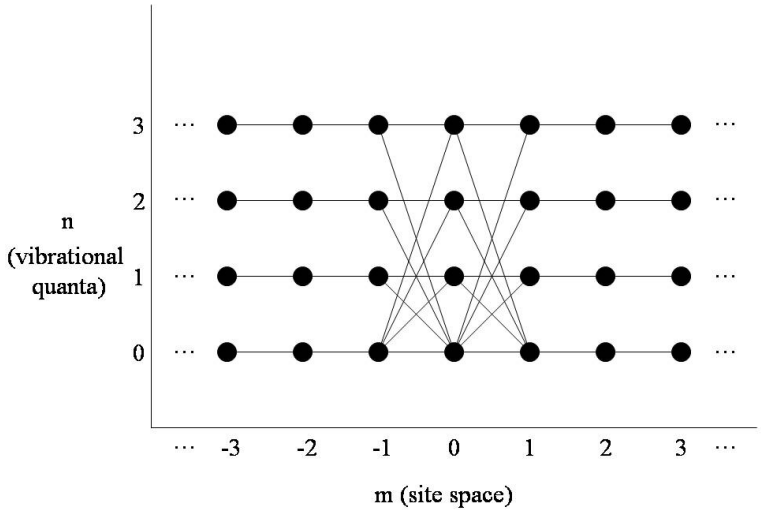

Figure 6.4: Two dimensional site space, where m is the site location of the electron and n is the vibrational quantum number of the oscillator. For $|m| \geq 1$ only horizontal transitions are allowed, however if $|m| \leq 1$ then diagonal transitions are allowed, which is a reflection of the vibrational coupling.

an excited state when the electron remains on the molecule is negligible. Thus, the quantity of interest is the Green function for the dominant process,

$$G_e(0,0;0,0) = \frac{1}{z - \varepsilon_0 + g^2\hbar\omega_0 + \lambda eU - \left(\Delta_L^{(e)} + \Delta_R^{(e)}\right)}. \tag{6.89}$$

Previously we were able to calculate the self energies exactly because we could easily enumerate all of the paths on the one-dimensional chain. With the addition of phonons, there are many diagonal paths forming loops that return to the origin. One example is shown in Figure 6.5. Since each path between the molecule and the leads contributes a factor of η, the term corresponding to the path that is depicted will be proportional to η^6. Assuming convergence of the perturbation expansion, for small enough η we can neglect these higher order terms. The dominant contributions will come from the η^2 terms, which are simple on and off paths, as shown in Figure

6.6.

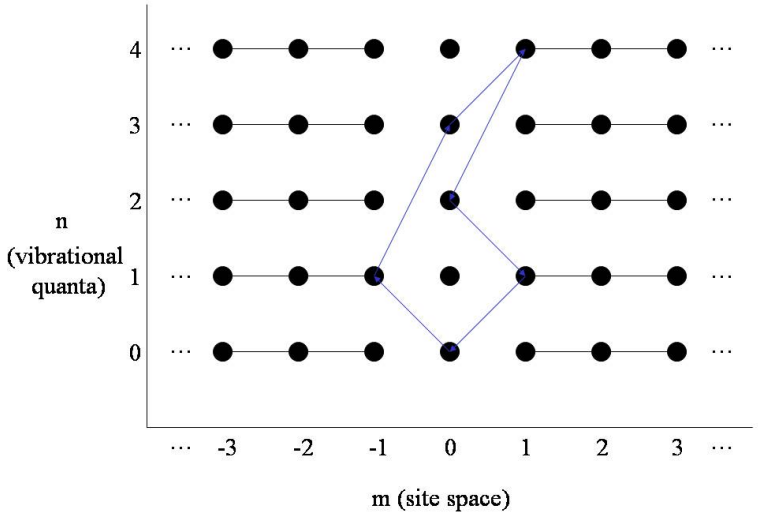

Figure 6.5: Example of a circular path in the two-dimensional site space {m,n}. Prior to the inclusion of phonons, for a one-dimensional system this type of path was referred to as a "decoration" of a skeleton path. Since a factor of ηV is included for each excursion between the molecule and the electrodes, this path is on the order of η^6.

The previous expression is modified by summing over the various self energies, Δ_L and Δ_R, for each vibrational quantum number. The sum is weighted by the square of the matrix obtained each diagonal path,

$$\Delta_L^{(e)} = \sum_{n=0}^{\infty} \left| \langle 0 | e^{\frac{i}{\hbar} x_{eq} \mathbb{P}} | n \rangle \right|^2 \Delta_L(n) \tag{6.90}$$

$$= \sum_{n=0}^{\infty} \frac{e^{-g^2} g^{2n}}{n!} \frac{\eta_L^2 \mathrm{w}}{8} \left(-i\pi + \ln \left(\frac{z - n\omega_0 - \mu + i\frac{4}{\pi} kT}{\mathrm{w}/2} \right) \right), \tag{6.91}$$

where

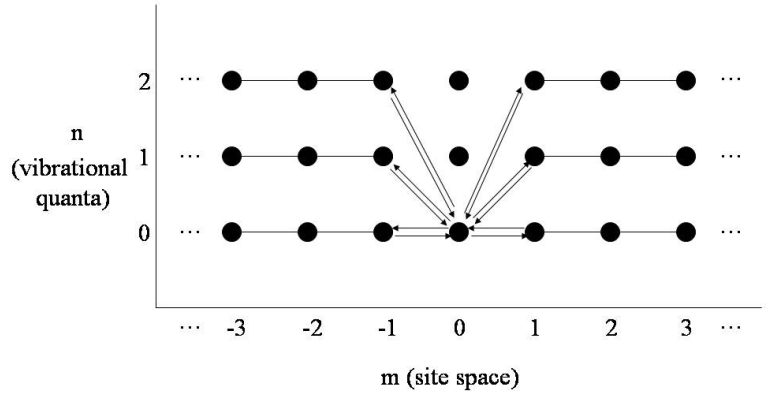

Figure 6.6: Illustration of the dominant paths (on the order of η^2) in the current.

$$\frac{e^{-g^2}g^{2n}}{n!} = \left|\langle 0|e^{\frac{i}{\hbar}x_{eq}\mathbb{P}}|n\rangle\right|^2 \tag{6.92}$$

is the square of the Franck-Condon overlap factor between an oscillator in the ground state and a displaced oscillator in the nth excited state. Similarly,

$$\Delta_R^{(e)} = \sum_{n=0}^{\infty} \frac{e^{-g^2}g^{2n}}{n!}\frac{\eta_R^2 \mathrm{w}}{8}\left(-i\pi + \ln\left(\frac{z - n\omega_0 - eU - \mu + i\frac{4}{\pi}kT}{\mathrm{w}/2}\right)\right). \tag{6.93}$$

The corresponding electron emission rates are

$$R_L^{(e)} = -\frac{\eta_L^2 \mathrm{w}}{4}\mathrm{Im}\sum_{n=0}^{\infty}\frac{e^{-g^2}g^{2n}}{n!}\left[-i\pi + ln\left(\frac{z_-^e - n\omega_0 + i\frac{4}{\pi}kT - \mu}{\mathrm{w}/2}\right)\right] \tag{6.94}$$

$$R_R^{(e)} = -\frac{\eta_R^2 \mathrm{w}}{4}\mathrm{Im}\sum_{n=0}^{\infty}\frac{e^{-g^2}g^{2n}}{n!}\left[-i\pi + ln\left(\frac{z_-^e - n\omega_0 + i\frac{4}{\pi}kT + eU - \mu}{\mathrm{w}/2}\right)\right] \tag{6.95}$$

where to lowest order, $z_{-}^{e} = \varepsilon_0^{'} - \lambda eU$, is the energy of the molecular ion if it is in isolation from the leads, where we define $\varepsilon_0^{'} \equiv \varepsilon_0 - g^2\hbar\omega_0$.

The terms in the sum that contribute to the emission rate are shown in Figure 6.7, where the molecular energy broadens into a "comb" of different energies for different values of n. For each level of the comb that is above the Fermi level of the anode, there is a contribution to electron emission into an unoccupied state. The physical process that corresponds to this is an electron leaving the molecule and creating n phonons in the process. Each contribution, or tooth of the comb, is weighted by the corresponding Franck-Condon factor.

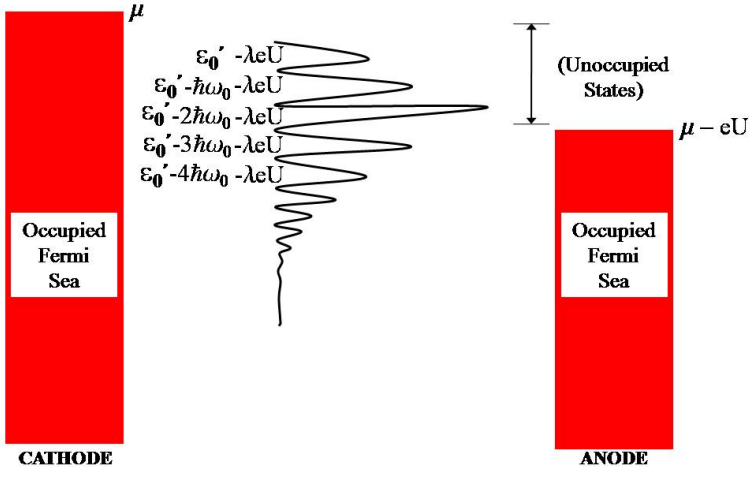

Figure 6.7: The molecular energy "comb". The levels that are above the Fermi level of the anode correspond to electron emission accompanied by the creation of n phonons.

As the source-drain voltage is increased, the molecular energy drops by λeU while the fermi level of the anode drops by eU. This means that the number of teeth that fit in the window of unoccupied states increases with the applied voltage. The emission rate increases abruptly whenever an additional tooth (vibrational mode) crosses the fermi energy of the anode. The emission rate saturates when the entire Franck-

Condon envelope has crossed this point. Figure 6.8 depicts the abrupt increases in the emission rate as the source-drain voltage is applied.

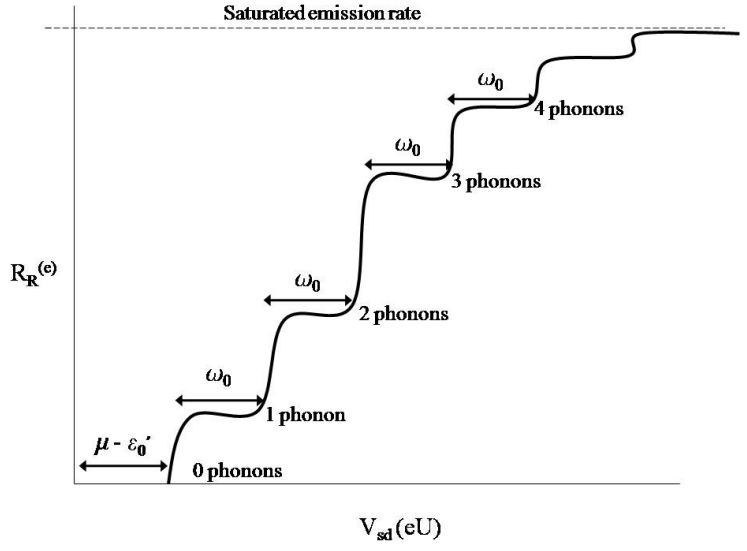

Figure 6.8: The emission rate $R_R^{(e)}$ as a function of the number of phonons emitted. It can be seen that as the bias voltage is applied, additional "teeth" of the molecular energy comb are made accessible to a tunnelling particle.

After the electron leaves the ion another electron will tunnel onto the molecule from the cathode to take its place. The rates for this correspond to electron absorption, however it is easier to consider these events as hole emissions. An illustration of the hole tunnelling process can be obtained by looking at the mirror image of the electron tunnelling process. The hole emission rates are obtained by simply changing the signs of the energy terms in the electron emission rates. Therefore, the site zero locator for a hole that is initially on the molecule is

$$G_h(0,0;0,0) = \frac{1}{z + \varepsilon_0 - g^2\hbar\omega_0 - \lambda eU - \left(\Delta_L^{(h)} + \Delta_R^{(h)}\right)}, \tag{6.96}$$

where

$$\Delta_L^{(h)} = \sum_{n=0}^{\infty} \frac{e^{-g^2} g^{2n}}{n!} \frac{\eta_L^2 \mathrm{w}}{8} \left(-i\pi + \ln \left(\frac{z - n\omega_0 + \mu + i\frac{4}{\pi} kT}{\mathrm{w}/2} \right) \right) \tag{6.97}$$

$$\Delta_R^{(h)} = \sum_{n=0}^{\infty} \frac{e^{-g^2} g^{2n}}{n!} \frac{\eta_R^2 \mathrm{w}}{8} \left(-i\pi + \ln \left(\frac{z - n\omega_0 - eU + \mu + i\frac{4}{\pi} kT}{\mathrm{w}/2} \right) \right). \tag{6.98}$$

The corresponding hole emission rates are

$$\begin{aligned} R_L^{(h)} &= -\frac{\eta_L^2 \mathrm{w}}{4} \mathrm{Im} \sum_{n=0}^{\infty} \frac{e^{-g^2} g^{2n}}{n!} \\ &\quad \times \left[-i\pi + ln \left(\frac{z_-^h - n\omega_0 + i\frac{4}{\pi} kT + \mu}{\mathrm{w}/2} \right) \right] \end{aligned} \tag{6.99}$$

$$\begin{aligned} R_R^{(h)} &= -\frac{\eta_R^2 \mathrm{w}}{4} \mathrm{Im} \sum_{n=0}^{\infty} \frac{e^{-g^2} g^{2n}}{n!} \\ &\quad \times \left[-i\pi + ln \left(\frac{z_-^h - n\omega_0 + i\frac{4}{\pi} kT - eU + \mu}{\mathrm{w}/2} \right) \right]. \end{aligned} \tag{6.100}$$

6.7 Phonon Broadening

In this section the model will be augmented to include phonon broadening. Our interest in this effect is to capture the basic physics that causes the rounding of the stair structure in the I-V curves. This has been conjectured to arise from dissipative coupling of the vibrational mode with the leads [BF03]. We will model this heuristically as coupling to a narrow band of optical phonons.

Consider the case where the electron is coupled to a narrow band of optical phonons of width δ. The final term in the Hamiltonian in Equation 6.75 will become,

$$\begin{aligned} & \frac{p^2}{2m} + \frac{1}{2}m\omega_0^2 x^2 + g\sqrt{2\hbar m\omega_0^3}|0><0| \\ \Longrightarrow \quad & \sum_{i=1}^{N}\left(\frac{p_i^2}{2m} + \frac{1}{2}m\omega_i^2 x_i^2\right) + \sum_{i=1}^{N} g_i\sqrt{2\hbar m\omega_i^3}x_i|0><0|. \end{aligned} \tag{6.101}$$

The sum is over the N vibrational modes in the band, each having a different natural frequency ω_i. The electron-phonon coupling, g_i, is assumed to be constant for all modes,

$$g_i = \frac{g}{\sqrt{N}}, \tag{6.102}$$

and the frequency distribution is assumed to be symmetric about a central frequency ω_0, and written as a Lorentzian for tractibility,

$$\rho(\omega) = \frac{\delta/\pi}{\delta^2 + (\omega - \omega_0)^2}. \tag{6.103}$$

The phonon bandwidth δ is assumed to be narrow in relation to ω_0.

These changes can be implemented in the model by re-considering the electron-phonon coupling calculation with the redefined variables. We begin by completing the square in the untransformed Hamiltonian,

$$
\begin{aligned}
H_{vib} &= \sum_i \frac{p_i^2}{2m} + \frac{1}{2}m\omega_i^2 \left(x_i + \frac{g}{\sqrt{N}}\sqrt{\frac{2\hbar}{m\omega_i}}|0><0| \right)^2 \\
&\quad - \sum_i \left(\frac{g}{\sqrt{N}} \right)^2 \hbar\omega_i |0><0| \qquad (6.104) \\
&= \sum_i \frac{p_i^2}{2m} + \frac{1}{2}m\omega_i^2 \left(x_i + \frac{g}{\sqrt{N}}\sqrt{\frac{2\hbar}{m\omega_i}}|0><0| \right)^2 \\
&\quad - g^2\hbar\omega_0 |0><0|. \qquad (6.105)
\end{aligned}
$$

In evaluating the last term, the polaron binding energy, the frequencies are averaged over the band,

$$\sum_i \frac{\omega_i}{\sqrt{N}} = \langle\omega\rangle = \omega_0. \qquad (6.106)$$

The next step is to perform the displaced oscillator transformation. If we define $x_{eq_i} = -\frac{g}{\sqrt{N}}\sqrt{\frac{2\hbar}{m\omega_i}}$, then the transformation takes the following form:

$$e^{\frac{i}{\hbar}x_{eq}p|0><0|} \Longrightarrow e^{\frac{i}{\hbar}\sum_i x_{eq_i}p_i|0><0|}. \qquad (6.107)$$

This replaces the displacement operator with a product of displacement operators, each representing a different vibrational mode. The transformed Hamiltonian is,

$$\begin{aligned}
\mathbb{H} &= e^{\frac{i}{\hbar}\sum_i x_{eq_i}p_i|0><0|} H e^{-\frac{i}{\hbar}\sum_i x_{eq_i}p_i|0><0|} \qquad (6.108)\\
&= \sum_{m\neq 0,-1} V\left(||m \gg\ll m+1|| + \text{c.c.}\right)\\
&\quad +\eta_L V\left(||-1 \gg\ll 0||e^{-\frac{i}{\hbar}\sum_i x_{eq_i}\mathbb{P}_i} + \text{c.c.}\right)\\
&\quad +\eta_R V\left(||1 \gg\ll 0||e^{-\frac{i}{\hbar}\sum_i x_{eq_i}\mathbb{P}_i} + \text{c.c.}\right)\\
&\quad +(\varepsilon_0 - \lambda eU)||0 \gg\ll 0|| - eU\sum_{m=1}^{\infty}||m \gg\ll m||\\
&\quad +\sum_i \frac{\mathbb{P}_i^2}{2m} + \frac{1}{2}m\omega_i^2\mathbb{X}_i^2 - g^2\hbar\omega_0||0 \gg\ll 0||. \qquad (6.109)
\end{aligned}$$

Using this Hamiltonian, we can now calculate the self-energy. It suffices to illustrate the effect of phonon broadening on the self-energy using $\Delta_L^{(e)}$ as an example. The space is now N+1 dimensional, where N is the number of vibrational modes, and the self energy is

$$\begin{aligned}
\Delta_L^{(e)} &= \sum_{n_1=0}^{\infty}\sum_{n_2=0}^{\infty}\cdots\sum_{n_N=0}^{\infty}\frac{\left(\frac{g}{\sqrt{N}}\right)^{2n_1}\left(\frac{g}{\sqrt{N}}\right)^{2n_2}\cdots\left(\frac{g}{\sqrt{N}}\right)^{2n_N}}{n_1!n_2!\ldots n_N!}\left(\frac{\eta_L^2\mathrm{w}}{8}\right)\\
&\times\left(-i\pi + \ln\left(\frac{z-(n_1\omega_1+n_2\omega_2+\ldots+n_N\omega_N)-\mu+i\frac{4}{\pi}kT}{\mathrm{w}/2}\right)\right). \qquad (6.110)
\end{aligned}$$

This can be evaluated analytically by writing

$$-i\pi + \ln\left(\frac{z-\alpha-\mu}{\mathrm{w}/2}\right) = \int_{\mu}^{\mathrm{w}/2} d\varepsilon \frac{1}{z-\alpha-\varepsilon}, \qquad (6.111)$$

for large w, and then expressing the denominator as a Fourier transform,

$$\frac{1}{z-\alpha-\mu} = \frac{1}{i}\int_0^\infty dt e^{-it(z-\alpha-\varepsilon)}, \tag{6.112}$$

where $\alpha = (n_1\omega_1 + n_2\omega_2 + \ldots + n_N\omega_N) + i\frac{4}{\pi}kT$. By putting the oscillator frequencies in the exponent, the nested sums over the states of each normal mode factorize,

$$\begin{aligned}
\Delta_L^{(e)} &= \sum_{n_1=0}^{\infty}\sum_{n_2=0}^{\infty}\cdots\sum_{n_N=0}^{\infty}\frac{\left(\frac{g}{\sqrt{N}}\right)^{2n_1}\left(\frac{g}{\sqrt{N}}\right)^{2n_2}\cdots\left(\frac{g}{\sqrt{N}}\right)^{2n_N}}{n_1!n_2!\ldots n_N!}\left(\frac{\eta_L^2\mathrm{w}}{8}\right) \\
&\times\frac{1}{i}\int_\mu^{\frac{\mathrm{W}}{2}} d\varepsilon\int_0^\infty dt e^{-it(z-\varepsilon)}e^{it(n_1\omega_1+n_2\omega_2+\ldots+n_N\omega_N)}e^{-t\frac{4}{\pi}kT} \qquad (6.113)\\
&= \frac{1}{i}\left(\frac{\eta_L^2\mathrm{w}}{8}\right)\int_\mu^{\frac{\mathrm{W}}{2}} d\varepsilon\int_0^\infty dt e^{-it(z-\varepsilon)}e^{-t\frac{4}{\pi}kT}\prod_i\sum_{n_i=0}^{\infty}\frac{\left(\frac{g^2}{N}\right)^{n_i}}{n_i!}e^{itn_i\omega_i} \qquad (6.114)\\
&= \frac{1}{i}\left(\frac{\eta_L^2\mathrm{w}}{8}\right)\int_\mu^{\frac{\mathrm{W}}{2}} d\varepsilon\int_0^\infty dt e^{-it(z-\varepsilon)}e^{-t\frac{4}{\pi}kT}\prod_i\left[e^{e^{-it\omega_i}\frac{g^2}{N}}\right] \qquad (6.115)\\
&= \frac{1}{i}\left(\frac{\eta_L^2\mathrm{w}}{8}\right)\int_\mu^{\frac{\mathrm{W}}{2}} d\varepsilon\int_0^\infty dt e^{it(z-\varepsilon)}e^{t\frac{4}{\pi}kT}e^{\frac{g^2}{N}\sum_{i=1}^{N}e^{it\omega_i}}. \qquad (6.116)
\end{aligned}$$

Taking the limit as $N\to\infty$, we replace the sum with an integration,

$$e^{g^2\int d\omega\rho(\omega)e^{-i\omega t}} = e^{g^2e^{-\delta|t|}e^{-i\omega_0 t}}. \tag{6.117}$$

Evaluating the integral over t gives

$$\begin{aligned}
&\frac{1}{i}\int_0^\infty dt e^{-it(z-\varepsilon)}e^{g^2e-i\omega_0 te^{-\delta|t|}}e^{-t\frac{4}{\pi}kT} \\
&= \sum_{m=0}^{\infty}\frac{(g^2)^2}{m!}\frac{1}{z-\varepsilon-m\omega_0+im\delta+i\frac{4}{\pi}kT}. \qquad (6.118)
\end{aligned}$$

Finally, integrating over ε returns the logarithmic form,

$$\begin{aligned} & \int_{\mu}^{\frac{\mathrm{W}}{2}} d\varepsilon \frac{1}{z-\varepsilon-m\omega_0+im\delta+i\frac{4}{\pi}kT} \\ = \; & \ln\left(\frac{z-\mu-m\omega_0+im\delta+i\frac{4}{\pi}kT}{z-\mathrm{w}/2-m\omega_0+im\delta+i\frac{4}{\pi}kT}\right). \end{aligned} \tag{6.119}$$

For large w, in the wide band limit, this can be written as

$$\left(-i\pi+\ln\left(\frac{z-m\omega_0-\mu+im\delta+i\frac{4}{\pi}kT}{\mathrm{w}/2}\right)\right). \tag{6.120}$$

Therefore the self energy $\Delta_L^{(e)}$ is,

$$\begin{aligned} \Delta_L^{(e)} \; = \; & \frac{\eta_L^2 \mathrm{w}}{8} e^{-g^2} \sum_{m=0}^{\infty} \frac{g^{2m}}{m!} \\ & \times \left(-i\pi+\ln\left(\frac{z-m\omega_0-\mu+im\delta+i\frac{4}{\pi}kT}{\mathrm{w}/2}\right)\right). \end{aligned} \tag{6.121}$$

This is almost the same expression that we found when considering only a single optical vibration, however there is an added imaginary term $im\delta$. This additional term combined with the factor of $i\frac{4}{\pi}kT$ causes the broadening of the stair structure.

Since the additional factor is proportional to m, one of the consequences of this is that the higher order steps will exhibit more broadening than the lower ones. Also, since δ and kT are added together, the effects of the phonon broadening will be more noticeable for $kT \ll \delta$.

6.8 Model I-V Curves

The expressions that have been derived for the electron and hole tunnelling rates may be combined and used to plot the current as a function of source drain voltage, producing I-V curves for the model C_{60} transistor system. In addition to confirming the validity of the model, these plots can be used to illustrate how the current responds to variations of certain parameters, allowing estimates for these parameters to be made via comparison with experimental data. The data of Park et al. [HP00] published in Nature, Volume 407, Page 57, 2000. In particular, the following parameters will be examined: the electron-phonon coupling (g), the extent of dissipative broadening (δ), the coupling of the molecule to the left and right electrodes (η_L, η_R), the position of the molecule in the junction (λ), the phonon energy (ω_0), and the temperature of the system (T). The bandwidth of the metal leads (w) is held constant at 4eV. The plots are produced using the Fortran code in Appendix A.

The effect of varying the parameters is illustrated in a series of plots, each illustrating the variation of one parameter while the rest are held at constant values. These constant values were determined by systematically scanning through the parameter space until a 'best fit' estimate was obtained for each one, except for the temperature which is known and is only included in the study for interest.

The estimates that are presented in this section are made by comparison with experimental data [Par00]. The dimensionless electron-phonon coupling parameter is found to be about $g \approx 1.1$. The molecular coupling parameters are found to be $\eta_R \mathrm{V} \approx 3.5 \times 10^{-3}\mathrm{V}$ and $\eta_L \mathrm{V} \approx 3.5 \times 10^{-4}\mathrm{V}$. The position of the molecule is found to be $\lambda \approx 0.6$, which places the molecule closer to the right electrode. The phonon energy is estimated to be $\hbar\omega_0 \approx 0.005\mathrm{eV}$, in accordance with the published data [Par00], and the extent of dissipative broadening is found to be about $\delta \approx \omega_0/10$. The temperature is held fixed at $T = 1.5K$.

For consistency, the gap voltage is kept fixed in all of the plots that explore

the parameter space. Recall that this represents the source-drain voltage drop that results in the alignment of the molecular level with the Fermi level of the electrode that receives the tunnelling electron.

6.8.1 Electron-Phonon Coupling - g

The dimensionless electron-phonon coupling constant influences the shape of the Franck-Condon overlap combs, and in particular affects how the size of the overlaps changes as a function of n, the oscillator level. A good estimate of the electron-phonon coupling can be found by comparing the rise of the steps in current for different values of g with data for the system. Figure 6.9 shows the effect of varying the linear electron-phonon coupling, where values of g in the vicinity of $g = 1$ are explored in particular.

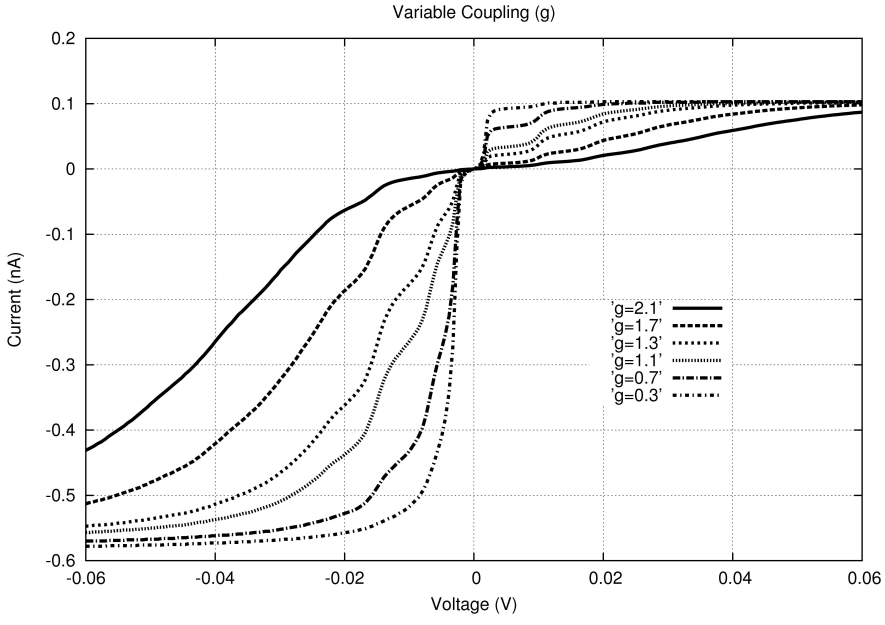

Figure 6.9: Illustration of different values of the dimensionless electron-phonon coupling constant g for $\omega_0 = 0.005$eV, $\delta = \omega_0/10$, $\eta_R = 0.0035$, $\eta_L = 0.00035$, $\lambda = 0.6$, $T = 1.5$K, w= 4eV.

By matching the size of the first, and most distinct, step in the current to the experimental data, the linear coupling parameter for C_{60} between gold electrodes is estimated to be $g \approx 1.1$. This value is slightly greater than predictions for the isolated C_{60} molecule. In particular, Joshi and Dresselhaus [JD92] have shown that the curvature of the C_{60} molecule leads to a slight decrease in the strength of the electron-phonon coupling interaction as compared to that of graphite. They find a value of $g \approx 0.9$ for the dimensionless coupling parameter for C_{60}. Park et al. [HP00] estimate the value of the coupling constant for isolated C_{60} to be $g \approx 0.8$.

6.8.2 Dissipative Broadening - δ

Coupling to the environment affects the width of the teeth in the overlap combs, which in turn affects the distinctness of the steps in the I-V curves. As discussed in Section 6.7, this dissipative broadening is incorporated into the model by considering the distribution of phonon energies as a Lorentzian distribution of width δ. We take δ to be some fraction of ω_0. Results for $\delta = \omega_0$, $\delta = \omega_0/10$, $\delta = \omega_0/100$ are shown in Figure 6.10.

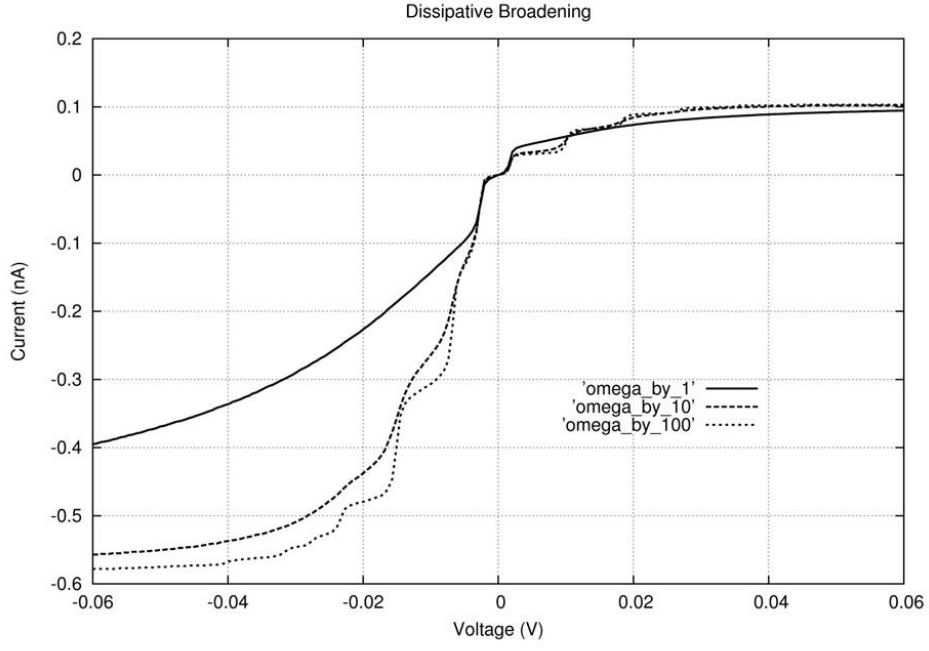

Figure 6.10: Illustration of the effect of varying the amount of dissipative broadening. Shown here are the results for $\delta = \omega_0$, $\delta = \omega_0/10$, $\delta = \omega_0/100$, with the remaining parameters held constant at $g = 1.1$, $\omega_0 = 0.005$eV, $\eta_R = 0.0035$, $\eta_L = 0.00035$, $\lambda = 0.6$, $T = 1.5$K, w= 4eV.

Comparison with the experimental plots yields an estimated value of $\omega_0/10$ for the width δ.

6.8.3 Molecule-Electrode Coupling - η

The strength of the coupling between the molecule and the electrodes affects the maximum value at which the current saturates. It can be seen in Figure 6.11 that increasing the coupling parameters increases these values.

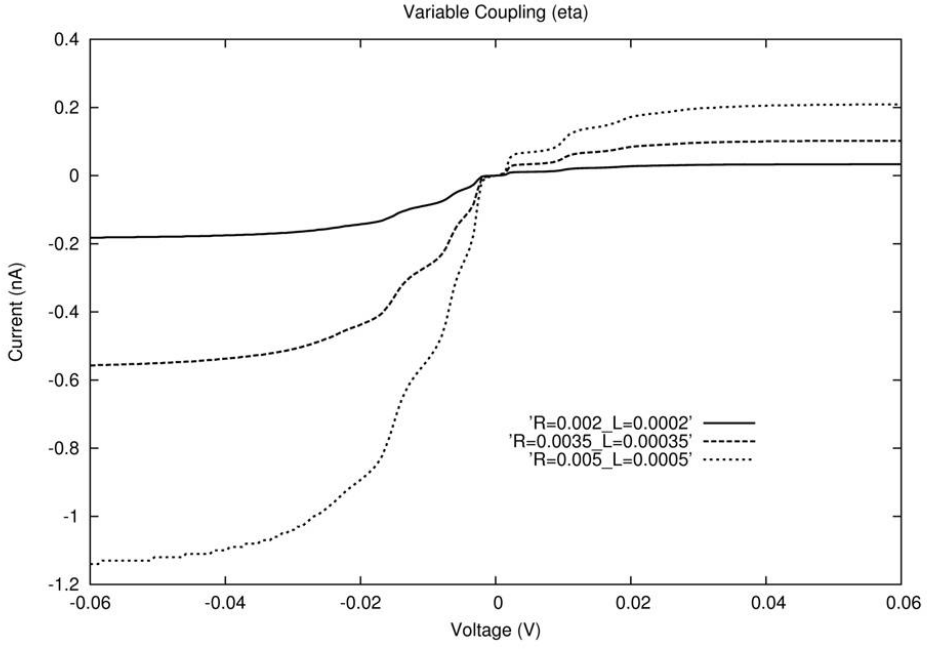

Figure 6.11: Illustration of the effect of varying the size of the dimensionless coupling constants between the molecule and the electrodes for $g = 1.1$, $\delta = \omega_0/10$, $\omega_0 = 0.005$eV, $\lambda = 0.6$, $T = 1.5$K, w= 4eV.

By examining the saturation values of the current for different coupling values, the dimensionless coupling factors are found to be $\eta_L \approx 3.5 \times 10^{-4}$ and $\eta_R \approx 3.5 \times 10^{-3}$. This means that the rate limiting step is between the molecule and the left electrode. If the rate limiting step was between the molecule and the right electrode, then the forward bias current would saturate at a value that is greater than the saturation value for the reverse bias current by a factor of 6, as shown in Figure 6.12.

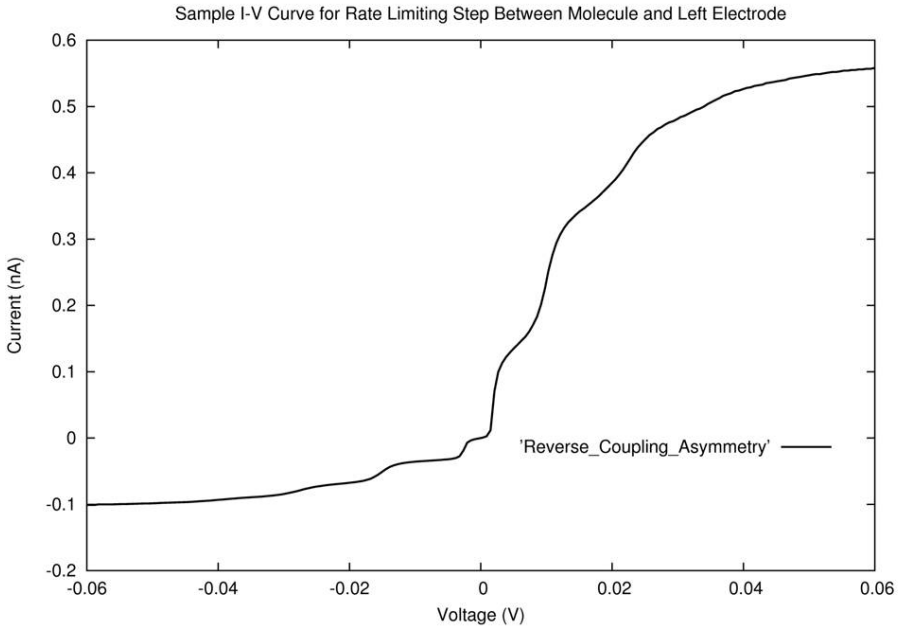

Figure 6.12: Rate limiting step between the molecule and the left electrode ($\eta_R > \eta_L$), for $\eta_R = 0.0035$, $\eta_L = 0.00035$, $g = 1.1$, $\delta = \omega_0/10$, $\omega_0 = 0.005$eV, $\lambda = 0.6$, $T = 1.5$K, w= 4eV.

6.8.4 Voltage Divider - λ

The distance between the molecule and the left and right electrodes affects the drop in source-drain voltage that turns on the current. This is reflected in the I-V plots as the sizes of the forward and reverse voltage gaps. The gaps would be equal if the molecule was equidistant from either electrode, and the gap increases as the molecule-electrode distance increases. The position of the molecule can be considered as a voltage divider, and is incorporated into the model as the factor λ, where λ is the ratio of the left electrode-molecule distance and the total size of the gap between the electrodes, $\lambda = d_1/l$.

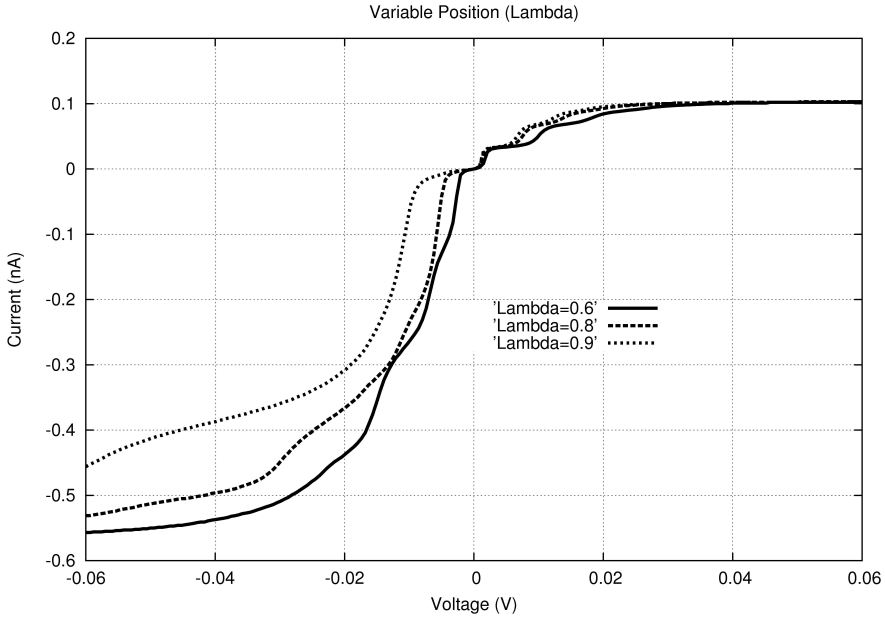

Figure 6.13: Illustration of the effect of shifting the position of the molecule in the gap between the electrodes. Increasing λ corresponds to moving the molecule closer to the right electrode. ($\eta_R = 0.0035$, $\eta_L = 0.00035$, $g = 1.1$, $\delta = \omega_0/10$, $\omega_0 = 0.005$eV, $T = 1.5$K, w= 4eV.

As shown in Figure 6.13, increasing λ increases the distance between the molecule and the left electrode, and increases the 'reverse bias' voltage gap while decreasing the 'forward bias' gap. This is expected because the current turns on when the tunnelling level aligns with the Fermi level of the electrode for hops off of the molecule. When λ increases, the fraction of the applied voltage that accomplishes this grows smaller for forward bias since the tunnelling level is getting closer to this electrode, and larger for reverse bias since the level is getting further from this electrode. Comparison yields a value of $\lambda \approx 0.6$.

6.8.5 Phonon Energy - ω_0

The vibrational quantum is estimated to have an energy of $\omega_0 = 0.005$eV [HP00], which corresponds to the centre of mass oscillation of the C_{60} molecule within the confinement potential of the electrodes [LYG97]. Altering this energy affects the width of the steps in the current. The direct correlation between various phonon energies and the step width can be seen in Figure 6.14.

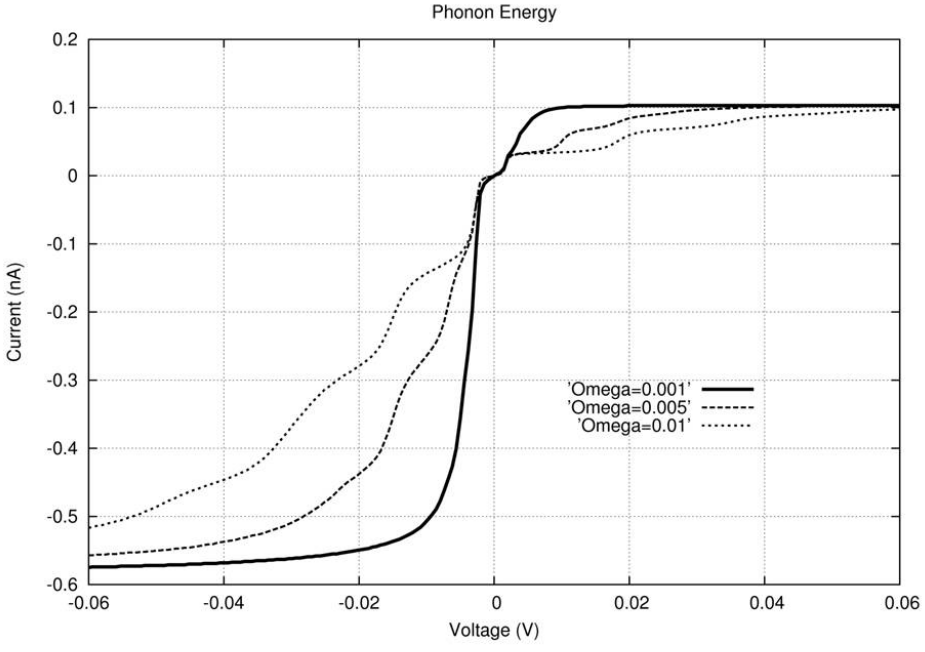

Figure 6.14: Illustration of different values for the vibrational quantum ω_0, for $\eta_R = 0.0035$, $\eta_L = 0.00035$, $g = 1.1$, $\delta = \omega_0/10$, $\lambda = 0.6$, $T = 1.5$K, w= 4eV.

6.8.6 Temperature - T

The effect of varying the temperature of the system is shown in Figure 6.15. The structure of the I-V curves becomes increasingly indistinct as the temperature of the system is raised.

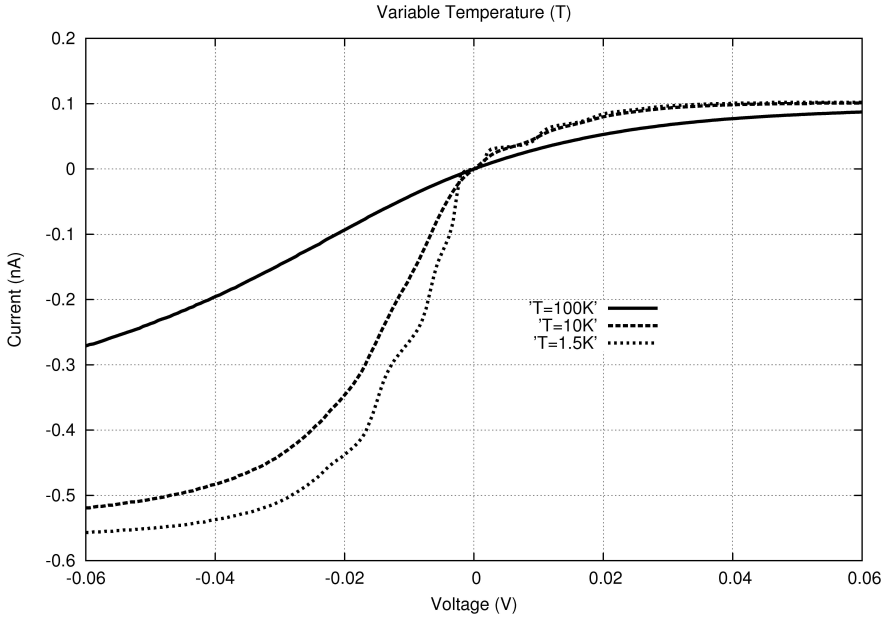

Figure 6.15: Illustration of the effect of varying the temperature of the system, for $\eta_R = 0.0035$, $\eta_L = 0.00035$, $g = 1.1$, $\delta = \omega_0/10$, $\omega_0 = 0.005$eV, $\lambda = 0.6$, w= 4eV.

6.8.7 Comparison with Experimental Curves

The prominent asymmetries that are exhibited in the I-V data for the molecular transistor system are reproduced in the model curves. Under reverse bias the curves saturate more quickly, which causes them to exhibit less distinct structure. The Franck-Condon overlap combs are almost entirely contained in the window of energetically allowed transitions when the current turns on for reverse bias, which results in the lack of distinction in the current steps. The off-centre position of the molecule in the junction causes the asymmetry in the gap voltages, however the difference in the saturation rates is caused by the factor of six that was introduced into the expression for the current because of the degeneracy of the LUMO. There is clearly another factor that influences the rate at which the current saturates, because the

reveres bias curves saturate at a faster rate than is observed in the data. Figure 6.9 shows that increasing the value of the electron phonon coupling constant causes the reverse bias curves to saturate more slowly. In particular, when $g = 2.1$ the reverse bias current increases at a rate that matches the data. The data could be replicated if very different values of the electron-phonon coupling are chosen for forward and reverse bias ($g \approx 1.1$ for forward bias and $g \approx 2.1$ for reverse bias), however there is no physical justification for this.

Figure 6.16 shows a comparison between the model curves and the experimental data of H. Park et al. published in Volume 407 of Nature magazine in 2000 [Par00] for our best estimates of the model parameters.

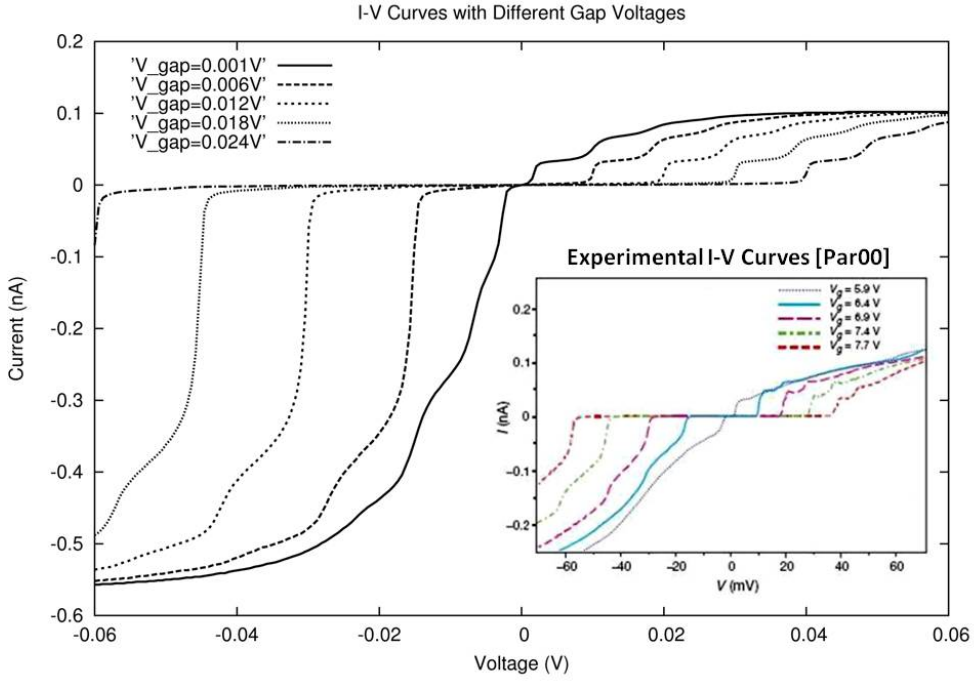

Figure 6.16: Comparison between the I-V relation predicted by our model and experimental data. Parameters are: $\eta_R = 0.0035$, $\eta_L = 0.00035$, $g = 1.1$, $\delta = \omega_0/10$, $\omega_0 = 0.005$eV, $\lambda = 0.6$, $T = 1.5$K, w= 4eV.

Summary:

The rates for an electron to tunnel between the left and right electrodes and the molecule are:

$$\begin{aligned} R_L^{(e)} &= -\frac{\eta_L^2 \mathrm{w}}{4} \mathrm{Im} \sum_{n=0}^{\infty} \frac{e^{-g^2} g^{2n}}{n!} \\ &\times \left[-i\pi + ln\left(\frac{z_-^e - n\omega_0 + i\frac{4}{\pi}kT - \mu + in\delta}{\mathrm{w}/2} \right) \right] \\ R_R^{(e)} &= -\frac{\eta_R^2 \mathrm{w}}{4} \mathrm{Im} \sum_{n=0}^{\infty} \frac{e^{-g^2} g^{2n}}{n!} \\ &\times \left[-i\pi + ln\left(\frac{z_-^e - n\omega_0 + i\frac{4}{\pi}kT + eU - \mu + in\delta}{\mathrm{w}/2} \right) \right], \end{aligned}$$

The corresponding hole tunnelling rates are:

$$\begin{aligned} R_L^{(h)} &= -\frac{\eta_L^2 \mathrm{w}}{4} \mathrm{Im} \sum_{n=0}^{\infty} \frac{e^{-g^2} g^{2n}}{n!} \\ &\times \left[-i\pi + ln\left(\frac{z_-^h - n\omega_0 + i\frac{4}{\pi}kT + \mu + in\delta}{\mathrm{w}/2} \right) \right] \\ R_R^{(h)} &= -\frac{\eta_R^2 \mathrm{w}}{4} \mathrm{Im} \sum_{n=0}^{\infty} \frac{e^{-g^2} g^{2n}}{n!} \\ &\times \left[-i\pi + ln\left(\frac{z_-^h - n\omega_0 + i\frac{4}{\pi}kT - eU + \mu + in\delta}{\mathrm{w}/2} \right) \right]. \end{aligned}$$

Using these rates in the previously derived expression for the current, the model parameters are estimated as follows:

Bandwidth (w)	4eV
Phonon Energy (ω_0)	0.005eV
Electron-Phonon Coupling Constant (g)	1.1
Molecule-Anode Coupling (η_R)	3.5×10^{-3}
Molecule-Cathode Coupling (η_L)	3.5×10^{-4}
Voltage Divider (λ)	0.6
Dissipative Broadening (δ)	$\omega_0/10$
Temperature (T)	1.5K

Chapter 7

Discussion

Our approach to modelling the I-V response of the C_{60} transistor of Park et al. [HP00] has confirmed existing theories [KF05, BS01, KM03a, GD92, LLS97] that explain the trends observed in experimental data for molecular transistors with strong electron-vibron coupling [JP02, WL02, RHMS02, NZB02], and has also uncovered new properties of the system. The hopping rate method by which the I-V relation is derived is not original [BF03],[MAM04], even as applied to to this system, however our execution includes details that were not previously explored. The I-V curves that are produced from our model replicate experimental data more closely than other published studies [BF03, MAM04, BS01, KM03b] because we have explored the parameter space more thoroughly. Our estimated values for the model parameters are listed in Table 7.1.

Table 7.1: Summary of the estimated values for the model parameters.

Parameter	Estimated Value
Bandwidth of Gold Electrodes (w)	4eV
Phonon Energy (ω_0)	0.005eV
Dimensionless Electron-Phonon Coupling Constant (g)	1.1
Dimensionless Molecule-Anode Coupling Parameter (η_R)	$3.5x10^{-3}$
Dimensionless Molecule-Cathode Coupling Parameter (η_L)	$3.5x10^{-4}$
Voltage Divider (λ)	0.6
Dissipative Broadening (δ)	$\omega_0/10$
Temperature (T)	1.5K

The single glaring discrepancy between our theory and experiment is the asymmetry in the curves of different bias. The inclusion of the degeneracy of the LUMO in the tunnelling rate expression for the current results in a predicted factor of six for the asymmetry in the current. Instead, the experimental curves appear to be asymmetric by a factor of about three, indicating that the LUMO degeneracy is not sufficient to explain that saturation asymmetry, however this model certainly improves upon the standard technique [BF03, MAM04] of considering only the spin asymmetry which predicts a factor of two.

The above problem notwithstanding, significant progress has been made in understanding the electronic properties of the C_{60} transistor system. In incorporating the degeneracy of the LUMO, a general technique for finding the tunnelling rates for degenerate systems was developed that we named the "molecular transition picture". The utility of this method lies in its generalization of the current expression based on the number of initial and final states that are available to a tunnelling particle.

Another detail about the system, that is treated somewhat ambiguously in the literature [CKS03, Par00], is the equilibrium charge state of the C_{60} molecule when sandwiched between the gold electrodes in the transistor configuration. It was shown in two ways in this thesis that the published data of Park et al., represents a system where the molecule is charged prior to the application of a bias voltage. Although

this alone is a fairly unremarkable result, the correlation of the asymmetries in the data with the charge state is an interesting result. If it is assumed that the molecule is asymmetrically coupled to the electrodes, and that the two charge states that participate in the current are C_{60}^{0} and C_{60}^{1-}, then there are four possible initial conditions for the molecule. Prior to the application of V_{SD} it can be closer to the cathode in either charge state, or closer to the anode in either charge state. Inspection of the voltage gap and current asymmetries reveals which initial condition correlates with the data. These results are listed in Table 7.2, and they are also summarized using the P function that was described in Chapter 4.

Table 7.2: Summary of the initial conditions associated with the asymmetries observed in experimental I-V curves for the C_{60} molecular transistor.

Initial Condition	Correlated Asymmetries	Sign of P
Closer to cathode; Neutral	$\|I_{FB}\| < \|I_{RB}\|$; $V_g^F < V_g^R$	P>0
Closer to cathode; Charged	$\|I_{FB}\| < \|I_{RB}\|$; $V_g^F > V_g^R$	P<0
Closer to anode; Neutral	$\|I_{FB}\| > \|I_{RB}\|$; $V_g^F > V_g^R$	P>0
Closer to anode; Charged	$\|I_{FB}\| > \|I_{RB}\|$; $V_g^F < V_g^R$	P<0

Finally, a method for measuring the difference in energy between the LUMO of C_{60} and the Fermi level of the electrodes for a particular gate voltage was uncovered in Section 4.3. This provides a simple experimental measure for obtaining a numerical relationship describing the effect that tuning the gate voltage has on the LUMO.

Clearly there is a lot of work to be done both theoretically and experimentally to capture the potential of nano-electronic systems for everyday use. Whether or not this ever occurs remains to be seen, and in no way diminishes the importance of the rapid progress that is being made in understanding this new field.

Appendices

Appendix A

Fortran Code for Producing I-V Curves

```
C Linear Coupling Code

program rates8a
implicit real*8 (a-h,o-z)
complex*16 pole1,pole2,z1,z2,z3,y,zg,mylog,term1,term2
     &,zgmax,zgmin,zginc,phononR,phononL
character*40 fname
common /parameters/ev,w,pi,etaR,etaL,gamma,eps0,alam,tol,
     &tol1,g,omega,width,akT,iflag,nmax

gamma=0.000001

C This program finds the poles of the green function G(0,0),
C   and then evaluates the self energy at these poles. Using
C   these values it deterimines the rates to hop off of the
```

```
C   molecule to the right and to the left. These rates are the
C   imaginary parts of the self energy. In lieu of calculating
C   the rates to hop on the molecule, the off rate is
C   evaluated for both electron and hole initial conditions
C   since the rate for a hole to leave the molecule is the
C   same as the rate for an electron to hop onto the molecule.
C   Combining these electron on/off rates gives the current
C   through the junction.

C The advantage of this method of calculation is that both
C   the real and imaginary parts of the self energy are
C   considered. The real part of the self energy causes shifts
C   in the locations of the voltage thresholds. Although these
C   shifts are insignificant in the limit of weak coupling,
C   there are regimes where the coupling is weak enough to
C   give a well-defined decay rate while at the same time
C   large enough so that the energy shifts are significant.
C   The effect is pronounced at T=0 because the real part of
C   the self energy diverges logarithmically when the energy
C   is equal to either the fermi level of the cathode or the
C   fermi level of the anode. The logarithmic divergence occurs
C   because the fermi function cuts off the integration of the
C   Green function over the density at a point where the
C   density of states is non-vanishing.

C These energies give the upper and lower limits in voltage
C   in electron volts.
ev1=-0.06
ev2=.06
```

```
npts=203
evstep=(ev2-ev1)/npts

C This is the bandwidth of the metal leads, in electron
C   volts.
w=4

C These are the dimensionless band narrowing factors, etaL
C   for the cathode-molecule bond, and etaR for the
C   anode-molecule bond.
etaR=0.0035
etaL=0.00035

C This is the voltage asymmetry factor (0.5 is symmetric)
C   reflecting the position of the molecule.
alam=0.6

C This is the electron-phonon coupling constant
g=1.1

C This is the upper limit on phonon states (>> g^2)
nmax=40

C This is the phonon energy in eV.
omega=0.005

C This is the width of the phonon density of states in eV
C   (assuming a Lorentizian distribution of phonons).
```

```
width = omega/10.

C This gives kT in electron volts for T=1.5 Kelvin
pi=3.141592654
akT=1.5/300*(1./38.6)*(4./pi)

C This prefactor gives the current in nanoamps.
pre=2.7e+5

C This is the ratio of the hole effective mass to the
C   electron effective mass.
ratio=1

C This input gives the gap voltage (position of the LUMO).
write(6,*)'Enter the offset energy'
read(5,*)offset
eps0=offset+g**2*omega
write(6,*)'Enter the datafile name'
read(5,*)fname

C These are the lower and upper limits of the guesses.
C The newton's method which is used to find the poles of the
C   Green function does not converge for any guess, but usually
C   there is a guess which will work if you can find it. Here
C   we sweep through 101 guesses until we find one which
C   converges in less than 100 iterations. If there is no
C   convergence in 100 iterations for any guess, the data point
C   is omitted from the set, and we go on to the next voltage.
nguess=101
```

```
zgmin=(5,-.005)
zgmax=(-5,-.005)
zginc=(zgmax-zgmin)/(nguess-1)



C This program solves for the roots of a complex function
C   using Newton's method.

C The tolerance tol1 is used as the step when I approximate
C   the derivative of the function by taking the difference
C   between two points. The tolerance tol is used to determine
C   when the root has been found to sufficient accuracy. Both
C   tol1 and tol are in electron volts.
tol1=1.d-9
tol=1.d-8

open(1,file=fname,status='unknown')
open(2,file='pole',status='unknown')

pi=3.141592654

zg=(5,0)
do 100 j=1,npts+1
ev=ev1+(j-1)*evstep

C The iflag is set to 1 for the emission of an electron, and
C   to 2 for the emmission of a hole.
iflag=1
ionce1=0
```

```
do 101 k1=1,nguess
zg=zgmin+(k1-1)*zginc
call root(zg,pole1,ierror)
if(ierror.eq.0)then
ionce1=1
go to 1010
endif
 101 continue
 1010 if(ionce1.ne.1)then
write(6,*)'ionce1 is zero'
endif
if((dimag(pole1).gt.0).and.(dabs(dimag(pole1)).gt.1.e-8))then
write(6,*)'Trouble with sign of pole'
pause
endif
iflag=2
ionce2=0
do 102 k1=1,nguess
zg=zgmin+(k1-1)*zginc
call root(zg,pole2,ierror)
if(ierror.eq.0)then
ionce2=1
go to 1020
endif
 102 continue
 1020 if(ionce2.ne.1)then
write(6,*)'ionce2 is zero'
endif
if((dimag(pole2).gt.0).and.(dabs(dimag(pole2)).gt.1.e-8))then
```

```
write(6,*)'Trouble with sign of pole'
pause
endif

if((ionce1.ne.0).and.(ionce2.ne.0))then

iflag=1
rateR1=-2*dimag(phononR(pole1))
rateL1=-2*dimag(phononL(pole1))

iflag=2
rateR2=-2*dimag(phononR(pole2))
rateL2=-2*dimag(phononL(pole2))

decayR1=rateR1*ratio**1.5
decayL1=rateL1*ratio**1.5
decayR2=rateR2
decayL2=rateL2

C The rate expression for the current is inserted here:
C   I = -6[(mc)(am)-(ma)(cm)]/(cm+am+6ma+6mc)
anum=decayR1*decayL2-decayL1*decayR2
denom=6.*decayR1+decayL2+6.*decayL1+decayR2
current=6.*pre*anum/denom
write(2,600)ev,Imag(pole1),Imag(pole2)
write(1,600)ev,current

else
```

```
write(6,600)'Skip data point'
endif

 100 continue
stop
 600 format(5(g10.3,1x))
end

subroutine root(zg,pole,ierror)
implicit real*8 (a-h,o-z)
complex*16 zg,func,z1,z2,z3,y,pole
common /parameters/ev,w,pi,etaR,etaL,gamma,eps0,alam,tol,
     &tol1,g,omega,width,akT,iflag,nmax

C A Newton's method routine to find the root of a complex
C   function.
jmax=100
z1=zg
j=0
 10 j=j+1
derivx=dreal(func(z1+(1.,0.)*tol1)-func(z1))/tol1
x2=x1-dreal(func(z1))/derivx
z2=(1,0)*x2+(0,1)*y1
derivy=dimag(func(z2+(0,1)*tol1)-func(z2))/tol1
y2=y1-dimag(func(z2))/derivy
z3=(1.,0.)*x2+(0.,1.)*y2
value=cdabs(func(z3))
if(value.gt.tol)then
x1=x2
```

```
y1=y2
z1=z3
if(j.gt.jmax)then
ierror=1
return
else
ierror=0
endif
go to 10
else
pole=z3
endif
return
end

complex*16 function func(z)
implicit real*8 (a-h,o-z)
complex*16 z,eps,term1,term2,term3,mylog,phononR,phononL
common /parameters/ev,w,pi,etaR,etaL,gamma,eps0,alam,tol,
     &tol1,g,omega,width,akT,iflag,nmax

C This routine calculates the denominator of G(0,0).
eps=z+(0.,1.)*gamma
if(iflag.eq.1)then
func=eps+g**2*omega+alam*ev-eps0-phononR(eps)-phononL(eps)
endif
if(iflag.eq.2)then
func=eps-g**2*omega-alam*ev+eps0-phononR(eps)-phononL(eps)
endif
```

```
return
end

complex*16 function phononR(eps)
implicit real*8 (a-h,o-z)
complex*16 eps,term,term1,term2,mylog
common /parameters/ev,w,pi,etaR,etaL,gamma,eps0,alam,tol,
     &tol1,g,omega,width,akT,iflag,nmax

C The self energy contibutions coming from the right hand
C   side (the anode).
if(iflag.eq.1)then
term=(0.,0.)
do 100 j=0,nmax
term2=mylog((eps-j*(omega-(0.,1.)*width)
     &+(0.,1.)*akT+ev)/(w/2.))-(0.,1.)*pi
term=term+(1./8.)*(etaR)**2*fcon(j)*w*term2
 100 continue
phononR=term
endif
if(iflag.eq.2)then
term=(0.,0.)
do 200 j=0,nmax
term2=mylog((eps-ev-j*(omega-(0.,1.)*width)
     &+(0.,1.)*akT)/(w/2.))-(0.,1.)*pi
term=term+(1./8.)*(etaR)**2*fcon(j)*w*term2
 200 continue
phononR=term
endif
```

```
return
end

complex*16 function phononL(eps)
implicit real*8 (a-h,o-z)
complex*16 eps,term,term1,term2,mylog
common /parameters/ev,w,pi,etaR,etaL,gamma,eps0,alam,tol,
     &tol1,g,omega,width,akT,iflag,nmax

C The self energy contibutions coming from the left hand
C   side (the cathode).
if(iflag.eq.1)then
term=(0.,0.)
do 100 j=0,nmax
term1=mylog((eps-j*(omega-(0.,1.)*width)
     &+(0.,1.)*akT)/(w/2.))-(0.,1.)*pi
term=term+(1./8.)*(etaL)**2*fcon(j)*w*term1
 100 continue
phononL=term
endif
if(iflag.eq.2)then
term=(0.,0.)
do 200 j=0,nmax
term1=mylog((eps-j*(omega-(0.,1.)*width)
     &+(0.,1.)*akT)/(w/2.))-(0.,1.)*pi
term=term+(1./8.)*(etaL)**2*fcon(j)*w*term1
 200 continue
phononL=term
endif
```

```
return
end

real*8 function fcon(n)
implicit real*8 (a-h,o-z)
common /parameters/ev,w,pi,etaR,etaL,gamma,eps0,alam,tol,
     &tol1,g,omega,width,akT,iflag,nmax

C This calculates the Frank-Condon overlap factor.
fcon=g**(2*n)/factorial(n)*exp(-g**2)
return
end

function factorial(m)
implicit real*8 (a-h,o-z)
factorial=1.
do 100 j=1,m
factorial=factorial*j
 100 continue
return
end



complex*16 function mylog(z)
complex*16 z

C This program puts the branch cuts for the log function
C   along the negative imaginary axis.
pi=3.141592654
```

```
if((dreal(z).lt.0).and.(dimag(z).lt.0))then
mylog=log(z)+(0.,1.)*(2*pi)
else
mylog=log(z)
endif
return
end



C complex*16 function mylog(z)
C This is a fake routine to return only the imaginary part
C of the log, but not the real part.
C complex*16 z
C pi=3.141592654
C if((dreal(z).lt.0).and.(dimag(z).lt.0))then
C mylog=(0.,1.)*dimag(log(z)+(0.,1.)*(2*pi))
C else
C mylog=(0.,1.)*dimag(log(z))
C endif
C return
C end
```

References

[AMAR98] A. Aviram and Eds. M. A. Ratner. *Molecular Electronics: Science and Technology (Annals of the New York Academy of Sciences), Vol. 852*. The New York Academy of Science, New York, NY, 1998.

[ANP05] C. Chang A. V. Soldatov S. Lebedkin R. C. Bialczak J. E. Grose L. A. K. Donev J. P. Sethna D. C. Ralph P. L. McEuen A. N. Pasupathy, J. Park. *Nano Letters*, 5:203, 2005.

[AP95] R. Aldrovandi and J. G. Pereira. *An Introduction to Geometrical Physics*. World Scientific, Singapore, 1995.

[AR74] A. Aviram and M. A. Ratner. *Chem. Phys. Lett.*, 29:257, 1974.

[Bev86] M. B. Bever. *Encyclopedia of Materials Science and Engineering*. MIT Press, Cambridge, MA, 1986.

[BF03] S. Braig and K. Flensberg. *Phys. Rev. B.*, 68:205324, 2003.

[BF04] S. Braig and K. Flensberg. *Phys. Rev. B*, 70:085317, 2004.

[BK99] F. Biscarini and V. M. Kenkre. *Surface Science*, 426:336, 1999.

[Bri] http://www.britannica.com/ebc/art-97949/The-Biosphere-Montreal.

[BS01] D. Boese and H. Schoeller. *Europhys. Lett.*, 54:668, 2001.

[Car83] F. Carter. *J. Vac. Sci. Technol. B*, 1:959, 1983.

[Cha88] R. Chang. *Chemistry, Third Edition*. McGraw Hill, Toronto, 1988.

[CJ00] A. Aviram C. Joachim, J. K. Gimzewski. *Nature*, 408:541, 2000.

[CJA93] C. Chavy, C. Joachim, and A. Altibelli. *Chem. Phys. Lett.*, 214:569, 1993.

[CKS03] A. Chakraborty, K. Kumar, and K. L. Sebastian. *Phys. Rev. B*, 68:85411, 2003.

[Dat95] S. Datta. *Electronic Transport in Mesoscopic Systems*. Cambridge University Press, Cambridge, MA, 1995.

[DDE96] M. S. Dresselhaus, G. Dresselhaus, and P. C. Eklund. *Science of Fullerenes and Carbon Nanotubes*. Academic Press, New York, 1996.

[EB02] D. C. Ralph E. Bonet, M. M. Deshmukh. *Phys. Rev. B*, 65:45317, 2002.

[Eco06] E. N. Economou. *Green Functions in Quantum Physics*. Springer-Verlag, Berlin, 2006.

[EK02] E. G. Emberly and G. Kirczenow. *Chem. Phys.*, 281:311, 2002.

[EK03] E. G. Emberly and G. Kirczenow. *Phys. Rev. Lett.*, 91:188, 2003.

[ET05] F. Elste and C. Timm. *Phys. Rev. B*, 71:155403, 2005.

[FB95] V. M. Kenkre F. Biscarini, C. Bustamante. *Phys. Rev. B*, 51:11089, 1995.

[GD92] H. Grabert and M. H. Devoret. *Single Charge Tunnelling*. Plenum, New York, 1992.

[GS71] M. Grover and R. Silbey. *J. Chem. Phys.*, 54:4843, 1971.

[Heb93] A. F. Hebard. *Annual Review of Materials Science*, 23:159, 1993.

[HH89] P. Horowitz and W. Hill. *The Art of Electronics*. Cambridge University Press, Cambridge, MA, 1989.

[HP99] A. P. Alivisatos J. Park P. L. McEuen H. Park, A. K. L. Lim. *Applied Physics Letters*, 75:301, 1999.

[HP00] J. Park A. K. L. Lim E. H. Anderson A. P. Alivisatos P. L. McEuen H. Park. *Nature*, 407:57, 2000.

[IG91] G. L. Ingold and H. Grabert. *Europhys. Lett.*, 14:371, 1991.

[JBY92] R. D. Johnson, B. S. Bethune, and C. S. Yannoni. *Accounts of Chem. Res.*, 25:169, 1992.

[JD92] R. A. Jishi and M. S. Dresselhaus. *Phys. Rev. B*, 45:2507, 1992.

[JMAR97] J. Jortner and Eds M. A. Ratner. *Molecular Electronics*. Blackwell Science, Cambridge, MA, 1997.

[Joa02] C. Joachim. *Nanotechnology*, 13:R1, 2002.

[JP02] J. I. Goldsmith C. Chang Y. Yaish J. R. Petta M. Rinkoski J. P. Sethna H. D. Abruna P. J. Park, A. N. Pasupathy. *Nature*, 417:722, 2002.

[Jr.91] D. E. Koshland Jr. *Science*, 254:5039, 1991.

[Ken75] V. M. Kenkre. *Phys. Rev. B.*, 12:2150, 1975.

[KF05] G. A. Kaat and K. Flensberg. *Phys. Rev. B*, 71:155408, 2005.

[KHOS85] H. W. Kroto, J. R. Heath, S. C. O'Brien, and R. E. Smalley. *Nature*, 318:162, 1985.

[KM03a] M. Tuominen K. McCarthy, N. Prokofev. *Phys. Rev. B*, 67:245415, 2003.

[KM03b] S. B. Arnason K. McCarthy, A. F. Hebard. *Phys. Rev. Lett.*, 90:117201, 2003.

[KN02] Y. Majima K. Nagano, A. Okuda. *Applied Physics Letters*, 81:544, 2002.

[Kro87] H. W. Kroto. *Nature*, 329:529, 1987.

[KvO05] J. Koch and F. von Oppen. *Phys. Rev. B*, 72:113308, 2005.

[LLS97] G. Schön L. L. Sohn, L. P. Kouwenhoven. *Mesoscopic Electron Transport*. Kluwer Academic, Dordrecht, 1997.

[LYG97] M. V. Voinova B. Kasemo R. I. Shekhter M. Jonson L. Y. Gorelik, A. Isacsson. *Phys. Rev. Lett.*, 80:4526, 1997.

[MA60] A. Miller and E. Abrahams. *Physical Review*, 120:745, 1960.

[MAM04] A. Mitra, I. Aleiner, and A. J. Millis. *Phys. Rev. B.*, 69:245302, 2004.

[MAR97] C. J. Muller T. P. Burgin J. M. Tour M. A. Reed, C. Zhou. *Science*, 278:252, 1997.

[MAR98] M. Kemp V. Mujica A. Roitberg S. Yaliraki M. A. Ratner, B. Davis. *Ann. N.Y. Acad. Sci.*, 852:22, 1998.

[Mat] http://mathworld.wolfram.com/TruncatedIcosahedron.html.

[MHD90] H. Grabert G. L. Ingold H. Pothier C. Urbina M. H. Devoret, D. Esteve. *Phys. Rev. Lett.*, 64:1824, 1990.

[MJ06] K. Baheti M. M. Deshmukh J. J. Sokol E. M. Rumberger D. N. Hendrickson J. R. Long H. Park D. C. Ralph M. Jo, J. E. Grose. *Nano Letters*, 6:2014, 2006.

[Naz89] Y. V. Nazarov. *Sov. Phys. JETP*, 68:561, 1989.

[NR03] A. Nitzan and M. A. Ratner. *Science*, 300:1384, 2003.

[NZB02] H. Meng N.B. Zhitenev and Z. Bao. *Phys. Rev. Lett.*, 88:226801, 2002.

[O'S05] J. N. O'Shea. *Science*, 310:453, 2005.

[Osa70] E. Osawa. *Kagaku*, 25:854, 1970.

[Par00] H. Park. *Science*, 407:57, 2000.

[RH93] R. S. Ruoff and A. P. Hickman. *J. Phys. Chem.*, 97:2494, 1993.

[RHMS02] C. Untiedt N. D. Lang M. C. van Hemert J. M. van Ruitenbeek R. H. M. Smit, Y. Noat. *Nature*, 419:906, 2002.

[Sak94] J. Sakurai. *Modern Quantum Mechanics*. Addison-Wesley, New York, 1994.

[SMG90] M. Jonson D. R. Penn M. D. Stiles S. M. Girvin, L. I. Glazman. *Phys. Rev. Lett.*, 64:3183, 1990.

[SR93] G. C. Schatz and M. A. Ratner. *Quantum Mechanics in Chemistry*. Prentice Hall, Englewood Cliffs, 1993.

[Tis33] L. Tisza. *Zeitschrift für Physik*, 82:48, 1933.

[TN02] R. I. Shekhter M. Jonson T. Nord, L. Y. Gorelik. *Phys. Rev. B*, 65:165312, 2002.

[VEH04] M. Di Ventra, S. Evoy, and J. R. Heflin. *Introduction to Nanoscale Science and Technology*. Springer, New York, 2004.

[VMK92] C. Bustamante V. M. Kenkre, F. Biscarini. *Ultramicroscopy*, 42-44:122, 1992.

[VMK95] C. Bustamante V. M. Kenkre, F. Biscarini. *Phys. Rev. B*, 51:11074, 1995.

[WL02] M. Bockrath J. R. Long H. Park W. Liang, M. P. Shores. *Nature*, 417:725, 2002.

[XR03] Y. Xue and M. A. Ratner. *Phys. Rev. B*, 68:115, 2003.

[YA03] Y. Majima Y. Azuma, K. Nagano. *Japanese Journal of Applied Physics*, 42:2458, 2003.